AD NUMBER

AD451409

LIMITATION CHANGES

TO:

Approved for public release; distribution is unlimited.

FROM:

**Distribution authorized to U.S. Gov't. agencies and their contractors;
Administrative/Operational Use; NOV 1964. Other requests shall be referred to Air Force Arnold Engineering Development Center, Arnold AFB, TN.**

AUTHORITY

aedc dtd 19 May 1965

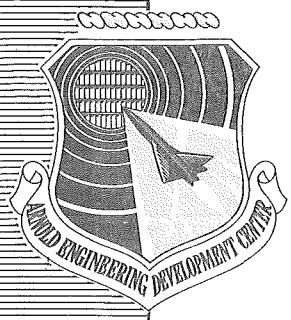

AN EXPERIMENTAL STUDY OF RADIANT ENERGY TRANSFER FROM A PLASMA

By

James M. Berry and Richard S. Tankin
Gas Dynamics Laboratory
Northwestern University
Evanston, Illinois

TECHNICAL DOCUMENTARY REPORT NO. AEDC-TDR-64-233

November 1964

Program Element 61405014/8951

(Prepared under Contract No. AF(600)-972 by
Northwestern University, Evanston, Illinois.)

ARNOLD ENGINEERING DEVELOPMENT CENTER
AIR FORCE SYSTEMS COMMAND
UNITED STATES AIR FORCE

NOTICES

Qualified requesters may obtain copies of this report from DDC, Cameron Station, Alexandria, Va. Orders will be expedited if placed through the librarian or other staff member designated to request and receive documents from DDC.

When Government drawings, specifications or other data are used for any purpose other than in connection with a definitely related Government procurement operation, the United States Government thereby incurs no responsibility nor any obligation whatsoever; and the fact that the Government may have formulated, furnished, or in any way supplied the said drawings, specifications, or other data, is not to be regarded by implication or otherwise as in any manner licensing the holder or any other person or corporation, or conveying any rights or permission to manufacture, use, or sell any patented invention that may in any way be related thereto.

AN EXPERIMENTAL STUDY OF RADIANT ENERGY TRANSFER FROM A PLASMA

By

James M. Berry* and Richard S. Tankin†

Gas Dynamics Laboratory

Northwestern University

Evanston, Illinois

(The reproducibles used in the reproduction of this report were supplied by the authors.)

November 1964

*Research Assistant

†Assistant Professor

AF - AEDC
Arnold AFS Tenn

ABSTRACT

A thermistor bolometer has been used to determine the radiant energy transfer from a typical laboratory plasma. Radiation has been found to be a significant mechanism of energy transfer from an atmospheric argon plasma jet, amounting to as much as 18 percent of the net power input to the plasma. The radiant energy transfer from an atmospheric nitrogen plasma jet under comparable conditions has been found to be less than 1 percent of the net power input to the plasma. The radiative power density in an atmospheric argon plasma has been determined. Contributions from both bremsstrahlung and recombination radiation have been found to be important. A model, based on the Kramers and the Unsöld approximations, has been used to predict the radiative power density in an atmospheric argon plasma.

PUBLICATION REVIEW

This report has been reviewed and publication is approved.

Terry L. Hershey
Capt, USAF
Aerospace Sciences Division
DCS/Research

Donald R. Eastman, Jr.
DCS/Research

CONTENTS

ILLUSTRATIONS

CHAPTER 1

INTRODUCTION

1.1 IMPORTANCE OF RADIATIVE PROCESSES IN GAS DYNAMICS

Work in the field of gas dynamics has frequently ignored radiative processes. The justification for this approximation is that most gas dynamics problems are concerned with relatively cool gases in which radiative processes are insignificant. In the realm of high temperature gas dynamics, however, radiation must be considered as a potentially significant mechanism of energy transport.

With the growing interest in flow problems involving plasmas, plasma generating facilities are becoming familiar items of laboratory equipment. The plasma torch is a common method of generating plasmas in the laboratory. The subject of this report is the measurement of the radiative energy transfer from plasmas generated in a typical laboratory plasma torch.

1.2 CLASSICAL APPROACH TO RADIATIVE HEAT TRANSFER

The basic relationship in problems involving radiative heat transfer is the Stefan-Boltzmann law, which relates the emissive power of an ideally black surface to its temperature

$$W_B = \sigma T^4 \tag{1-1}$$

where W_B is the emissive power of an ideally black surface (Btu/hr ft^2)

σ is the Stefan-Boltzmann constant, 0.1713×10^{-8} Btu/hr ft^2 $^oR^4$

T is the absolute temperature of the surface (^oR)

The spectral distribution of black-body radiation is given by Planck's law

$$W_{B\lambda} = \frac{2\pi hc^2}{\lambda^5 (e^{ch/k\lambda T} - 1)} \tag{1-2}$$

where $W_{B\lambda}$ is the monochromatic emissive power of a black surface at wavelength λ (ergs/sec cm^3)

h is Planck's constant, 6.63×10^{-27} erg sec

c is the velocity of light, 3.0×10^{10} cm/sec

λ is the wavelength of radiation (cm)

k is Boltzmann's constant, 1.38×10^{-16} erg/°K

T is the absolute temperature of the surface (°K)

The emissive power of a real surface is always less than the emissive power of a black surface at the same temperature. The classical approach to the problem of radiative heat transfer between solid surfaces uses the definition of the emissivity of a real surface

$$\epsilon = \frac{W}{W_B} \tag{1-3}$$

where ϵ is the emissivity of the real surface

W is the emissive power of the real surface (Btu/hr ft^2)

W_B is the emissive power of a black surface at the same temperature (Btu/hr ft^2)

In general, the emissivity of a real surface is a function of wavelength

and temperature. If the radiation emitted by a particular surface has the same spectral distribution as the radiation from a black surface at the same temperature, the emissivity of that surface is independent of wavelength. A surface having this property is referred to as a gray body. For most engineering purposes, radiators are considered as gray bodies. In this case, the emissive power of a real surface is expressed as

$$W = \epsilon \sigma T^4 \tag{1-4}$$

where W is the emissive power of the real surface (Btu/hr ft^2)

ϵ is the emissivity of the surface

σ is the Stefan-Boltzmann constant, 0.1713 x 10^{-8} Btu/hr ft^2 $^oR^4$

T is the absolute temperature of the surface (^oR)

Whereas the proportionality between the emissive power of a black surface and the fourth power of its absolute temperature can be derived from thermodynamic considerations, Eq. 1-4 is an empirical relationship.

The spectrum of radiation emitted from a plasma does not resemble black-body radiation. Since a plasma is nearly transparent, the radiation is emitted throughout the volume of the plasma. Very strong temperature gradients exist in a plasma jet. For these reasons, the classical approach to radiative heat transfer embodied in Eq. 1-4 is an inappropriate and inconvenient method to describe the radiation emitted from a plasma jet.

1.3 MACROSCOPIC DESCRIPTION OF RADIATION EMITTED FROM A PLASMA JET

The radiation emitted from a transparent plasma is a unique function

of the thermodynamic state of the plasma provided the plasma is in local thermodynamic equilibrium. In order to calculate the radiant energy emitted from a transparent plasma of any given geometrical configuration, the thermodynamic state of the plasma at every point and the radiation emitted per unit volume of the plasma as a function of the thermodynamic state of the plasma must be known.

In determining the radiation emitted from a plasma jet generated with a plasma torch, this approach meets with a serious practical difficulty. For a plasma jet issuing into atmospheric pressure, a knowledge of the thermodynamic state of the plasma is provided by a knowledge of the temperature at every point in the plasma jet. The determination of the temperature at every point in the plasma jet is a difficult task. It is desirable to find some more easily determined property of the plasma jet to use as an independent variable when measuring the radiation emitted from the plasma jet.

The net power input to the plasma is used in this report as the independent variable with which the macroscopic radiation measurements are correlated. The use of the net power input in this context requires the implicit assumption that the temperature distribution in the plasma jet at a given flow rate is a unique function of the net power input. The validity of this assumption for the plasma jets studied in this investigation has been verified indirectly.

1.4 MICROSCOPIC DESCRIPTION OF RADIATION EMITTED FROM A PLASMA

As discussed in Section 1.3, the radiation emitted per unit volume from a plasma in local thermodynamic equilibrium is a unique function

of the thermodynamic state of the plasma. This relationship has been determined experimentally for an argon plasma at atmospheric pressure. These results are only applicable to transparent argon plasmas at atmospheric pressure which are in local thermodynamic equilibrium, but are not otherwise restricted.

1.5 EXPERIMENTAL INVESTIGATIONS

The intensity of radiation emitted from a plasma jet generated in a plasma torch and exhausted to atmospheric pressure has been measured with a thermistor bolometer. The results presented in Chapter 3 are based on the macroscopic description of the plasma jet using the net power input as the independent variable. The results include determinations of the total radiation from an argon plasma jet, the total radiation from a nitrogen plasma jet, and the total radiation from an argon plasma jet seeded with carbon particles. Pointwise radiation measurements were used to determine the distribution of the radiative flux along the axis of the argon plasma jet. The angular distribution of the radiation from the argon plasma jet and the plasma torch was measured and was used to calculate the actual radiative heat transfer from the plasma jet and torch. Measurements of the temperature and radiation distributions leading to a determination of the intensity of radiation emitted per unit volume from an atmospheric argon plasma as a function of temperature are discussed in Chapter 5.

CHAPTER 2

EXPERIMENTAL APPARATUS AND PROCEDURE

Detailed descriptions of the plasma generating facility and the experimental procedure are given in Appendix A.

2.1 PLASMA TORCH

The plasmas studied in these experiments were generated in a Model F-40 plasma torch manufactured by Thermal Dynamics Corporation. In the plasma torch the gas is heated as it flows through a direct current arc between two electrodes, thereby generating the plasma. The gas enters the arc chamber through a straight-flow ceramic disc. The replaceable copper anode acts as the exit nozzle for the plasma. The replaceable tungsten cathode is located upstream from the anode. The arc is formed in the annular region between the nozzle (anode) and the electrode (cathode). A #57 x 15 nozzle and a #4-A electrode were used to generate an argon plasma; a #57 x 22 nozzle and a #3-M electrode were used to generate a nitrogen plasma. Both the electrode and nozzle are water cooled.

2.2 BOLOMETER

A Model 1312 thermistor bolometer manufactured by Servo Corporation of America was used to detect the radiation from the plasma. The bolometer sensing element is a small flake of semiconductor material, 0.5 mm square, which has a large negative temperature coefficient of resistance. The flake is blackened so that it absorbs about 80 per cent

of the radiation incident upon it (Ref. 1).

The bolometer sensing element is mounted in a sealed cylindrical case 5/8 in. long by 5/8 in. in diameter as shown in Figure 2-1. Radiation is transmitted to the bolometer sensing element through a sodium chloride window which transmits radiation in the frequency range from 0.175×10^{14} sec^{-1} to 11.2×10^{14} sec^{-1} (Ref. 2). A second element, shielded from radiation but otherwise identical to the bolometer sensing element, is also mounted in the cylindrical case. This element is used to compensate for variations in the ambient temperature.

Both bolometer elements are part of the bridge circuit shown in Figure 2-2. A Ballantine Model 801 a.c. voltmeter is used to measure the output signal of the bridge amplifier. The radiation incident on the bolometer is chopped at 30 c.p.s. to provide an a.c. signal to the amplifier. The chopping is accomplished with a 6 in. disc having 30 equally spaced 1/4 in. holes which is rotated at 1 r.p.s. by a synchronous motor. The chopper assembly is mounted on top of the box containing the bolometer, bridge, and amplifier. The power supplies are external.

2.3 EXPERIMENTAL ARRANGEMENT

A photograph of the basic arrangement of the experimental apparatus is shown in Figure 2-3. The bolometer unit is mounted on a laboratory jack which permits adjustment of its height. The laboratory jack is mounted on a table which can be moved in two horizontal directions with lead screws. This table rests on rails which run the length of the

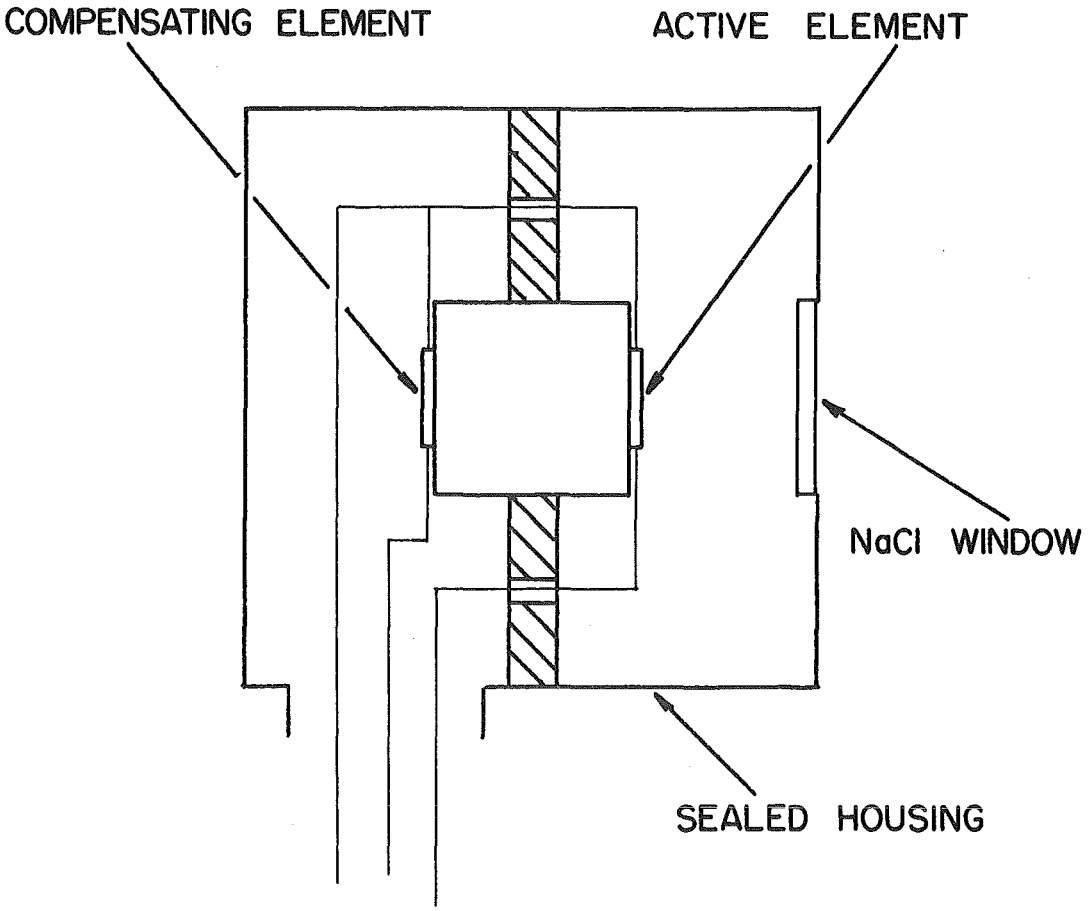

Fig. 2-1 Bolometer

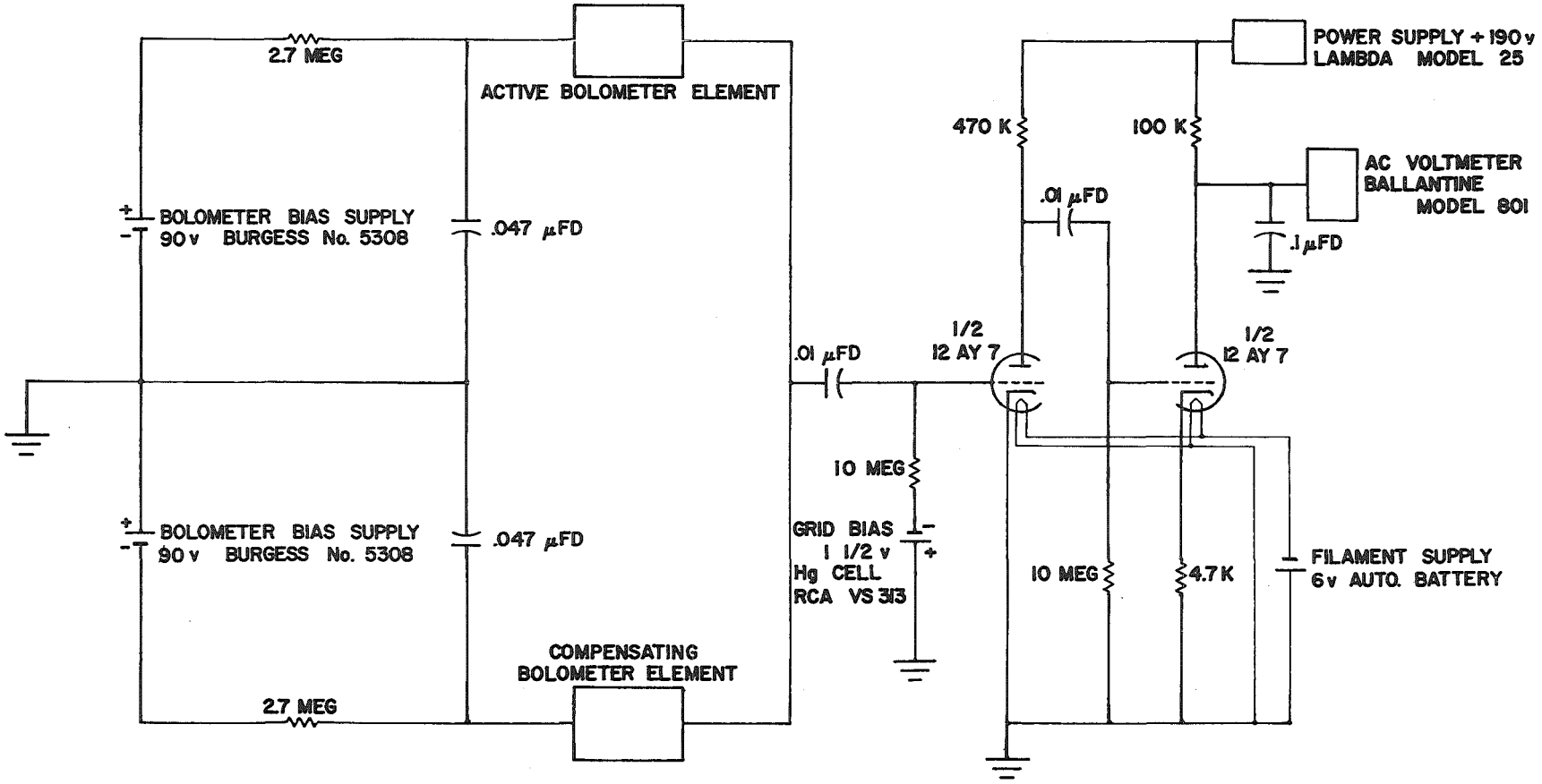

Fig. 2-2 Bolometer Bridge and Preamplifier

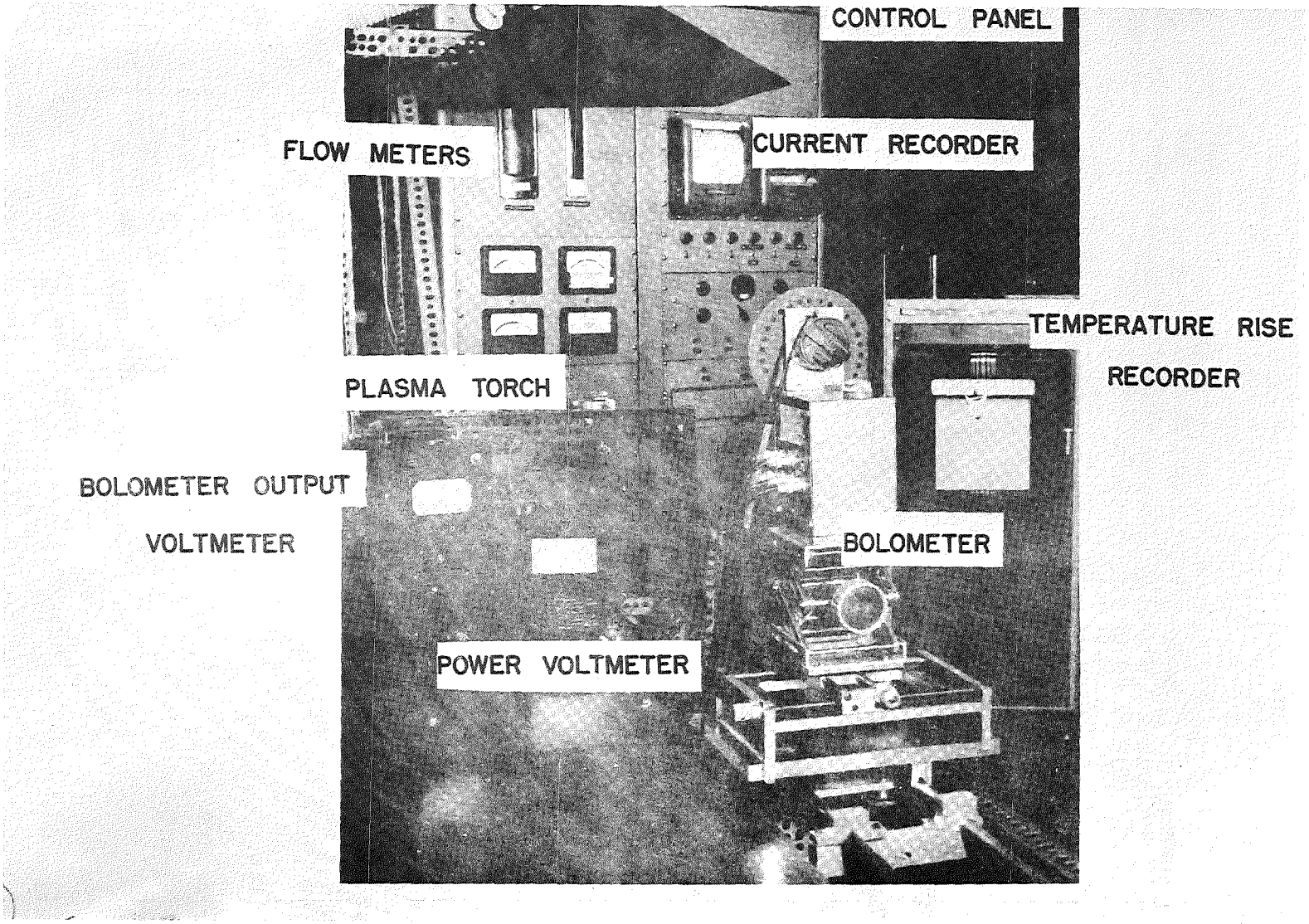

Fig. 2-3 Photograph of Experimental Apparatus

bench. With the unit clamped to the rails at some nominal location, the bolometer sensing element can be moved about nine inches in any direction in space. The position of the sensing element is determined by indicating dials on the lead screws and by a vertical scale attached to the laboratory jack.

The plasma torch is operated from a control panel. The current to the plasma torch and the temperature rise of the cooling water were recorded continuously. Instruments indicating the temperature, pressure, and flow rate of the gas and the flow rate of the cooling water are housed in the control panel. The voltmeter indicating the voltage drop across the plasma torch and the voltmeter indicating the bolometer output are located on the bench.

2.4 EXPERIMENTAL PROCEDURE

The output signal of the bolometer is proportional to the radiative flux incident on the bolometer element, as determined by calibrating the instrument. With appropriate mathematical models and physical arrangements of the apparatus, the bolometer was used to measure the total radiation from the plasma jet, the actual radiative heat transfer from the plasma jet and the plasma torch, the distribution of the radiative flux along the axis of the plasma jet, and the internal radiative power density in the plasma jet. Since the net power input to the plasma jet is used as the independent variable with which to represent the macroscopic radiation measurements and as the parameter of torch operation with the microscopic radiation measurements, the plasma torch

is instrumented to provide knowledge of the instantaneous net power input to the plasma. During the experimental runs the bolometer output signal and the voltage drop across the plasma torch were recorded simultaneously, noting the time of each reading on a stopwatch synchronized with the current and the cooling water temperature recorders.

Descriptions of the physical arrangements of the bolometer and plasma torch are given in the sections of the report describing the experiments.

CHAPTER 3

EXPERIMENTAL DETERMINATION OF RADIANT ENERGY TRANSFER FROM A LABORATORY PLASMA

When measuring the radiant energy transfer from a plasma generated in a plasma torch, that portion of the plasma emitting the radiation being measured must be defined. The luminous tongue of gas which protrudes from the exit nozzle of the plasma torch is referred to as the plasma jet. The model used to determine the total radiation from the plasma jet is described in Section 3.1. The method of making the pointwise radiation measurements along the axis of the plasma jet is discussed in Section 3.5.

In addition to the radiation emitted from the plasma jet, radiation is emitted from the plasma contained within the exit nozzle of the plasma torch, which is referred to as the hot core of plasma within the exit nozzle. The measurements used to determine the amount of radiant energy which is actually transferred from the plasma torch during operation are described in Section 3.8. This radiant energy transfer is referred to as the actual radiative heat transfer from the plasma and plasma torch.

3.1 MODEL FOR TOTAL RADIATION FROM A PLASMA JET

The luminous portion of the plasma which protrudes from the plasma torch is referred to as the plasma jet. The plasma jets studied in these experiments were roughly conical in shape resembling flames. For a transparent plasma, the intensity of the radiation emitted from the plasma depends on the volume of plasma observed. If the plasma jet could be detached from the plasma torch and placed at the center of a sphere, the radiation emitted from the plasma jet would be distributed uniformly over the sphere. Measurements on combustion flames demonstrate this fact (Ref. 3).

In order to represent the radiation emitted from the plasma jet, the plasma jet is imagined to lie at the center of a sphere as shown in Figure 3-1. The radius of this sphere is taken as the distance from the axis of the plasma jet to the bolometer sensing element. The total radiation emitted from the plasma jet is defined as the radiation crossing the sphere, assuming that this radiation is distributed uniformly over the sphere. To calculate the total radiation from the plasma jet, the radiative flux at the bolometer element is multiplied by the area of the sphere surrounding the plasma jet.

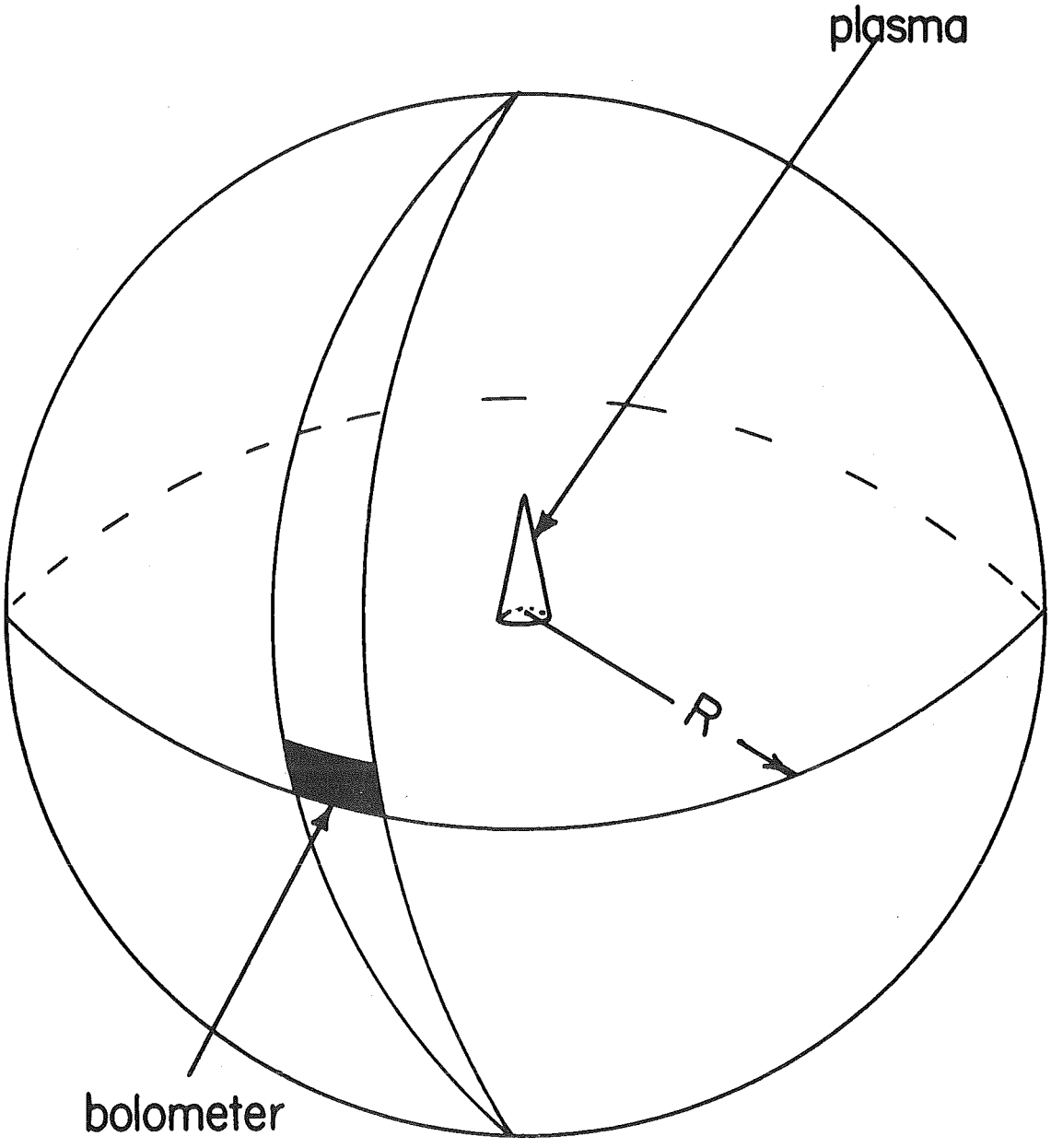

Fig. 3-1 Model Used to Calculate Total Radiation from Plasma

3.2 TOTAL RADIATION FROM AN ARGON PLASMA JET

All of the total radiation measurements were made with the bolometer and plasma torch positioned as shown in Figure 3-2. The bolometer was positioned so that a normal to the surface of the bolometer sensing element would intersect the axis of the plasma jet at a right angle at the base of the plasma jet. The distance from the bolometer sensing element to the axis of the plasma jet was 40 3/8 in. The bolometer was calibrated in this position as discussed in Appendix B. In all of the experiments the plasma jet was exhausted to the atmosphere.

Radiation readings were recorded over the maximum operating range of the plasma torch by varying the current to the plasma torch incrementally. The current was usually changed in 50 amp increments. A minimum of one minute was allowed after each change in the current to permit the plasma torch and all instruments to reach a state of steady operation. The net power input to the plasma was calculated for each radiation reading. The total radiation from the plasma jet was calculated as discussed in Section 3.1. Sample calculations are given in Appendix C.

The results of the measurements of the total radiation from an argon plasma jet are indicated in Figure 3-3 by the open circles. The total radiation from the plasma jet calculated for each radiation reading is expressed as a percentage of the net power input to the plasma at that radiation reading. The experimental curve has been drawn by hand as the best apparent representation of the data.

The effect of the flow rate of argon on the total radiation from

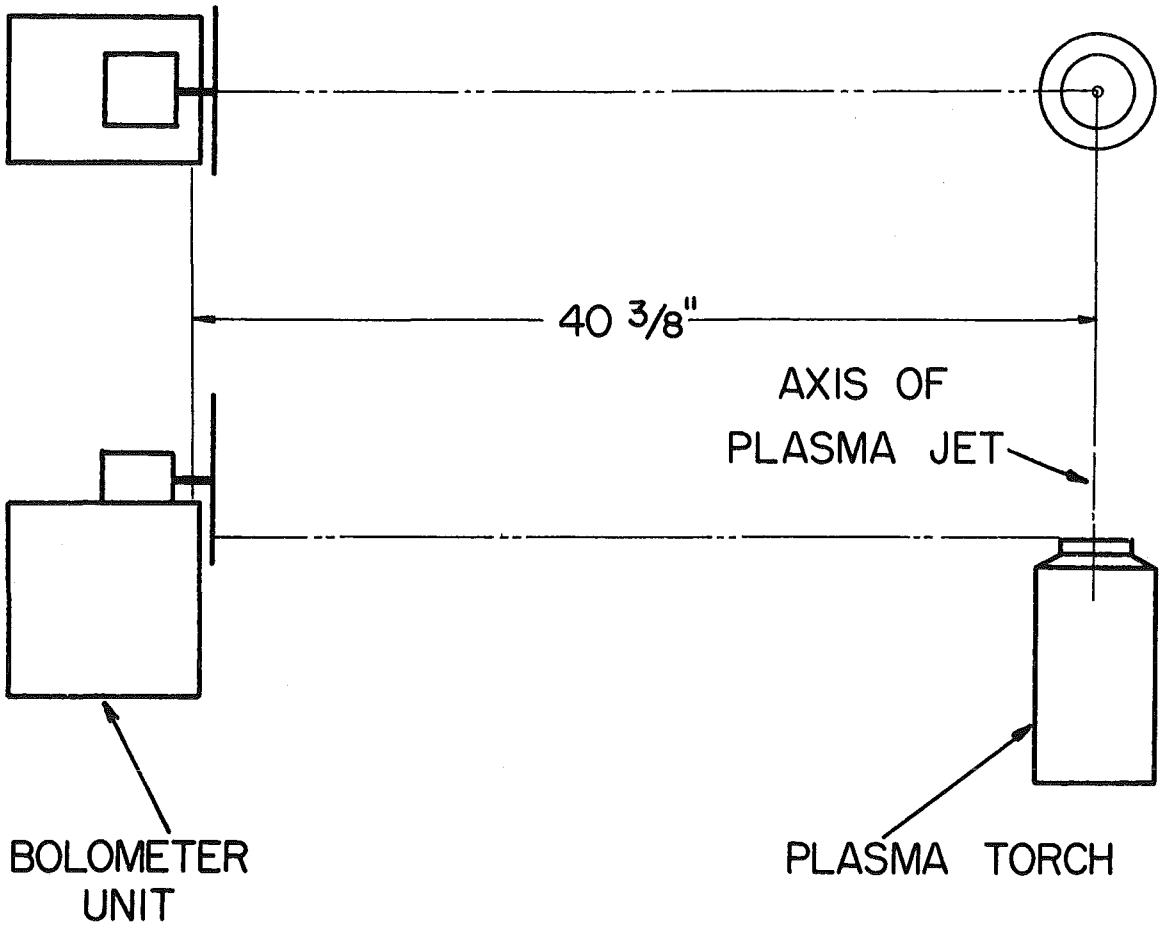

Fig. 3-2 Arrangement for Total Radiation Measurements

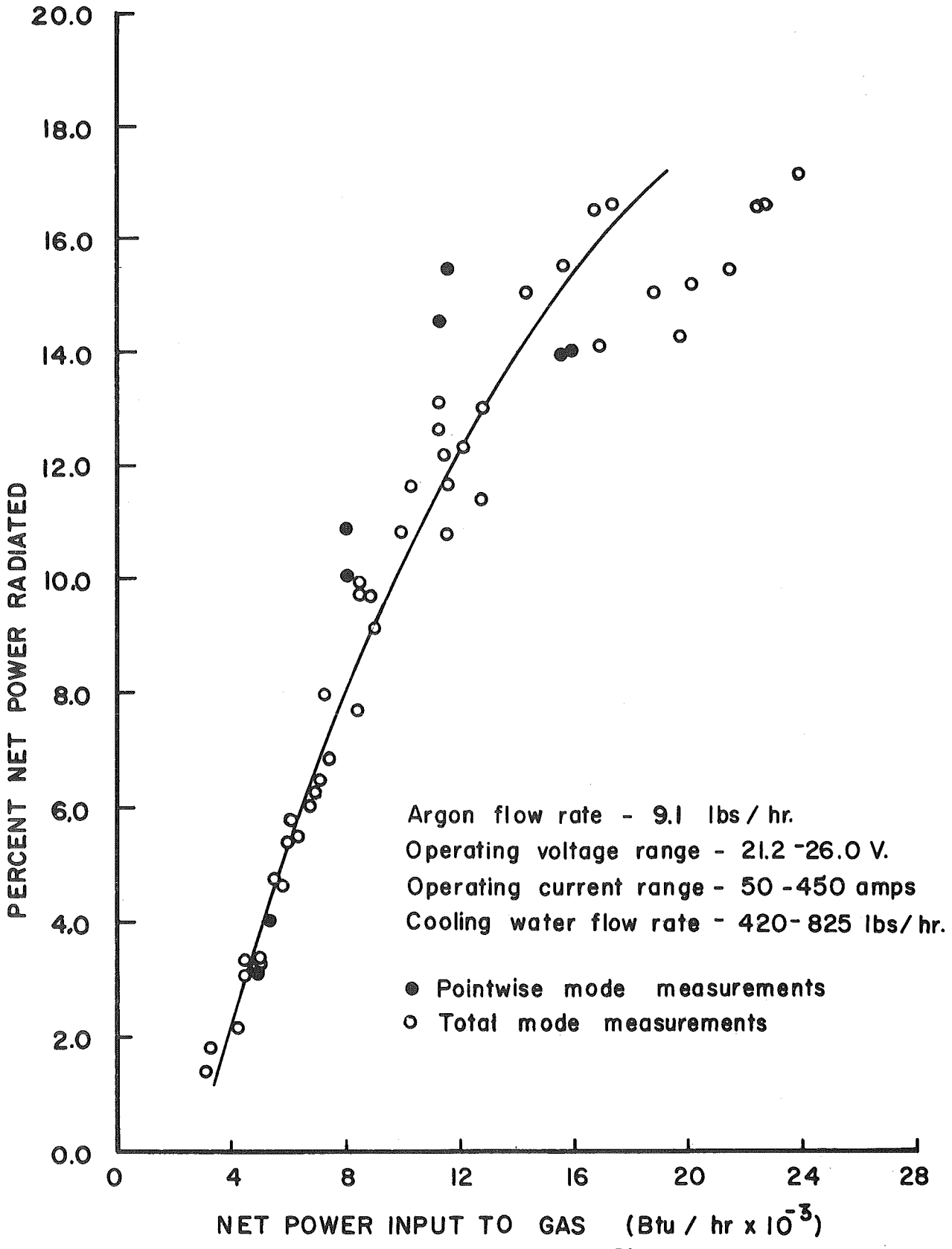

Fig. 3-3 Total Radiation from an Argon Plasma

an argon plasma jet is shown in Figure 3-4. The curves are similar in shape and the data is reproducible. It was observed that for an argon flow rate of 2.44 lbs/hr the plasma jet was quiet at all power levels and this was interpreted to be laminar flow. Also it was noted that these quiet, laminar jets were much longer than the turbulent jets (higher argon flow rates); indicating that turbulent mixing between the plasma and the surrounding air has a quenching effect. At intermediate and low power inputs for the flow rate 3.97 lbs/hr the jet was laminar; for high power inputs the jet was turbulent. Only for the lowest power inputs was the jet laminar for an argon flow rate of 5.51 lbs/hr. For all other power inputs and flow rates shown in Figure 3-4 the jet was turbulent.

A parameter used by experimentalists to describe the state of the plasma jet is the average enthalpy input per pound of gas. This quantity is defined as the net power input divided by the gas flow rate, and is represented by the 45° line shown in Figure 3-4a. This line is labeled "radiation loss neglected". To take into account the radiation loss, the following expression was used to calculate the enthalpy rise:

Net Energy Input - Radiant Energy Loss = Enthalpy Rise. All the data points shown in Figure 3-4 were used to calculate the enthalpy rise and the results are seen in Figure 3-4a. There appear to be two distinct sets of data points - one for the laminar plasma jet and the other for the turbulent plasma jet.

In defining the enthalpy rise many quantities have been neglected; such as, kinetic energy of the gases, viscous dissipation, heat conduction

etc. It is believed that the neglect of viscous dissipation may account for laminar curve being above the turbulent curve. Viscous dissipation is higher for turbulent flows than for corresponding laminar flows. However it is not claimed, but only weakly suggested that viscous dissipation may account for most of the spread between the laminar and turbulent curves in Figure 3-4a.

3.3 TOTAL RADIATION FROM A NITROGEN PLASMA JET

Measurements of the total radiation from a nitrogen plasma jet were made in the same manner as the measurements of the total radiation from an argon plasma jet.

The operation of the plasma torch with nitrogen was much more difficult than with argon. While generating a nitrogen plasma the current recorder trace was unsteady, making it possible to read the value of the current only to within $\pm$ 30 amps. Due to the high power level necessary to generate a nitrogen plasma, the nozzle inserts and "O"-ring water seals were short-lived. The nitrogen plasma jet was much different in appearance than the argon plasma jet, being two or three times longer and ragged in appearance. The nitrogen plasma jet was slightly yellow in color as opposed to the bluish-shite argon plasma jet and was not nearly as intense.

The results of the total radiation measurements from a nitrogen plasma jet are shown in Figure 3-5. A straight line has been used to

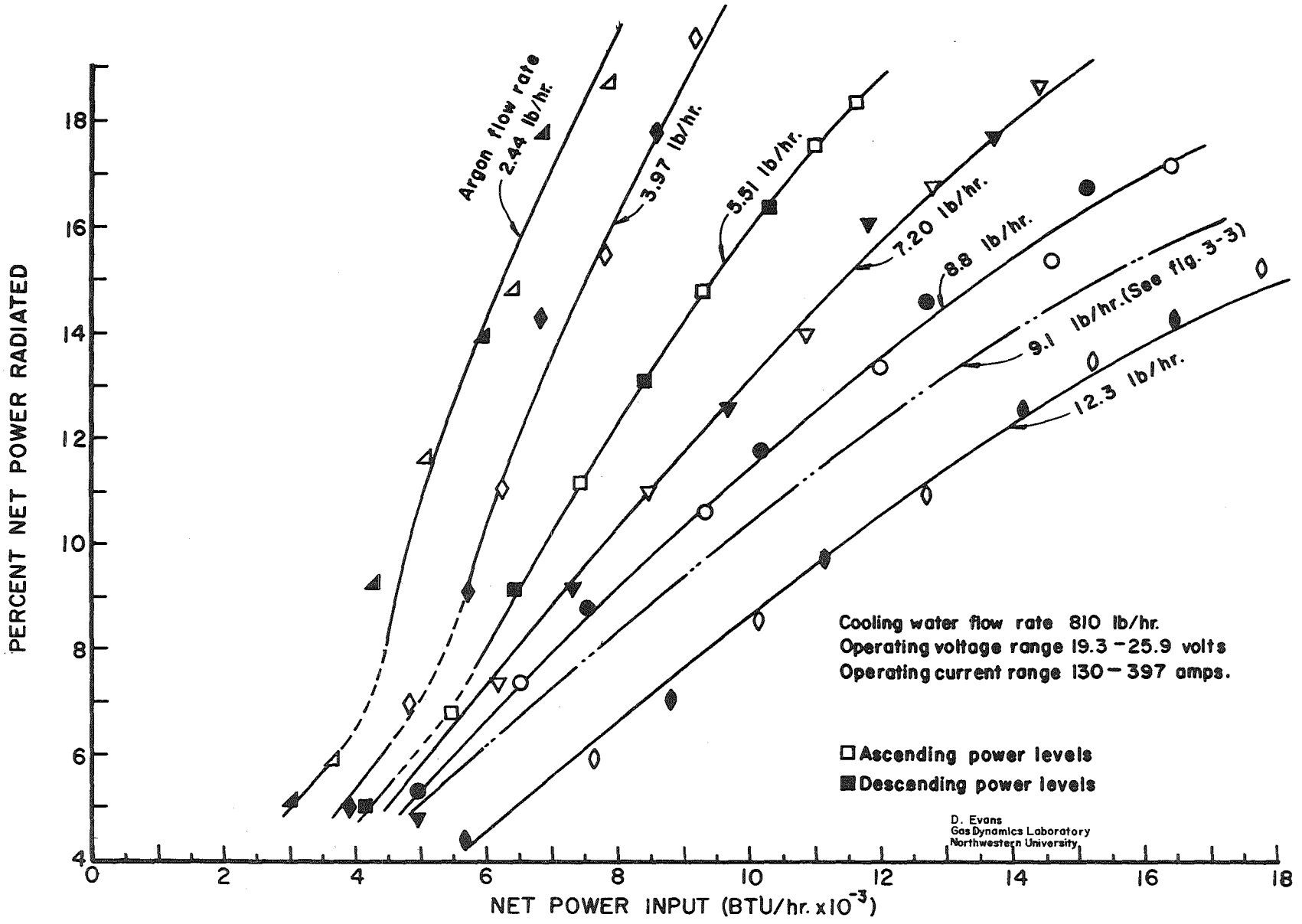

Fig. 3-4 Effect of Flow Rate on Total Radiation

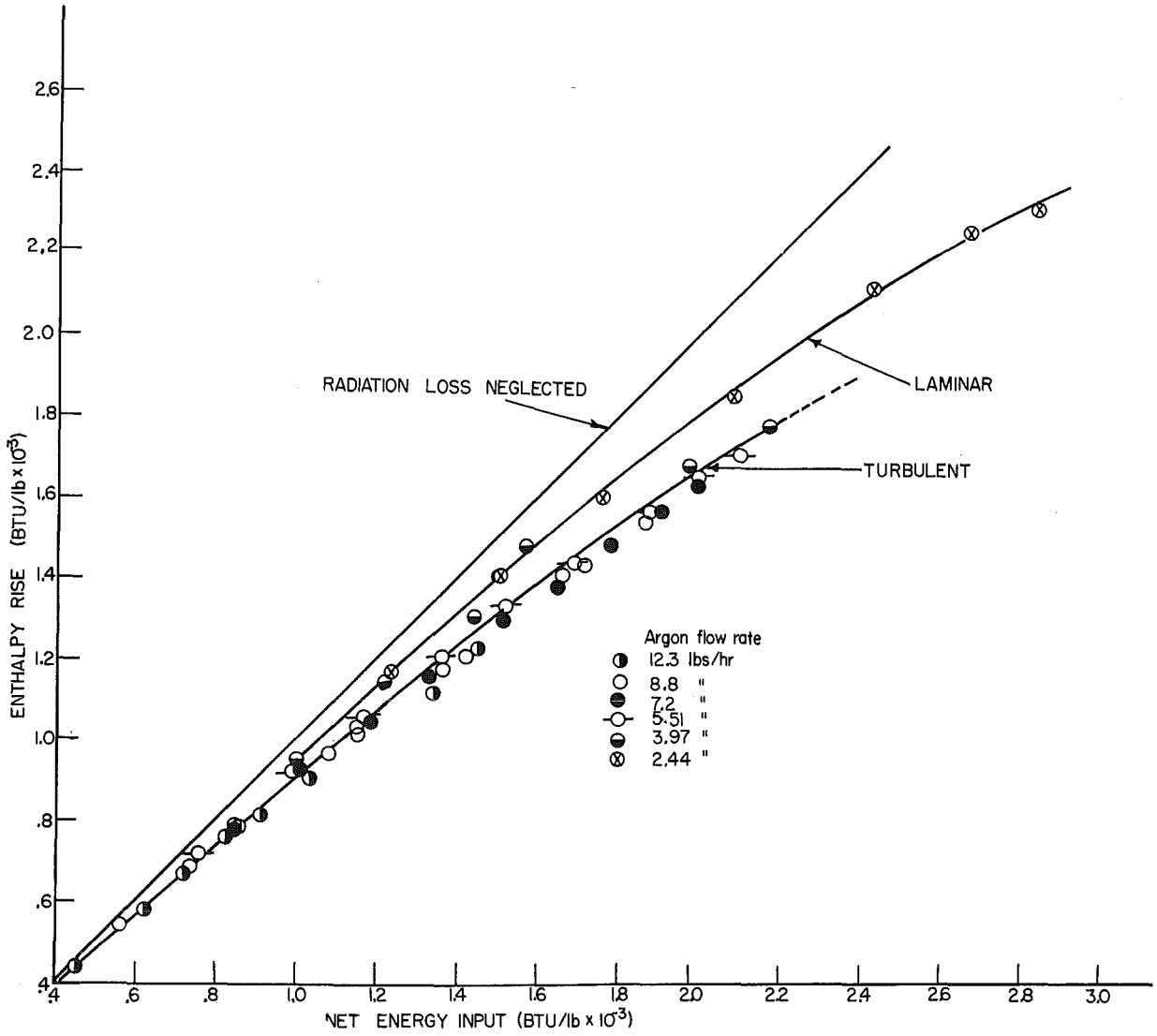

Fig. 3-4a Effect of Radiation on Enthalpy Rise

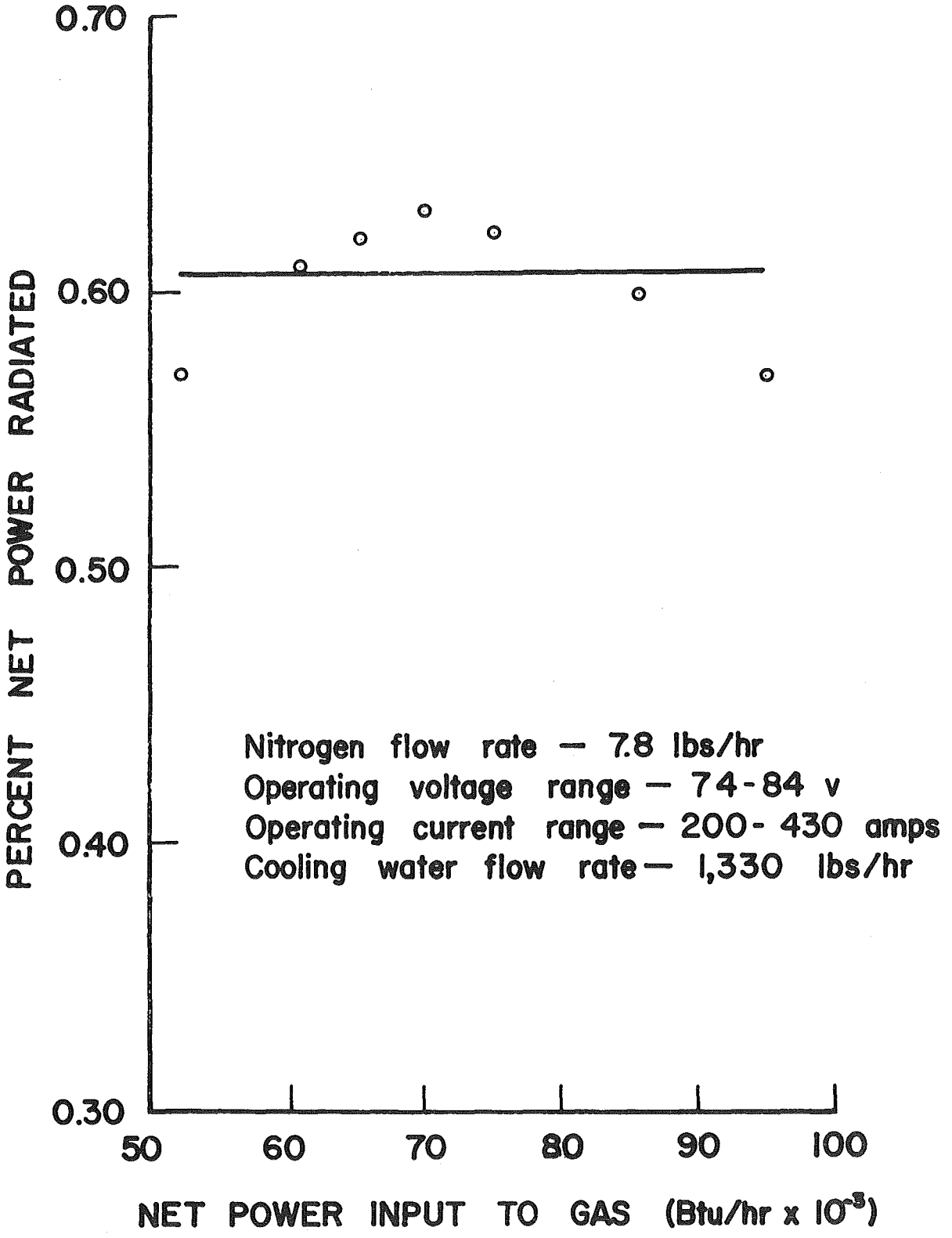

Fig. 3-5 Total Radiation from a Nitrogen Plasma

represent the data due to the expanded scale along the ordinate and the increased error in the power measurements.

3.4 TOTAL RADIATION FROM AN ARGON PLASMA JET SEEDED WITH CARBON PARTICLES

An argon plasma jet was seeded with finely divided carbon particles in an attempt to increase the optical thickness of the plasma jet. Carbon black manufactured by Cabot Corporation under the brand name Supercarbovar was used as the seeding material. The carbon particles used have a mean diameter of 1.4×10^{-8} m. (Ref. 4). A Sylco CCC Mark VII fine powder feeder manufactured by Sylvester and Company was used to feed the carbon to the plasma jet.

The total radiation from the seeded argon plasma jet was measured with carbon being fed to the plasma jet at four different mass flow rates. Total radiation measurements with no carbon being fed to the plasma jet were taken preceding each reading with carbon particles present in the jet. In this manner eight readings were taken at each of six different power levels. The measurements were made in the same manner as the total radiation measurements from the argon and nitrogen plasma jets.

The results of these measurements are shown in Figure 3-6. Fluctuations in the voltage across the plasma torch and a slight amount of electrical noise in the current recorder trace due to the seeder account for the fact that each group of data points is not at precisely the same net power input level. The plasma jet took on a slight yellow coloration

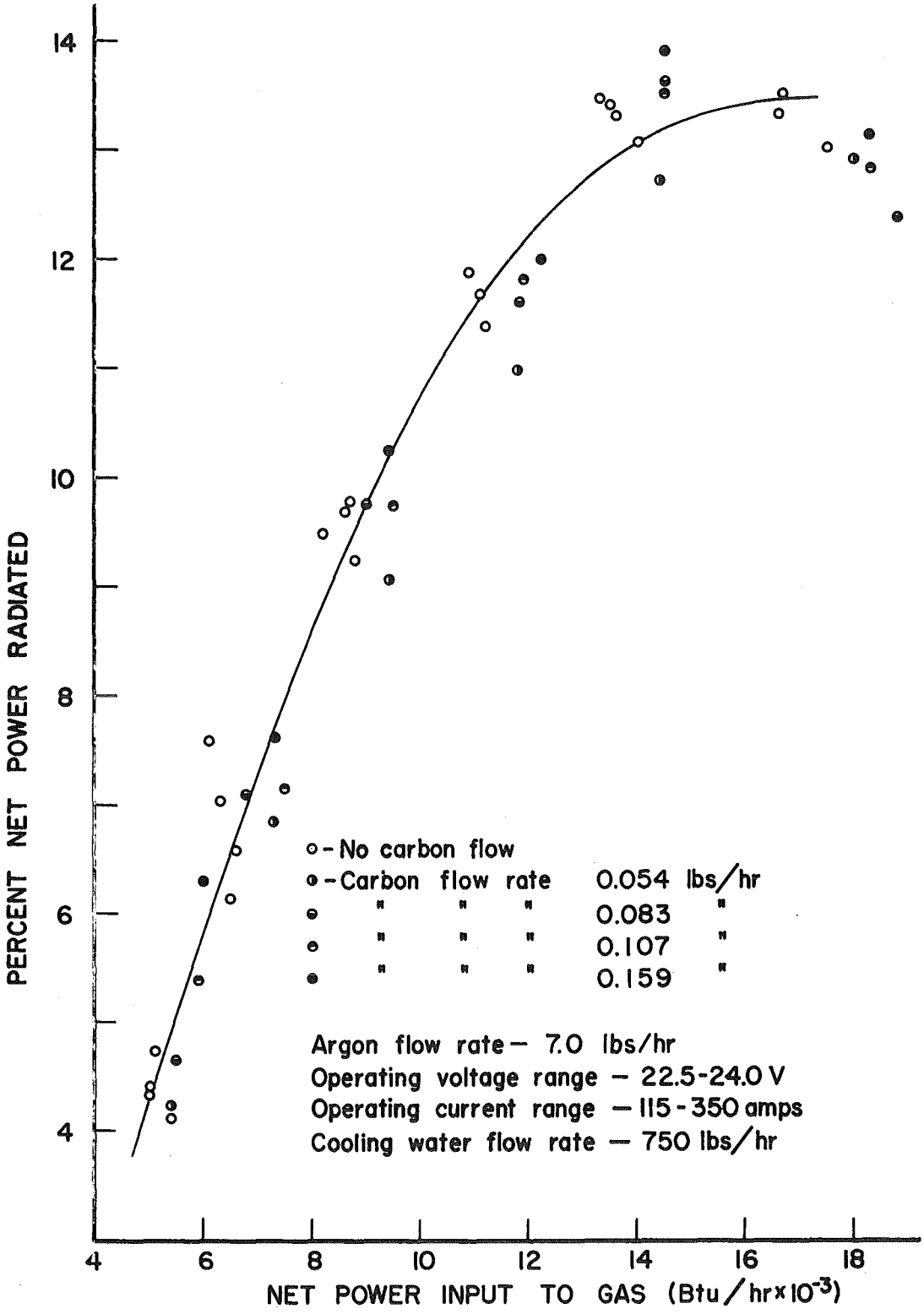

Fig. 3-6 Total Radiation from an Argon Plasma Seeded with Carbon Particles

with carbon particles present, an effect which was more pronounced at the higher carbon flow rates. Carbon was observed leaving the tip of the plasma jet as a fine black smoke, giving the jet an appearance similar to a sooty flame.

3.5 POINTWISE RADIATION MEASUREMENTS

Measurements of the radiative flux at the surface of the plasma jet were made by projecting an image of the plasma jet in the plane of the bolometer sensing element. These measurements are referred to as pointwise radiation measurements.

The optical system shown in Figure 3-7 was used to project an image of the plasma jet in the plane of the bolometer element. Two-fold magnification was used for convenience to provide a larger image with which to work and to increase the resolution of the bolometer. The mirror used is a 10 in. diameter front-surfaced paraboloid having a 45 in. focal length. The optical system was aligned using a transparent focusing grid and a light source as an object. The calibration of the bolometer for use with this optical system is discussed in Appendix B.

3.6 DISTRIBUTION OF RADIATIVE FLUX ALONG THE AXIS OF AN ARGON PLASMA JET

With the arrangement shown in Figure 3-7, the bolometer was moved horizontally across the image of the plasma jet until a maximum output signal was obtained. This position corresponds to the location of the axis of the plasma jet in its image. Maintaining the current to the plasma torch at a constant value, the image was traversed vertically

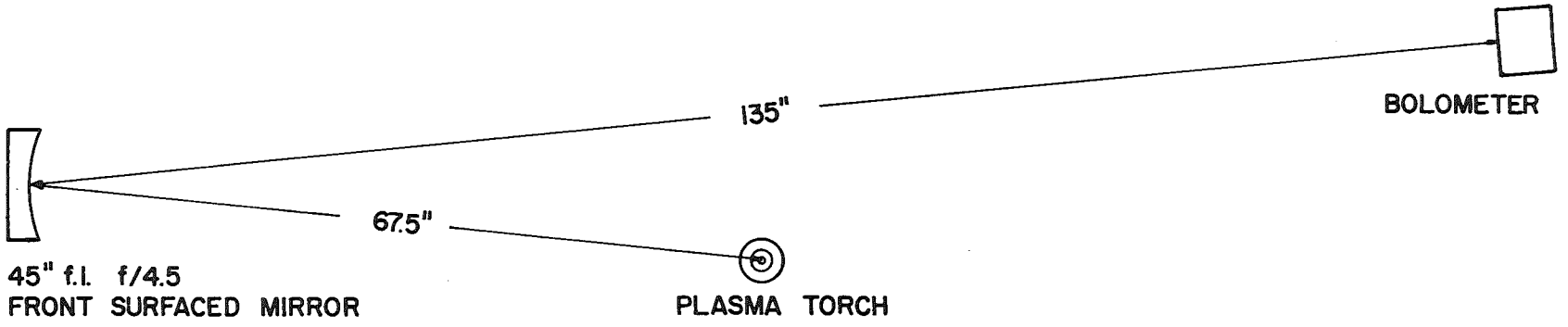

Fig. 3-7 Mirror Arrangement Pointwise Measurements 2:1 Magnification

along the axis. The bolometer output signal and the voltage drop across the plasma torch were recorded simultaneously at 1/8 in. increments. Ascending and descending traverses were taken at each of four power levels. The data from four of these eight traverses are shown in Figure 3-8. The net power input to the plasma was calculated for each radiation reading. These values were then averaged to compute the average net power for each traverse. The standard deviation from this average was also calculated, and was less than one per cent in all but one case. In Figure 3-8, the argon flow rate at the three higher power levels was 8.5 lbs/hr; the flow rate at the lowest power level was 9.5 lbs/hr. Figure 3-8a shows this data plotted logarithmically.

If the maximum output signal along the axis of the image of the plasma jet is taken as the base of the plasma jet, the distribution of the radiative flux along the axis of the plasma jet is represented closely by the expression

$$F = F_{max} \left(\frac{x}{L}\right)^{2.1}$$

where F is the radiative flux at any point x along the axis of the plasma jet (Btu/hr ft^2)

F_{max} is the maximum radiative flux, i.e., the radiative flux at the base of the plasma jet (Btu/hr ft^2)

x is the distance from the tip of the plasma jet to the observation point (in)

L is the length of the plasma jet from base to tip (in)

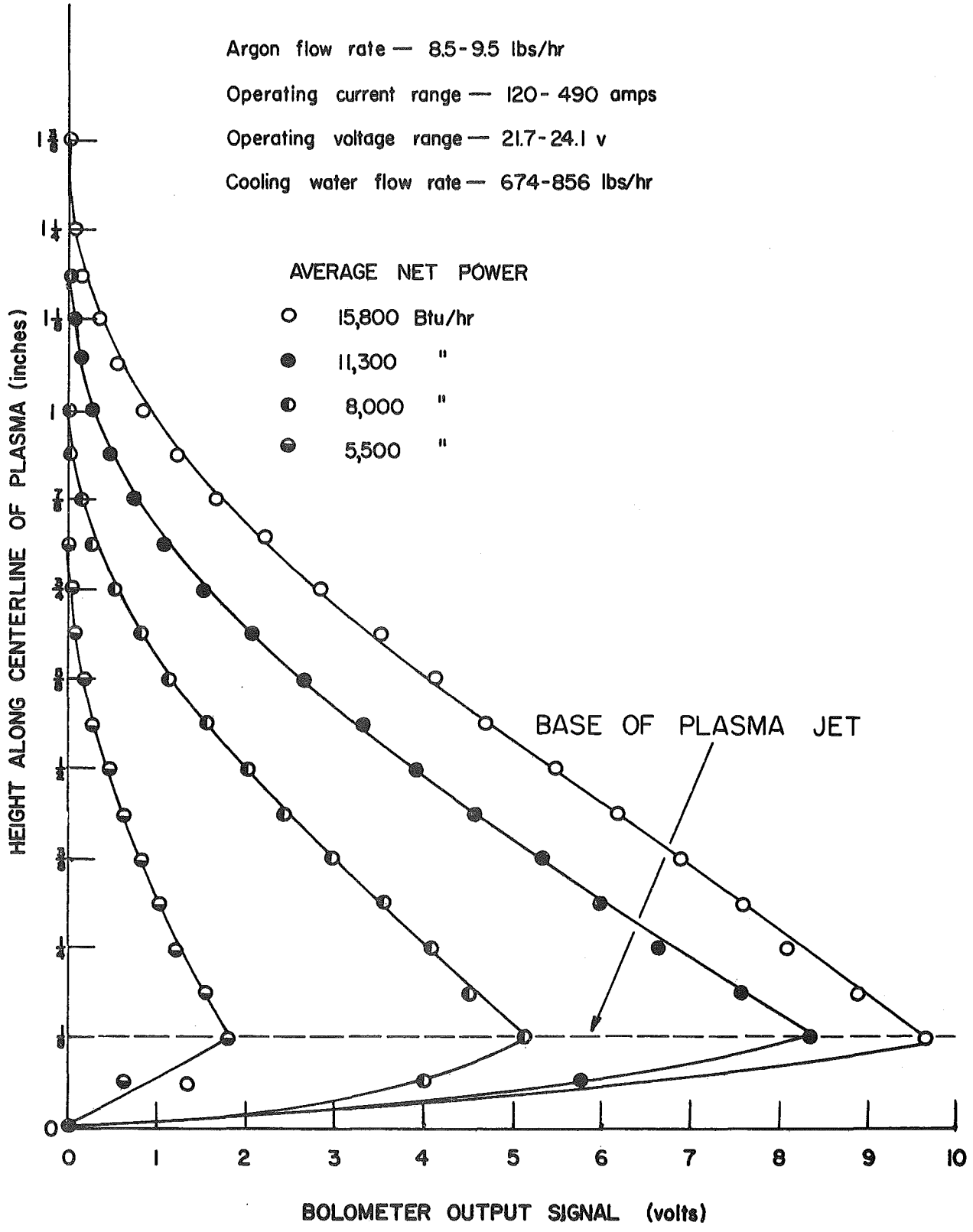

Fig. 3-8 Pointwise Radiation Measurements of Argon Plasma

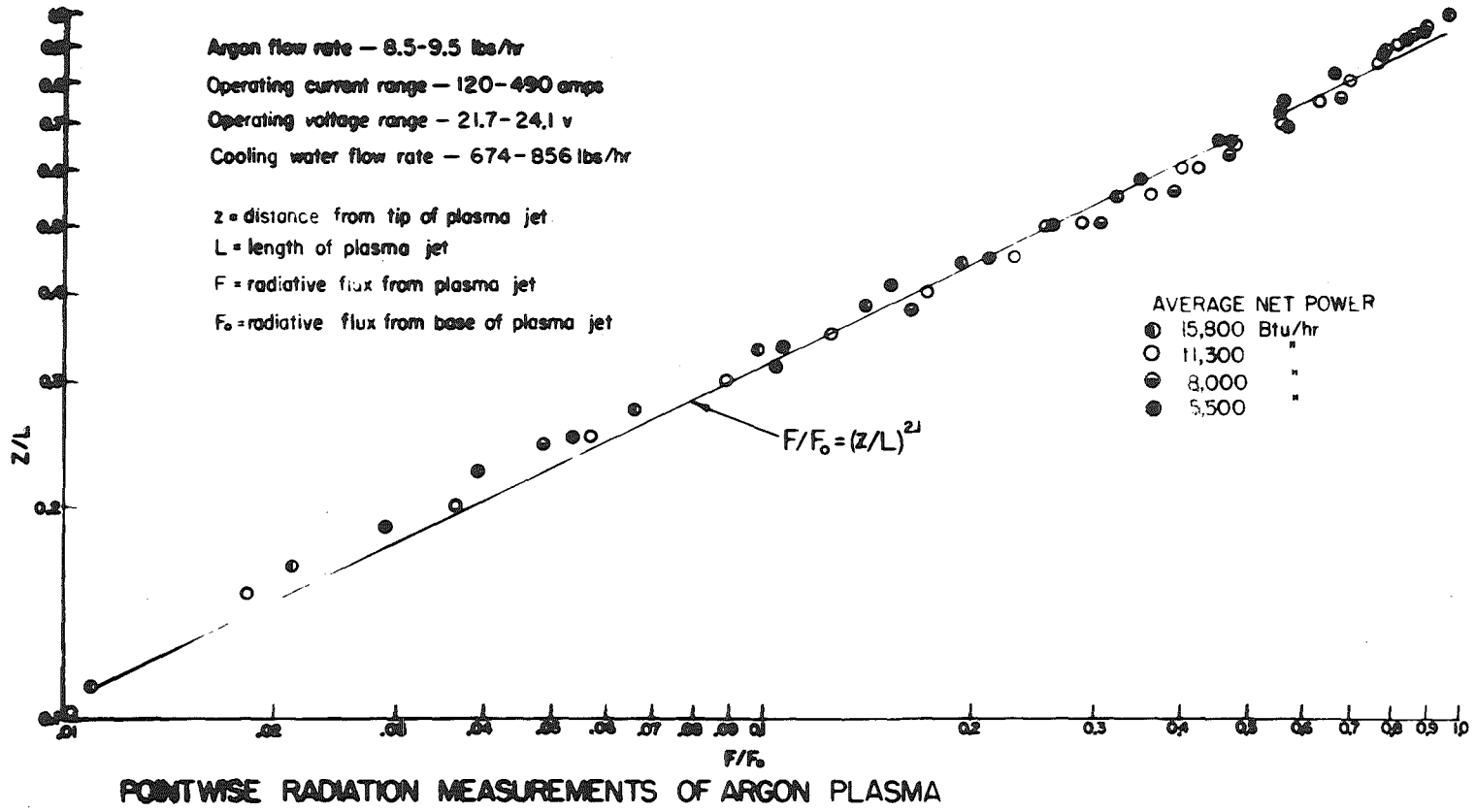

POINTWISE RADIATION MEASUREMENTS OF ARGON PLASMA

Fig. 3-8 Concluded

Both the length of the plasma jet and the maximum radiative flux at the base of the plasma jet depend on the net power input to the plasma and the flow rate of the gas. To convert the bolometer output signals given in Figure 3-8 to values of radiative flux at the surface of the plasma jet, the calibration value of 1.94×10^5 Btu/hr ft^2 volt can be used (see Appendix B).

3.7 CALCULATION OF TOTAL RADIATION USING POINTWISE RADIATION DATA

The total radiation from an argon plasma jet was calculated using the pointwise radiation data shown in Figure 3-8. The calculations are based on the model shown in Figure 3-9. The plasma jet is assumed to be conical in shape having a base with diameter equal to the diameter of the exit nozzle opening, 5/16 in., and having a height as determined from the pointwise radiation measurements. The cone is imagined to be sectioned into frustums of equal altitude, such that each pointwise radiation measurement lies at the vertical midpoint of its corresponding frustum. The total radiation from the argon plasma jet was calculated by multiplying the radiative flux at the vertical midpoint of each frustum by the area of that frustum, and summing the contributions from all frustums of the cone. Examples of these calculations are given in Appendix C. The results of these calculations are plotted on Figure 3-3 as the closed circles.

3.8 ANGULAR DISTRIBUTION OF RADIATION FROM PLASMA TORCH

The angular distribution of the radiation from the plasma torch was determined by mounting the plasma torch on a small rotary machinist's

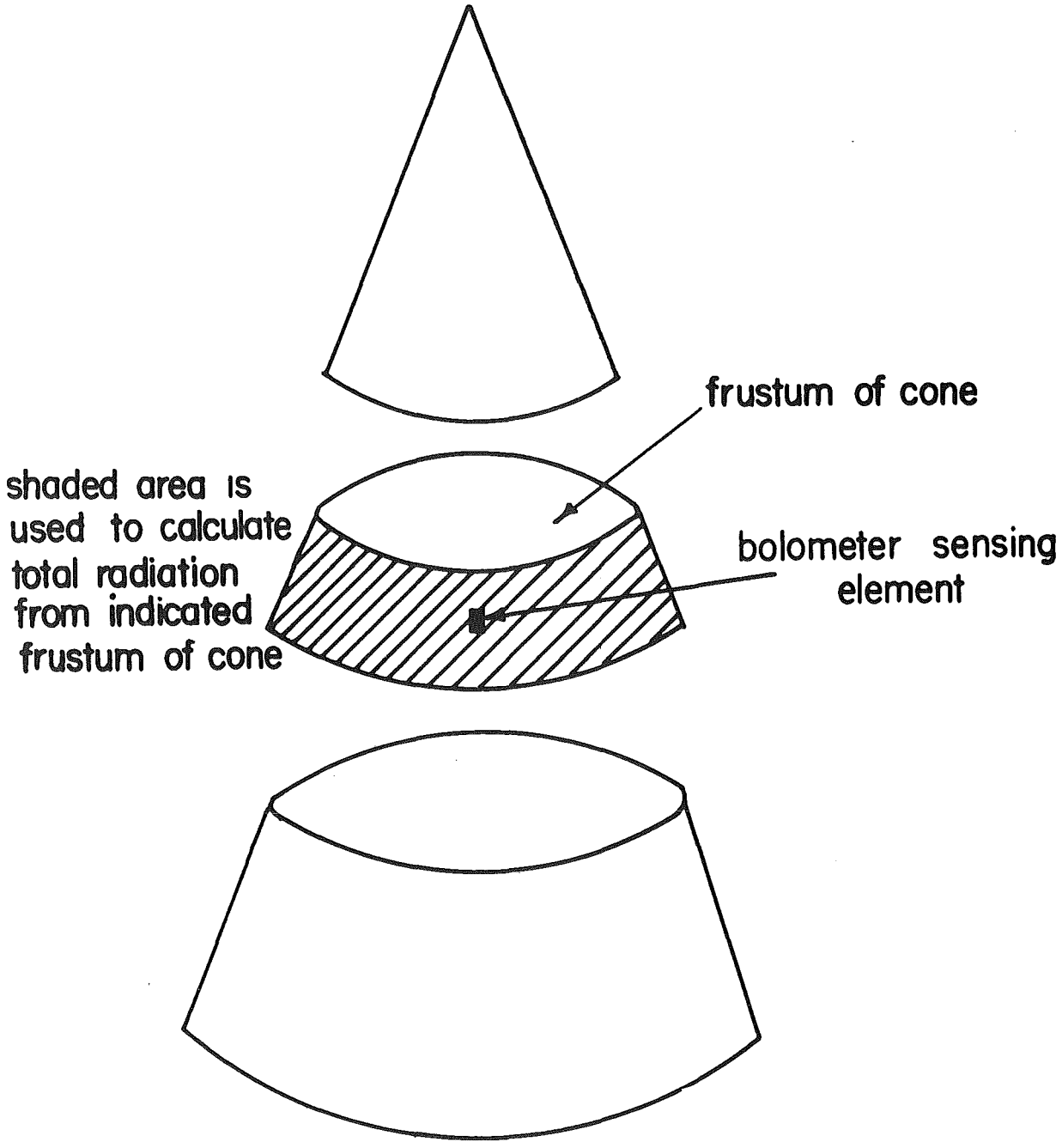

Fig. 3-9 Model used to Calculate Total Radiation from Plasma using Pointwise Data

table, as shown in Figure 3-10. The plasma torch was positioned on the table so that the center of rotation was on the axis of the plasma jet at its base. The bolometer sensing element was located 47 5/8 in. from the center of rotation in the plane of rotation.

The experiment was performed with the plasma torch generating an argon plasma. The angular distribution of the radiation from the plasma torch was determined by rotating the plasma torch in angular increments. Radiation readings were recorded at 5^{o} increments at the smaller viewing angles and at 10^{o} increments at the larger viewing angles. The voltage drop across the plasma torch was recorded simultaneously with each radiation reading. The readings were begun at a viewing angle of 0^{o}, with the bolometer sensing element lying on the extended axis of the plasma jet. The plasma torch was rotated until the bolometer output signal fell to the noise level in the shadow of the plasma torch. The air current from a household fan was directed transverse to the line from the bolometer sensing element to the center of rotation of the plasma torch to prevent convective heating at the bolometer.

The angular distribution of the radiation was determined at four power levels. The results of these measurements are shown in Figure 3-11. The net power input to the plasma was calculated at each radiation reading and these values were averaged over each run to compute the average net power.

3.9 ACTUAL RADIATIVE HEAT TRANSFER FROM AN ARGON PLASMA AND THE PLASMA TORCH

With the plasma torch operating at a given set of conditions, there

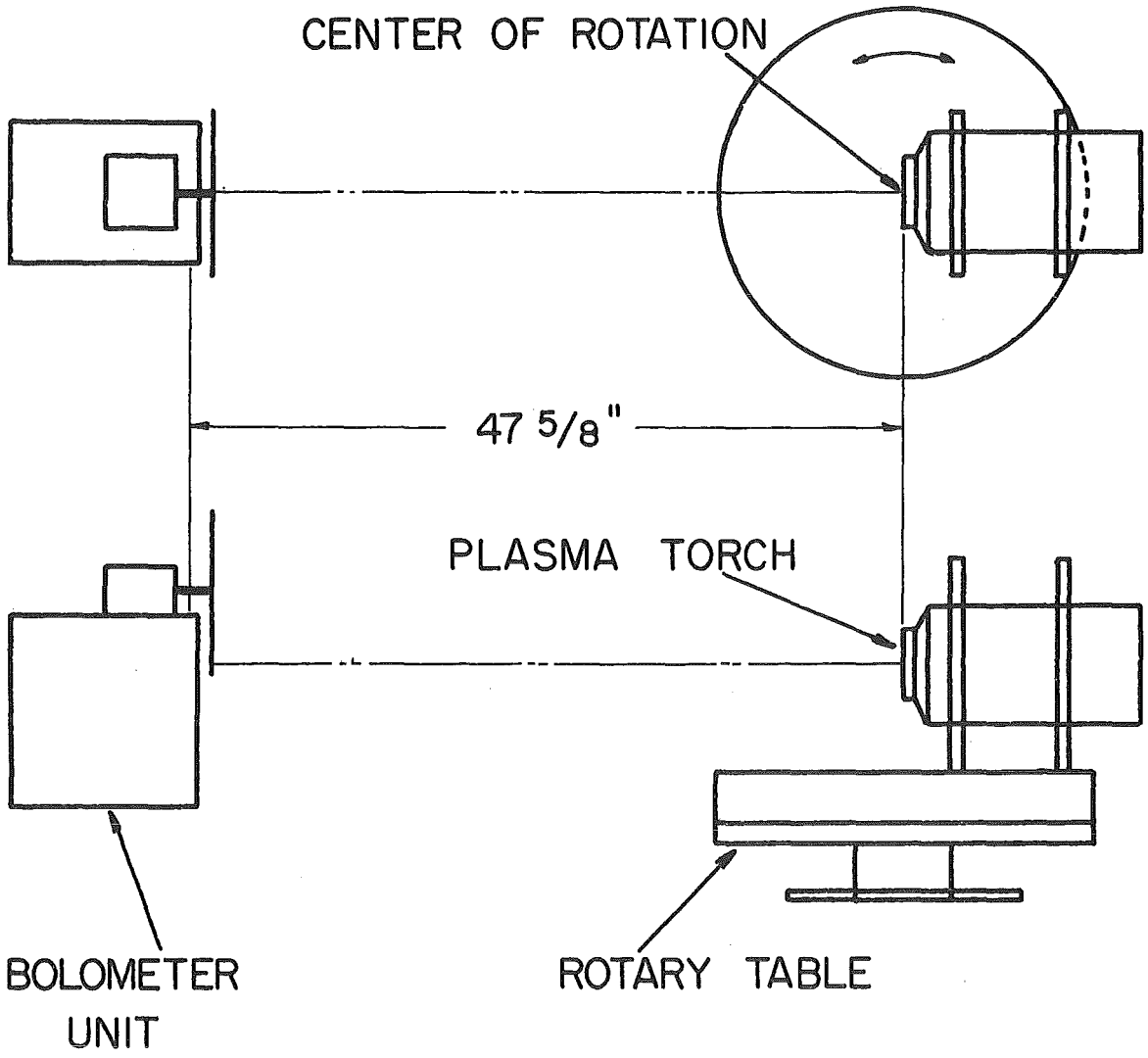

Fig. 3-10 Arrangement for Measurement of Angular Distribution of Radiation

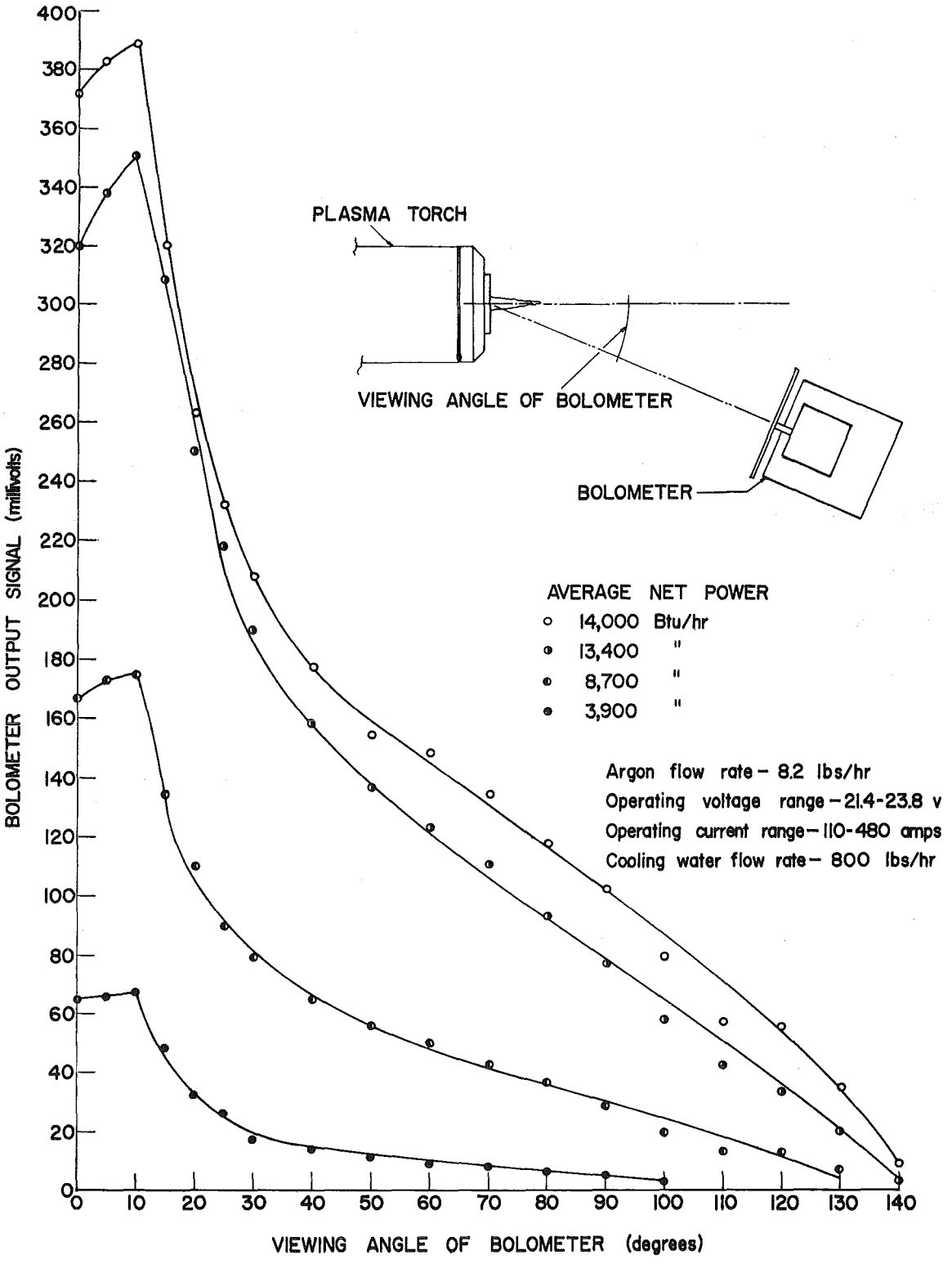

Fig. 3-11 Angular Distribution of Radiation from Plasma Torch

is a definite amount of radiant energy transferred to the surroundings. This is referred to as the actual radiative heat transfer from the plasma and plasma torch.

The data of the angular distribution of the radiation from the plasma torch shown in Figure 3-11 were used to calculate the actual radiative heat transfer from an argon plasma and the plasma torch. These calculations are based on the model shown in Figure 3-12. The bolometer is imagined to lie on the surface of a sphere whose center is the center of rotation of the plasma torch. At a viewing angle of 0° the bolometer sensing element lies on the south pole of this sphere. The surface is imagined to be divided into ring-like segments, such that each radiation reading lies in the latitudinal center of its corresponding segment. The radiation crossing each segment of the surface was calculated by multiplying the flux at that segment by the area of the segment. The actual radiative heat transfer was taken as the sum of the radiation crossing all segments of the spherical surface. Examples of these calculations are shown in Appendix C.

The results of these calculations are shown in Figure 3-13. The actual radiative heat transfer from the argon plasma and the plasma torch is expressed as a percentage of the average net power input to the plasma for each determination.

3.10 DISCUSSION OF RESULTS

The efficiency of the plasma torch is defined as the ratio of the net power input to the plasma to the gross electrical power input to the plasma torch. While generating an argon plasma, the efficiency of

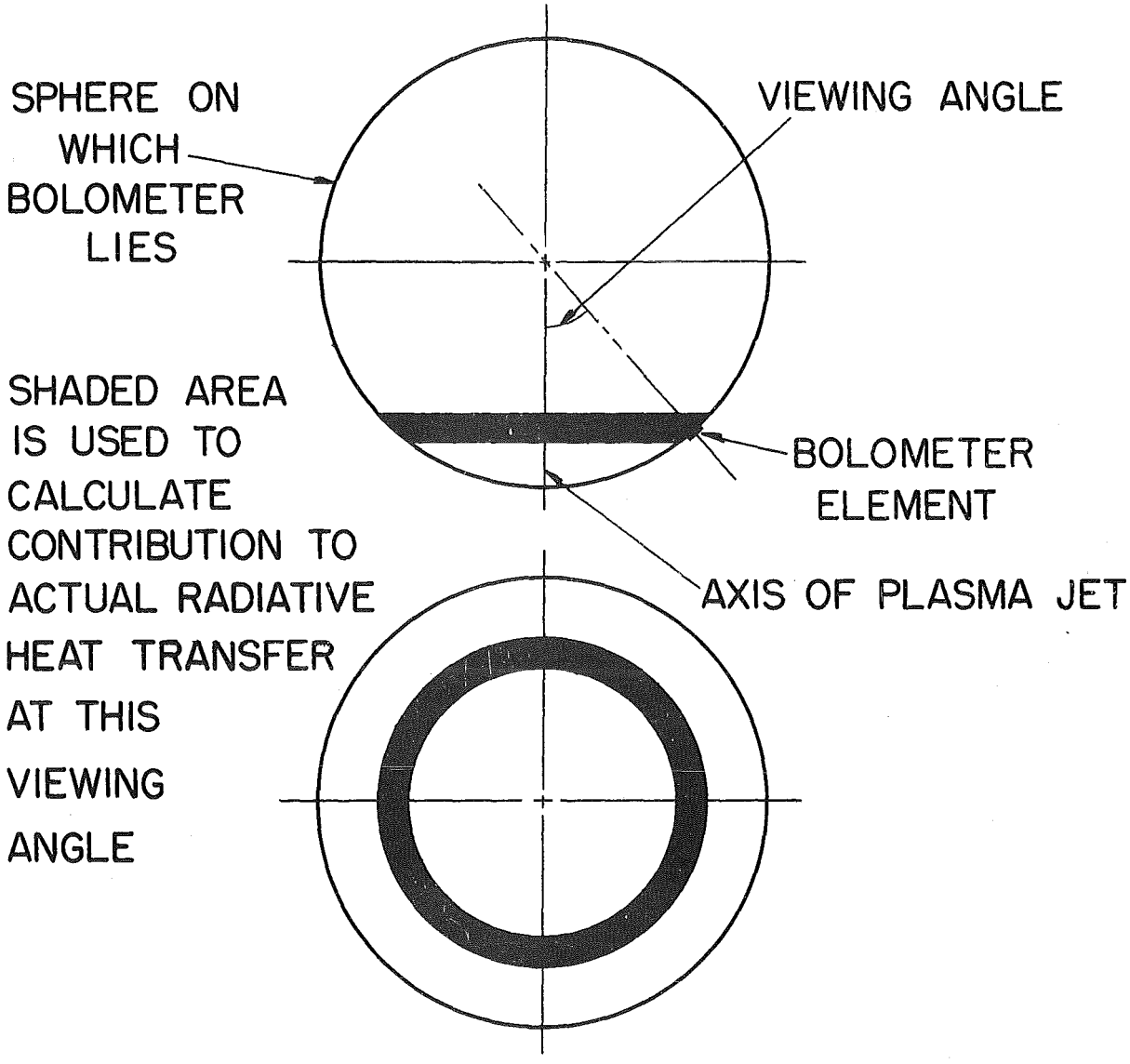

Fig. 3-12 Model for Calculation of Actual Radiative Heat Transfer

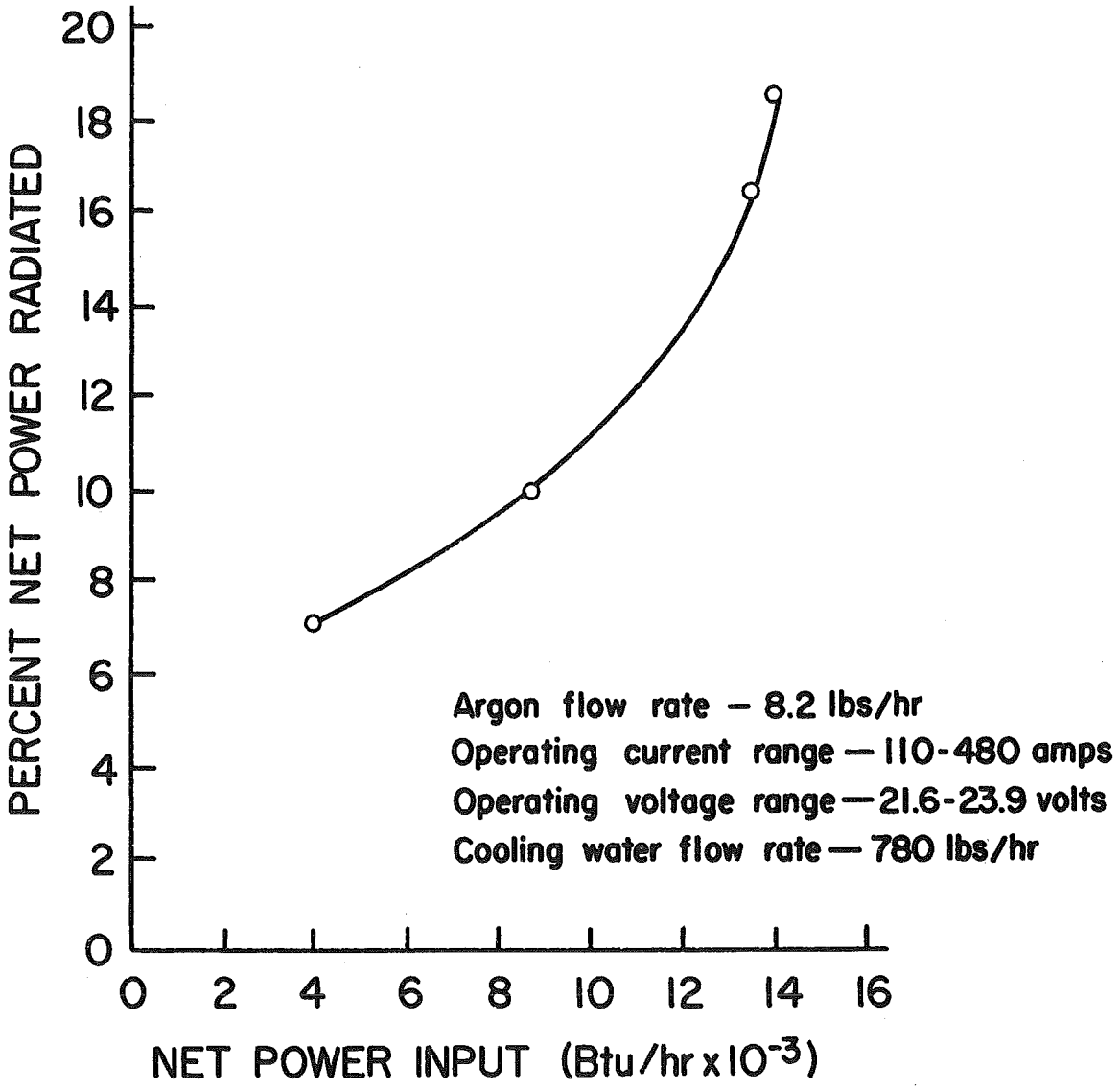

Fig. 3-13 Actual Radiative Heat Transfer from Argon Plasma and Plasma Torch

the plasma torch remained nearly constant at 0.5. For the forty data points recorded in the determination of the total radiation from an argon plasma (Figure 3-3), the efficiency varied from 0.48 to 0.54 with an average of 0.51. The efficiency of the plasma torch while generating an argon plasma is taken as constant at 0.5 over the range of power levels investigated.

The primary source of errors in the experiments described above is the power measurements. The cooling water flow rate was observed to fluctuate in a random manner approximately ± 5 per cent. The dead band of the current recorder is 1 per cent. The accuracy of the power voltmeter is 2 per cent. This gives an overall possible error of ± 11 per cent in the determination of the net power input.

Referring to Figure 3-3, most of the scatter of the data can be attributed to the errors incurred in the power measurements. There is, however, an additional source of error worth considering. As mentioned in Section 1.3, the use of the net power input to the plasma as the independent variable requires the implicit assumption that the net power input to the plasma uniquely determines the temperature distribution in the plasma jet. The fact that the radiation emitted from the plasma jet shows a strong correlation with the net power input to the plasma indirectly verifies this assumption.

The total radiation from an atmospheric argon plasma jet is significant, varying between 1 per cent and 18 per cent of the net power input to the plasma over the range of power levels investigated. At a constant net power input, the total radiation from an argon plasma jet increases

with decreasing flow rate, due to the higher temperatures generated in the plasma jet at the lower flow rates.

The total radiation from an atmospheric nitrogen plasma jet is less than 1 per cent of the net power input to the plasma over the range of power levels investigated. Since nitrogen is a diatomic gas, most of the energy input to the gas is expended in dissociating the molecules. As a result, the population of the free charged particles, which is the source of the radiation emitted from a plasma, is relatively small. For this reason, the total radiation from a nitrogen plasma jet is at least an order of magnitude smaller than the total radiation from an argon plasma jet at the same net power input to the plasma. The total radiation from an atmospheric nitrogen plasma jet may be considered insignificant for most purposes over the range of power levels investigated.

The calculation of the total radiation from the argon plasma jet using the pointwise radiation data agrees reasonably well with the direct measurements. The fact that this independent method of determining the total radiation from an argon plasma jet agrees with the results of the direct measurements tends to confirm the results of the direct measurements of the total radiation from an argon plasma jet.

The question of the effect of the presence of finely divided carbon particles on the total radiation from an argon plasma jet must be left unanswered. The results of the experiments reported here reveal no measurable effect due to the carbon. Further investigations in this area were not attempted.

The data on the angular distribution of the radiation from the

plasma and plasma torch reveal the presence of a hot core of plasma within the exit nozzle which radiates intensely. As the viewing angle decreases, more of the radiation from this hot core of plasma is detected by the bolometer. Thus, the intensity of radiation increases with decreasing viewing angle. The attenuation of the radiation as the viewing angle decreases from 10° to 0° is evidence of absorption of the radiation from the hot core of plasma by the plasma jet. At a viewing angle of 0°, the radiation emanating from within the exit nozzle must traverse the entire length of the plasma jet before being detected by the bolometer. Thus, the argon plasma generated in these experiments begins to exhibit a measureable absorptivity at a depth of about one inch.

The determination of the actual radiative heat transfer from the argon plasma and the plasma torch indicates that radiation is a significant mechanism of heat transfer from an atmospheric argon plasma generated in a plasma torch. Assuming a constant efficiency of 0.5 for the plasma torch, these data can be used to calculate an overall energy balance about the plasma torch including radiative losses from the argon plasma.

CHAPTER 4

THEORETICAL PREDICTION OF RADIATION EMITTED FROM A PARTIALLY IONIZED GAS

4.1 SOURCE OF CONTINUUM RADIATION

The major portion (energetically) of the radiation emitted by a hot, partially ionized gas (plasma) at atmospheric pressure is a continuous function of frequency. The source of this continuum radiation is the motion of free charges in the plasma. It is known from electrodynamics that a free charge, when accelerated, emits electromagnetic radiation. In a plasma the free charges (electrons) are accelerated as they collide with other particles (atoms, ions, and electrons), thus emitting electromagnetic radiation.

According to quantum mechanics, the energy of electromagnetic radiation is proportional to frequency through Planck's constant

$$E = h\nu \tag{4-1}$$

where h is Planck's constant, 6.63×10^{-27} erg sec

ν is the frequency (sec^{-1})

E is the energy (ergs)

Since energy is conserved, an electron undergoing a collision has some of its kinetic energy converted to radiation. The frequency of the radiation emitted by the electron is proportional to the energy loss of the electron. A free electron, upon colliding with another particle, can undergo a transition to any lower energy state; thus the radiation emitted from such collisions is continuous in frequency. This continuous

radiation is sometimes referred to as bremsstrahlung.

4.2 FREE-FREE TRANSITIONS

An electron, upon colliding with an ion, has some of its kinetic energy converted to radiation. If the energy loss of the electron is not too great, it leaves the influence of the ion's Coulombic field and maintains its status as a free electron. This is an example of a collision classified as a free-free transition.

The radiation emitted by an electron undergoing a free-free transition in a collision with an ion has been analyzed by Oster (Ref. 5). His treatment is a classical one, in which the radiant energy loss of the electron is ignored in solving the mechanics of the collision. As a result of this assumption, the electron describes a hyperbolic orbit in a reference frame attached to the ion. A Fourier analysis of the components of the electronic acceleration yields the classical emission coefficient of a free-free electron-ion collision.

Because of the mathematical complexity of the expression thus obtained, one of two approximations to the hyperbolic orbit of the electron is commonly made. In one case, the hyperbolic orbit is approximated by a straight line, in the other by a parabola. Each of these approximations yields results which are valid over certain frequency ranges. Using Kramers' parabolic approximation to the electronic orbit (Ref. 6), a simple expression for the emission coefficient is obtained from a Fourier analysis of the electron's acceleration (Refs. 7, 8)

$$\epsilon_\nu = \frac{64\pi^{3/2} e^6}{3\sqrt{6}\, m_e^{3/2} c^3 k^{1/2}} Z^2 \frac{n_e n_i}{T^{1/2}} e^{-h\nu/kT} \qquad (4\text{-}2)$$

where e is the electronic charge, 4.81×10^{-10} statcoul

m_e is the electronic mass, 9.12×10^{-28} gms

c is the velocity of light, 3×10^{10} cm/sec

Z is the integral ionic charge

n_e, n_i are the electron, ion number densities respectively (cm^{-3})

T is the temperature (^oK)

h is Planck's constant, 6.63×10^{-27} erg sec

k is Boltzmann's constant, 1.38×10^{-16} erg/^oK

ν is the frequency of radiation (sec^{-1})

ϵ_ν is the radiant energy of frequency ν emitted in all directions per unit volume of gas ($ergs/cm^3$)

Evaluating the constant term, this equation reduces to

$$\epsilon_\nu = 6.8 \times 10^{-38} Z^2 \frac{n_e n_i}{T^{1/2}} e^{-h\nu/kT} \qquad (4\text{-}3)$$

Integrating this expression over all frequencies gives the power radiated per unit volume of gas at temperature T

$$P(T) = \int_0^\infty \epsilon_\nu \, d\nu \qquad (4\text{-}4)$$

where P(T) is the power radiated per unit volume ($ergs/cm^3$ sec). Substituting Eq. 4-3 into Eq. 4-4 yields

$$P(T) = \int_0^\infty 6.8 \times 10^{-38} \; Z^2 \; \frac{n_e n_i}{T^{1/2}} \; e^{-h\nu/kT} \; d\nu \qquad (4\text{-}5)$$

Since the ionic charge, number densities, and temperature are independent of frequency, this gives

$$P(T) = 6.8 \times 10^{-38} \; Z^2 \; \frac{n_e n_i}{T^{1/2}} \int_0^\infty e^{-h\nu/kT} \; d\nu$$

$$= 6.8 \times 10^{-38} \; Z^2 \; \frac{n_e n_i}{T^{1/2}} \left(-\frac{kT}{h}\right) e^{-h\nu/kT} \Big|_0^\infty$$

$$= 6.8 \times 10^{-38} \; \frac{k}{h} \; Z^2 \; n_e n_i \; T^{1/2}$$

Evaluating the constant term and expressing the result in watts/cm^3 gives (Ref. 9)

$$P(T) = 1.4 \times 10^{-34} \; Z^2 \; n_e n_i \; T^{1/2} \qquad (4\text{-}6)$$

In applying the Kramers approximation to the work discussed in Chapter 5, the limits of integration used were the upper and lower cut-off frequencies of the sodium chloride window. Substituting these limits into Eq. 4-5 gives

$$P(T) = 1.4 \times 10^{-34} \; Z^2 \; n_e n_i \; T^{1/2} \left[e^{-840/T} - e^{-53{,}800/T}\right] \qquad (4\text{-}7)$$

This result is plotted as a function of temperature in Figure 5-19. The values of electron and ion number densities were taken from the

tables computed by Drellishak, et al. (Ref. 10) for the equilibrium composition of atmospheric argon plasma. Calculations were performed at thousand degree intervals from 10,000°K to 23,000°K. Two calculations were performed at each temperature, one for the radiation from collisions with the first ions (Z = 1) and one for the radiation from collisions with the second ions (Z = 2). These two contributions were added. The effect of radiation from electrons colliding with second ions calculated from Eq. 4-7 is negligible below 18,000°K. Sample calculations are shown in Appendix D.

4.3 QUANTUM CORRECTIONS TO CLASSICAL RESULTS

The basic assumption which allows a classical treatment of the radiation emitted by an electron upon colliding with an ion is the disregard for the energy lost by the electron to radiation during the encounter. A comprehensive quantum mechanical analysis of the electron-ion encounters which takes account of the energy loss of the electron was achieved by Sommerfeld in his book (1939) on atomic spectra. Greene (Ref. 11) gives a correction to Kramers' classical equation in the form of a multiplicative factor which adjusts the classical Kramers equation to agree with Sommerfeld's analysis

$$P(T) = 1.4 \times 10^{-34} \; Z^2 \; n_e n_i \; T^{1/2} \; \bar{g}(T) \qquad (4\text{-}8)$$

The multiplicative factor, $\bar{g}(T)$, is a frequency averaged Gaunt factor and is a slowly varying function of temperature. A plot of Eq. 4-8, calculated using values of $\bar{g}(T)$ given by Greene is shown on Figure 5-19 as the Sommerfeld solution.

4.4 FREE-BOUND TRANSITIONS

Consider now the radiation emitted by a free electron as it collides with and is captured by an ion. Such encounters are called free-bound transitions. A free-bound transition occurs when a free electron loses a sufficient amount of its energy and is captured by an ion. The radiation emitted by electrons undergoing free-bound transitions is often referred to as recombination radiation.

One of the basic tenets of quantum theory is that electrons are bound to their nuclei in discreet energy levels or orbits. Elementary quantum theory predicts that the energy difference between successively more energetic orbits decreases, approaching zero as the orbital energy approaches the ionization energy.

A free electron which undergoes a free-bound transition becomes bound to the ion in one of these discreet energy levels or orbits. A calculation of the radiation emitted by electrons experiencing free-bound transitions would involve a sum over these discreet levels or states.

In a hot plasma, however, the ions are excited so that the probability is greatest that an electron will become bound to an ion in one of the highest energy levels. Olsen (Ref. 12) discusses an approximation which Unsöld has made to calculate the radiation emitted during free-bound transitions.

Unsöld replaces the sum over discreet states by an integral. This amounts to assuming that the upper orbits of an ion which are available to accept an incoming electron are so energetically dense

that the substitution of an integral is valid. Unsöld adds the radiation from free-bound transitions to that from free-free transitions as calculated from Kramers' approximation and arrives at a spectrum for the continuum which is independent of frequency (Ref. 12)

$$\epsilon_\nu = 6.8 \times 10^{-45} \, Z^2 \frac{n_e n_i}{T^{1/2}} \tag{4-9}$$

where ϵ_ν is the radiant energy of frequency ν emitted in all directions per unit volume of gas (watt sec/cm^3)

Z is the integral ionic charge

n_e, n_i are the number densities of the electrons and ions, respectively (cm^{-3})

T is the temperature ($^\circ$K)

Unsöld's approximation, Eq. 4-9, is valid up to a cutoff frequency, ν_g. This cutoff frequency is defined by the energy difference between the effective ionization potential and the energy level below which the assumption of dense states becomes invalid. The theory is based on recombination into hydrogen-like states.

The total power radiated from the gas over the range of validity of Unsöld's approximation is easily calculated by integrating the emission coefficient, Eq. 4-9, over the appropriate frequency interval

$$P(T) = \int_0^{\nu_g} \epsilon_\nu \, d\nu$$

$$= \int_0^{\nu_g} 6.8 \times 10^{-45} \, Z^2 \, \frac{n_e n_i}{T^{1/2}} \, d\nu$$

$$= 6.8 \times 10^{-45} \, Z^2 \, \frac{n_e n_i}{T^{1/2}} \, \nu \Big|_0^{\nu_g}$$

$$P(T) = 6.8 \times 10^{-45} \, Z^2 \, \frac{n_e n_i}{T^{1/2}} \, \nu_g \qquad (4\text{-}10)$$

This expression gives the radiation from free-bound and free-free transitions in the frequency range up to the cutoff frequency.

Olsen (Ref. 12) has attempted to measure the cutoff frequency, ν_g, above which the Unsöld approximation is invalid. He made measurements of the intensity of the continuum at 16,000°K in an atmospheric argon plasma as a function of frequency. According to Unsöld's approximation, a plot of the intensity of the continuum radiation as a function of frequency should be flat out to the cutoff frequency, ν_g, and then, according to Kramers' approximation, should fall off exponentially (Ref. 8). Olsen apparently never reaches the cutoff frequency in his measurements, although it appears from his experimental data that he may be only slightly above it. He concludes only that the cutoff frequency in an atmospheric argon plasma at 16,000°K is less than 3×10^{14} sec^{-1}.

4.5 KRAMERS-UNSÖLD MODEL FOR CONTINUUM RADIATION

It is now possible to formulate a simple model of the continuum

radiation from a plasma which will account for the radiation from free-free and free-bound transitions. This is done by matching the Unsöld approximation, Eq. 4-9, to the Kramers approximation, Eq. 4-3, at the cutoff frequency, and then integrating both approximations over the appropriate frequency intervals.

Details of the calculations are shown in Appendix D. The cutoff frequency was taken as constant at 3×10^{14} sec^{-1}. The contribution to the continuum radiation below the cutoff frequency by free-bound and free-free transitions was calculated from the Unsöld approximation as indicated in Eq. 4-10. However, in order to match the experimental work, the lower limit of integration was taken as 0.175×10^{14} sec^{-1}, the lower limit of transmissibility of the sodium chloride window. The emission coefficient as given by the Kramers approximation, Eq. 4-3, was forced to match the emission coefficient as given by the Unsöld approximation, Eq. 4-9, at the cutoff frequency, ν_g, at each temperature. This was done by adjusting the constant term in the Kramers approximation, Eq. 4-3. The resulting expression, with the new constant, was then integrated, using as the lower limit of integration the cutoff frequency, ν_g, and as the upper limit 11.2×10^{14} sec^{-1}, which is the upper limit of transmissibility of the sodium chloride window. These calculations were performed at thousand degree increments from 10,000°K to 23,000°K, to cover the range of experimental observation. The resulting curve is shown on Figure 5-19 as the Kramers-Unsöld approximation.

CHAPTER 5

RADIATION FROM AN ATMOSPHERIC ARGON PLASMA AS A FUNCTION OF TEMPERATURE

5.1 LOCAL THERMODYNAMIC EQUILIBRIUM

The radiation emitted from a plasma will be a function of the thermodynamic state of the plasma provided the plasma is in local thermodynamic equilibrium. Local thermodynamic equilibrium implies that the various components of the plasma are at the same temperature at each point within the plasma.

Knopp (Ref. 13) has investigated the existence of local thermodynamic equilibrium in an argon plasma jet at atmospheric pressure. This investigation is based on the elastic nature of collisions between electrons and heavy particles in the plasma. Compton (Refs. 14, 15) has shown that these collisions are elastic provided

$$\frac{E}{p} < 1 \qquad (5\text{-}1)$$

where E is the electric field intensity (volts/cm)

p is the pressure of the plasma (mm Hg)

The electrode-nozzle spacing used in these experiments was about 0.25 cm. Using a representative voltage drop of 25 volts, the criterion of elastic collisions is satisfied for an atmospheric argon plasma jet. The argon plasma jet may be considered to be in local thermodynamic equilibrium under these conditions (Ref. 13).

McGregor (Ref. 15a) states that this criterion may be inadequate for flowing systems at high densities such as are encountered in a plasma torch exhausting to atmospheric pressure. He mentions that a criterion for equilibrium in such a flow system should at least consider the dwell time of the particles in the arc. A detailed investigation

of the flow between the electrodes and the structure of the arc in the plasma torch used in this report was not undertaken. The plasmas studied in this report areassumed to be in local thermodynamic equilibrium.

5.2 DETERMINATION OF TEMPERATURE DISTRIBUTION IN AN ARGON PLASMA JET

The temperature distribution in the argon plasma jet was determined by a method previously employed by several investigators (Refs. 13, 16, 17, 18). The method is based on a knowledge of the intensity of a spectral line of argon as a function of temperature. The theoretical basis for this method of temperature determination is discussed in Appendix E.

A Perkin-Elmer Model 12C spectrometer was used to measure the relative intensity of the radiation from the plasma jet in appropriate frequency intervals. The arrangement of the apparatus used in these measurements is shown in Figure 5-1. An f/4.5 optical system consisting of two compound lenses mounted on an optical bench was used to project an image of the plasma jet without magnification in the plane of the entrance slit of the spectrometer. The plasma torch was mounted vertically on a small rotary machinist's table with one lead screw of the table oriented perpendicular to the axis of the optical system. This lead screw was driven by a reversible 1 r.p.m. synchronous motor. With this mechanism, the plasma jet was traversed past the spectroscope at 0.100 in/min. Two razor blades spaced 0.005 in. apart were used to provide a horizontal entrance slit directly in front of the vertical entrance slit of the spectrometer. This combination of entrance slits allowed the spectroscope to view only a small area of the image of the plasma jet.

The traverses were taken at a height 0.1 in. above the base of

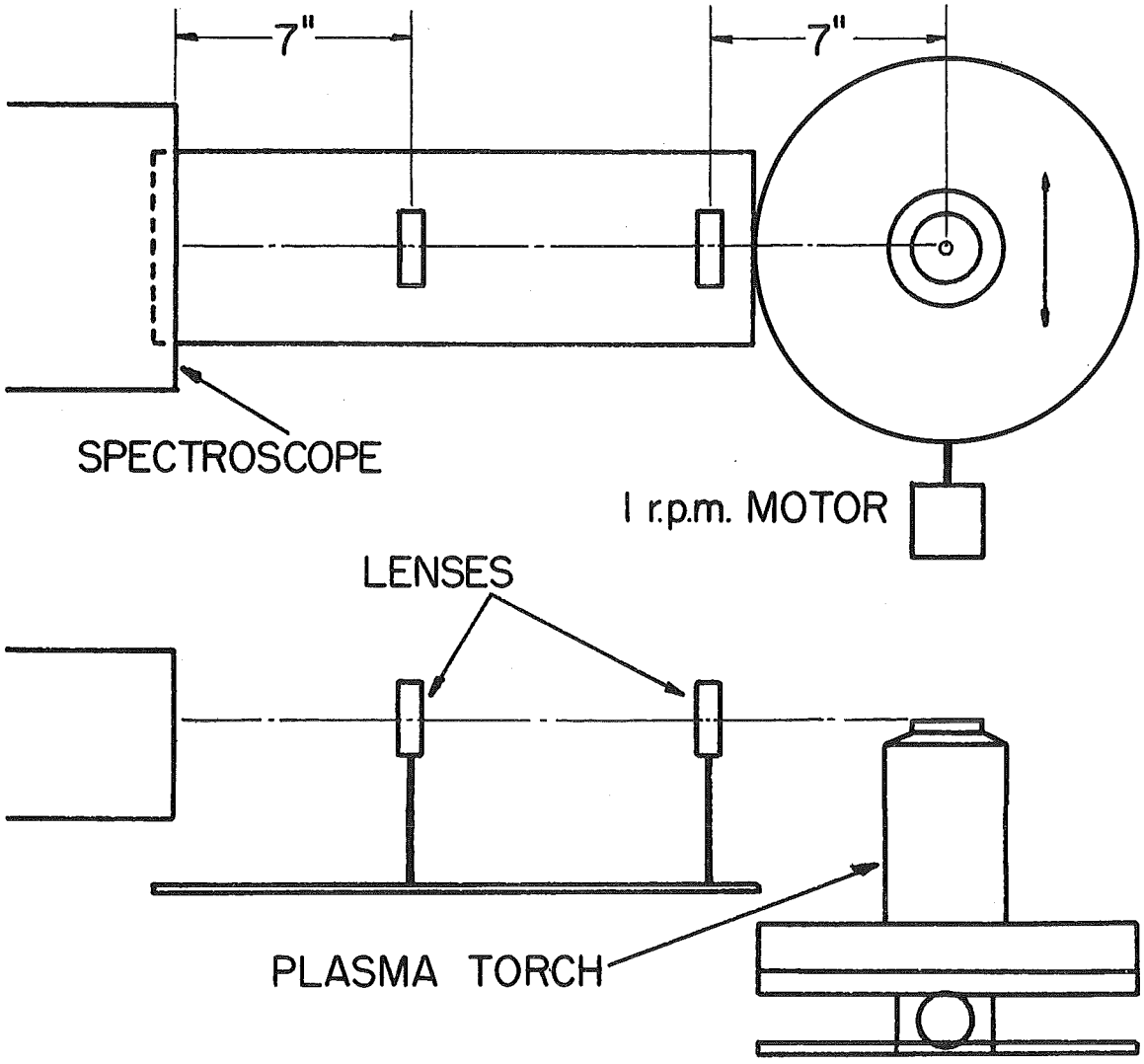

Fig. 5-1 Arrangement for Spectroscopic Measurements

the plasma jet. During a traverse the voltage drop across the plasma torch was recorded every fifteen seconds. The net power input to the plasma was calculated for each voltage drop reading and these values were averaged to compute the average net power for each traverse.

The radiation seen by the spectroscope within any bandwidth is the sum of the spectral line radiation and the continuum radiation within that bandwidth. In order to determine the intensity of the spectral line, two traverses were made at each power level. The first traverse was made with the spectroscope set to receive all of the radiation underneath the spectral line, including the continuum. The data thus obtained is referred to as the total intensity. The spectroscope was then set just far enough away from this frequency range to exclude the spectral line radiation, thus measuring just the continuum intensity. The continuum intensity was subtracted from the total intensity to yield the lateral spectral line intensity. The details of the settings of the spectroscope for these various measurements are discussed in Appendix E.

The two pairs of traces which were used to determine the temperature distribution in the plasma jet are shown in Figures 5-2, 5-3, 5-4, and 5-5. The chart speed was 4 in/min so that one inch on the recorder chart corresponds to 0.025 in. in the plasma jet. The argon flow rate to the plasma torch in these traverses was 5.1 lbs/hr; the cooling water flow rate was 1,260 lbs/hr. The average net power input for the traverses in Figures 5-2 and 5-3 was 10,100 Btu/hr, for Figures 5-4 and 5-5, 15,000 Btu/hr.

The data were taken from a smooth curve drawn directly on the spectroscope recorder traces. The maximum of each curve was determined

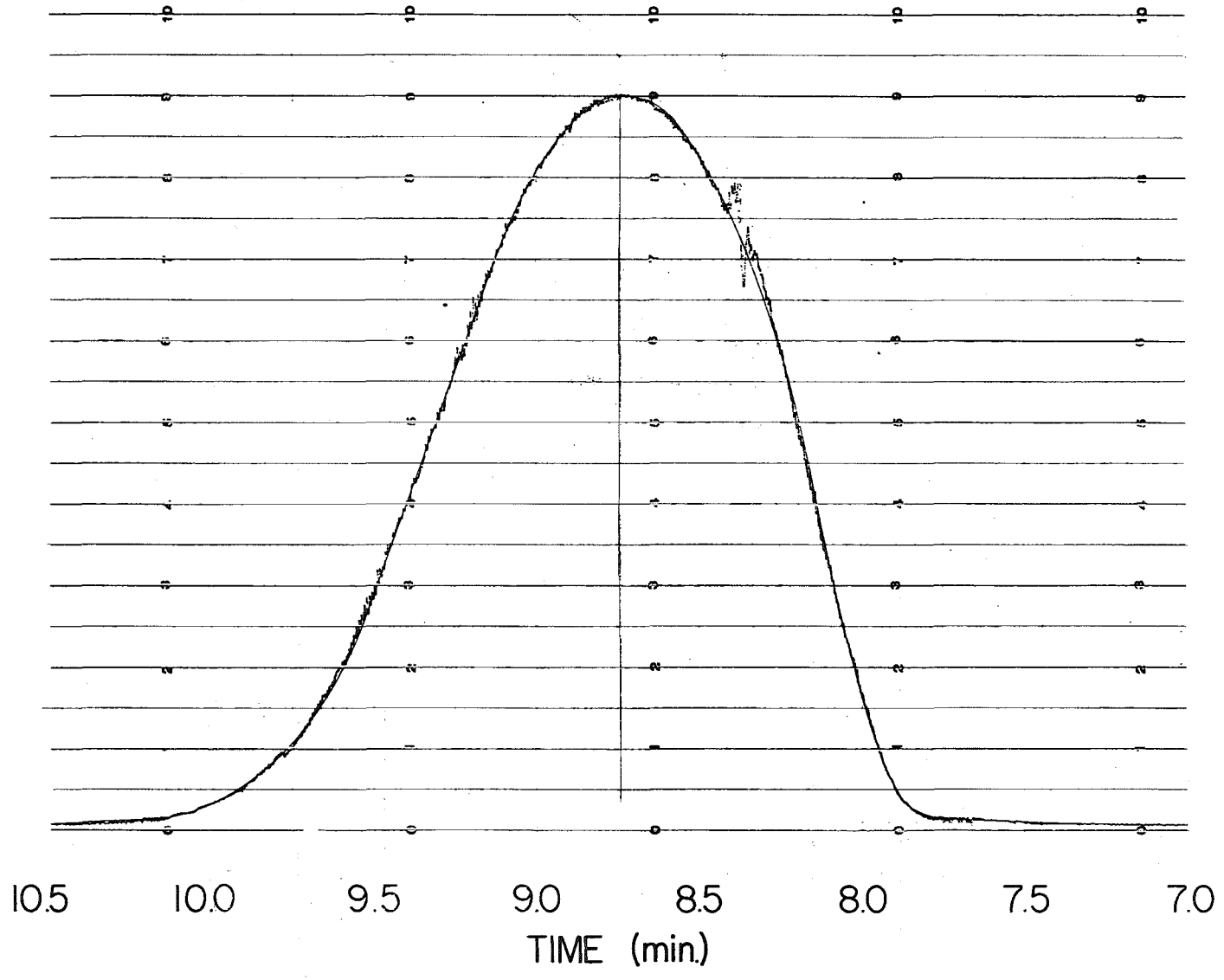

Fig. 5-2 Traverse of Plasma Jet; Argon Atom Line 4158.59 Å and Continuum

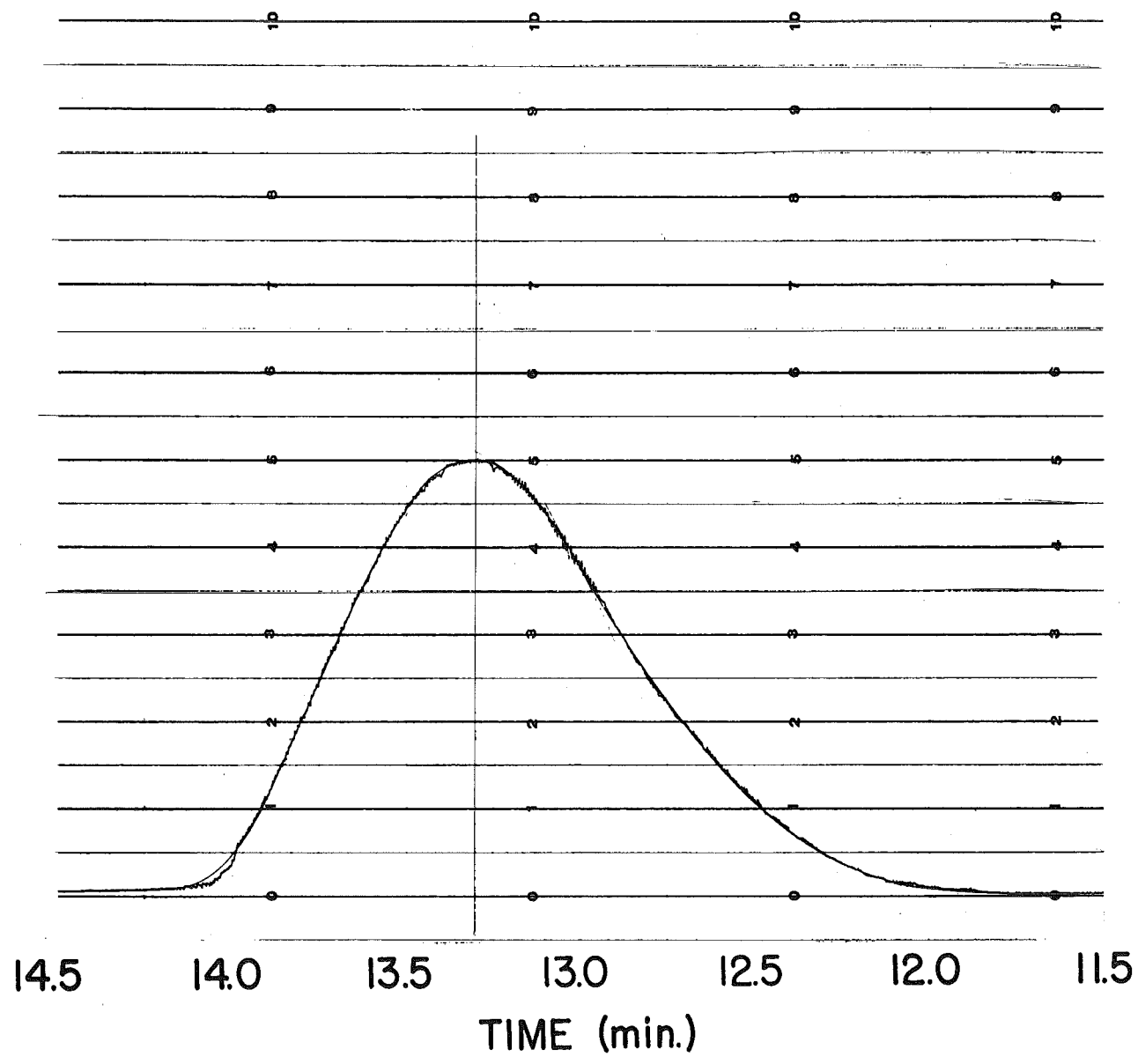

Fig. 5-3 Traverse of Plasma Jet; Continuum

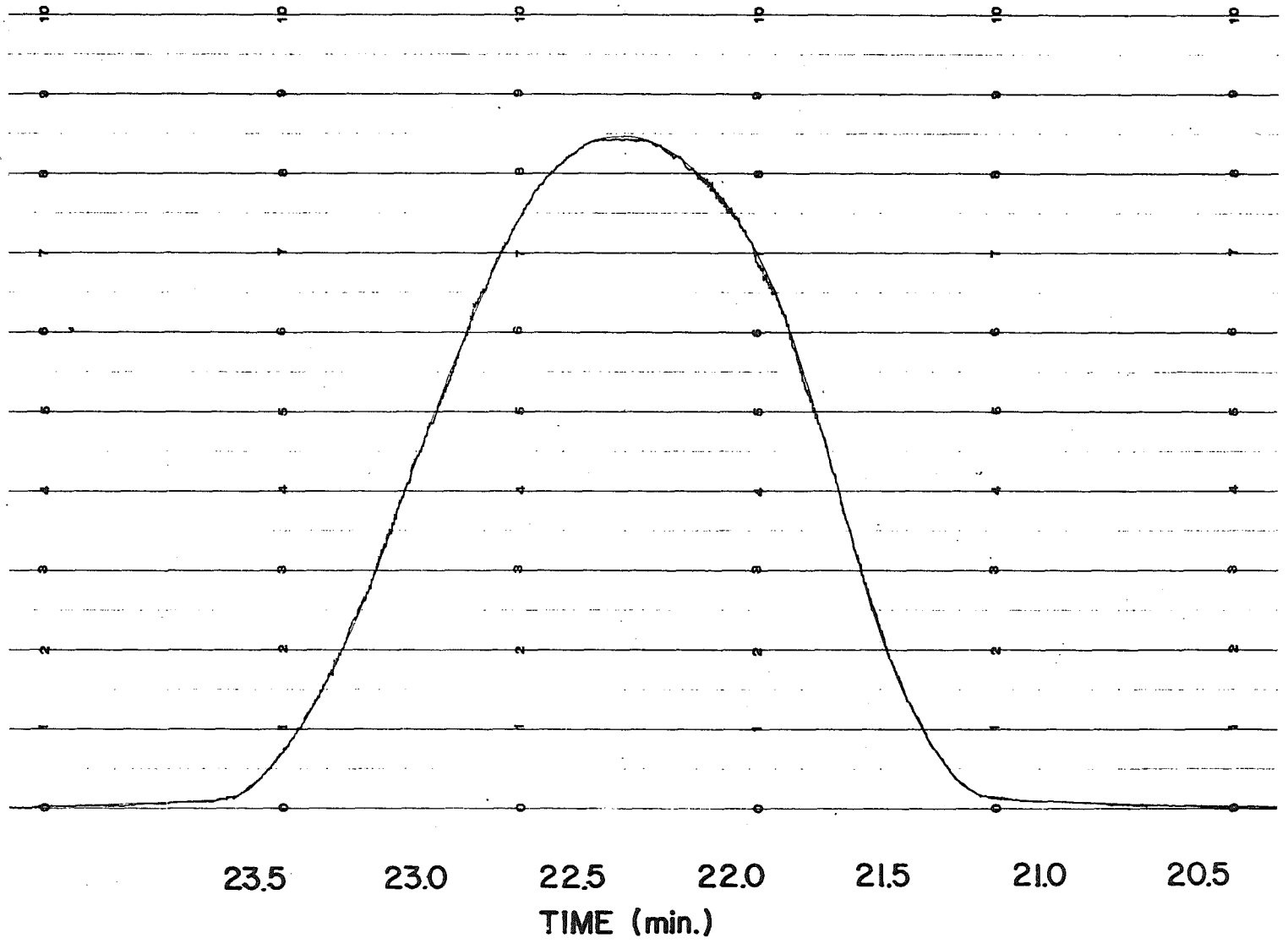

Fig. 5-4 Traverse of Plasma Jet; Argon Atom Line 4158.59Å and Continuum

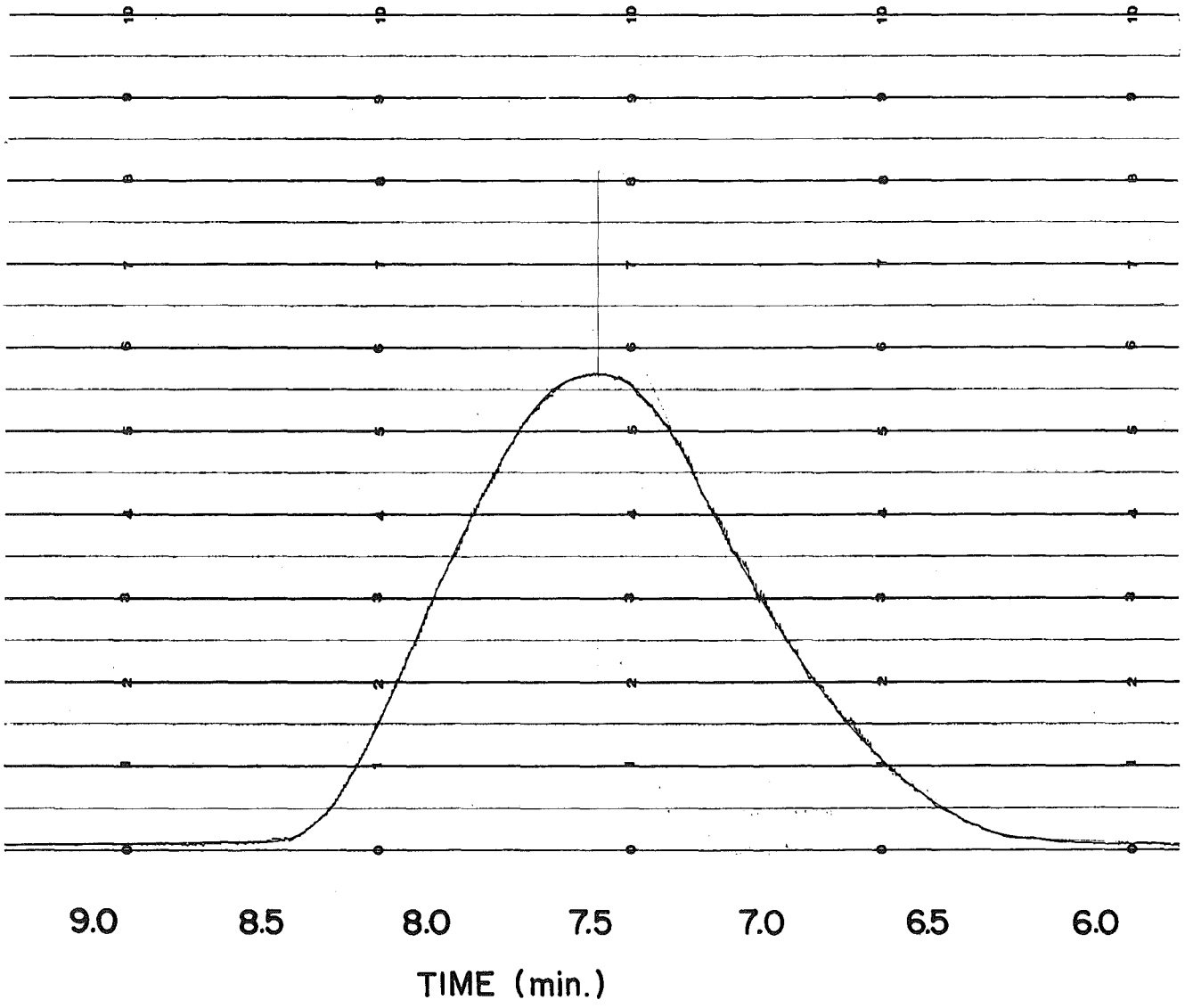

Fig. 5-5 Traverse of Plasma Jet; Continuum

and a vertical line was dropped from the maximum. The relative intensity was read at horizontal increments of 0.2 in. from the maximum on the recorder trace, which corresponds to horizontal increments of 0.005 in. in the plasma jet. The values of the relative intensity at equal distances on both sides of the maximum were averaged. This averaging procedure amounts to folding the recorder trace along a vertical line at the maximum and drawing an average curve through the two superposed curves. The folding process was used to adjust for any asymmetry in the plasma jet and to eliminate the asymmetry introduced by the hysteresis in the recorder. This procedure was used on both the total and continuum intensity traces. The folded continuum intensity was then subtracted from the folded total intensity at corresponding horizontal increments to yield the relative lateral spectral line intensity at the two power levels. These data are shown in Figure 5-6 and 5-7.

Nestor and Olsen (Ref. 18) have developed a numerical technique based on the Abel integral equation to invert the lateral intensity distribution to a radial intensity distribution. The occurrence of the Abel integral equation in this connection is discussed in Appendix E. This numerical technique has been programmed for use on an I.B.M. 709 digital computer by Enright (Ref. 17). The lateral spectral line intensities shown in Figures 5-6 and 5-7 were inverted to radial spectral line intensities using the computer program. The computer output was normalized at its maximum and plotted. The plots of the radial spectral line intensity are shown in Figures 5-8 and 5-9. The maxima on these curves corresponds to a temperature of 15,550°K in the plasma jet. The

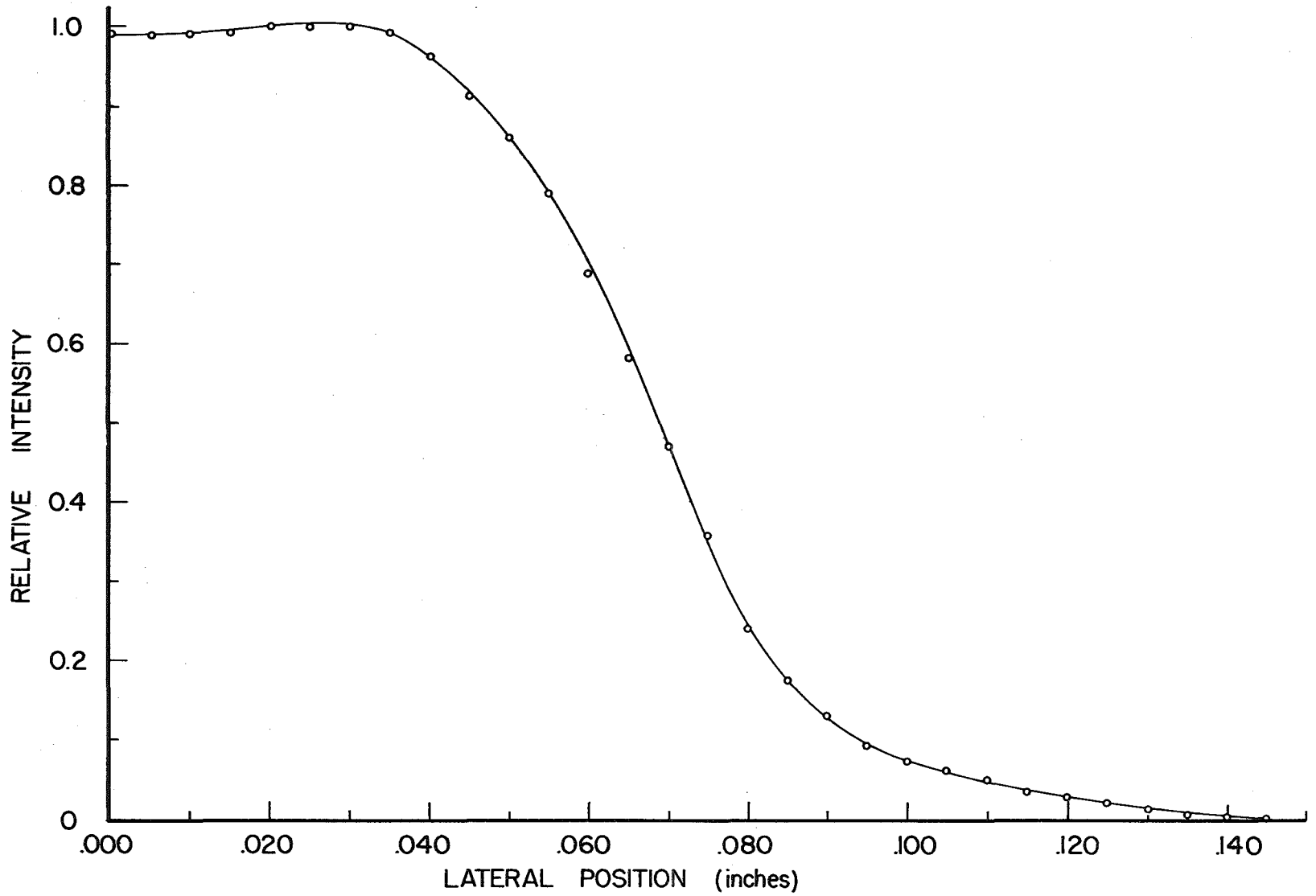

Fig. 5-6 Lateral Intensity; Argon Atom Line 4158.59Å; Average Net Power 10,100 Btu/hr

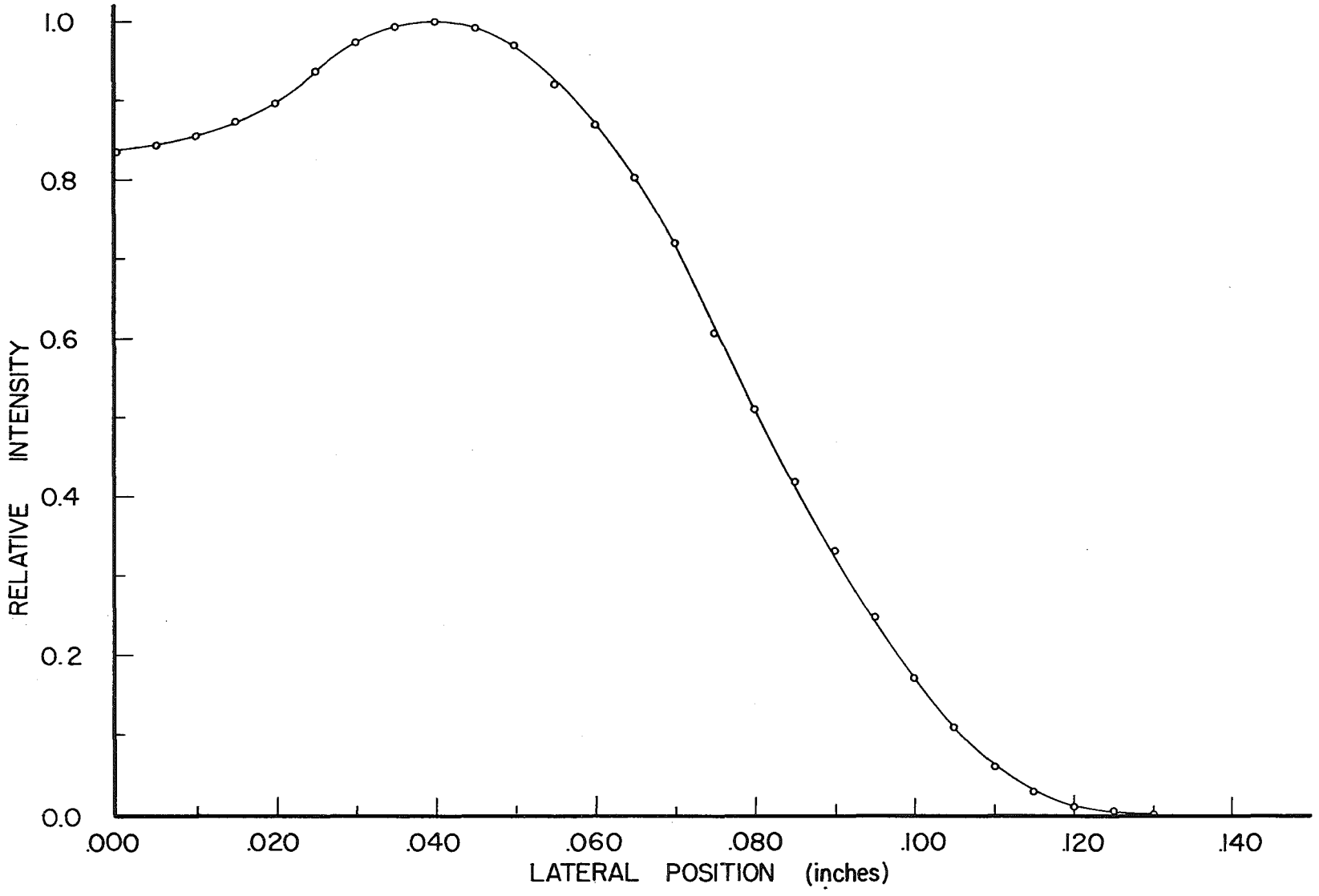

Fig. 5-7 Lateral Intensity; Argon Atom Line 4158.59Å; Average Net Power 15,000 Btu/hr

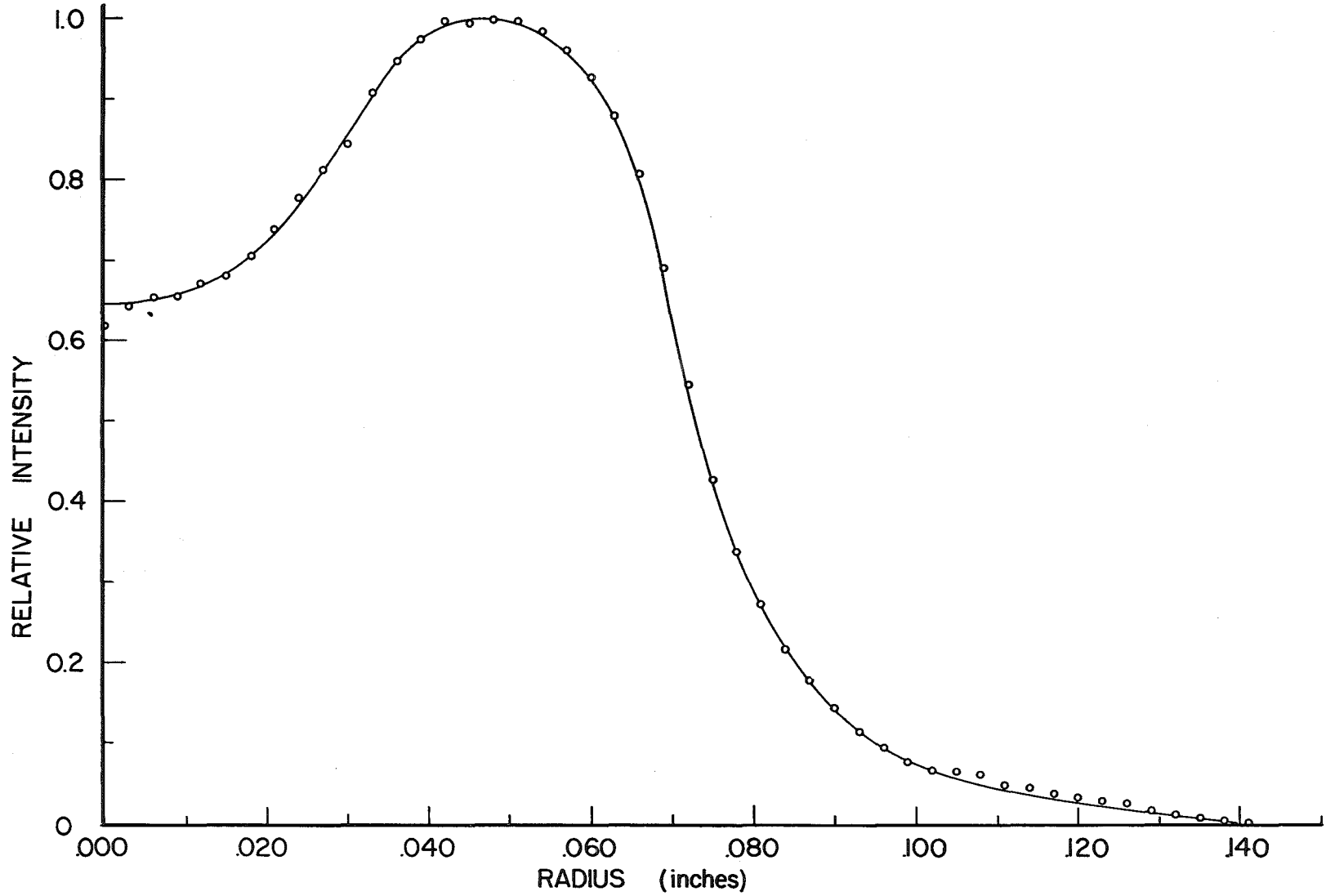

Fig. 5-8 Radial Intensity; Argon Atom Line 4158.59Å; Average Net Power 10,000 Btu/hr

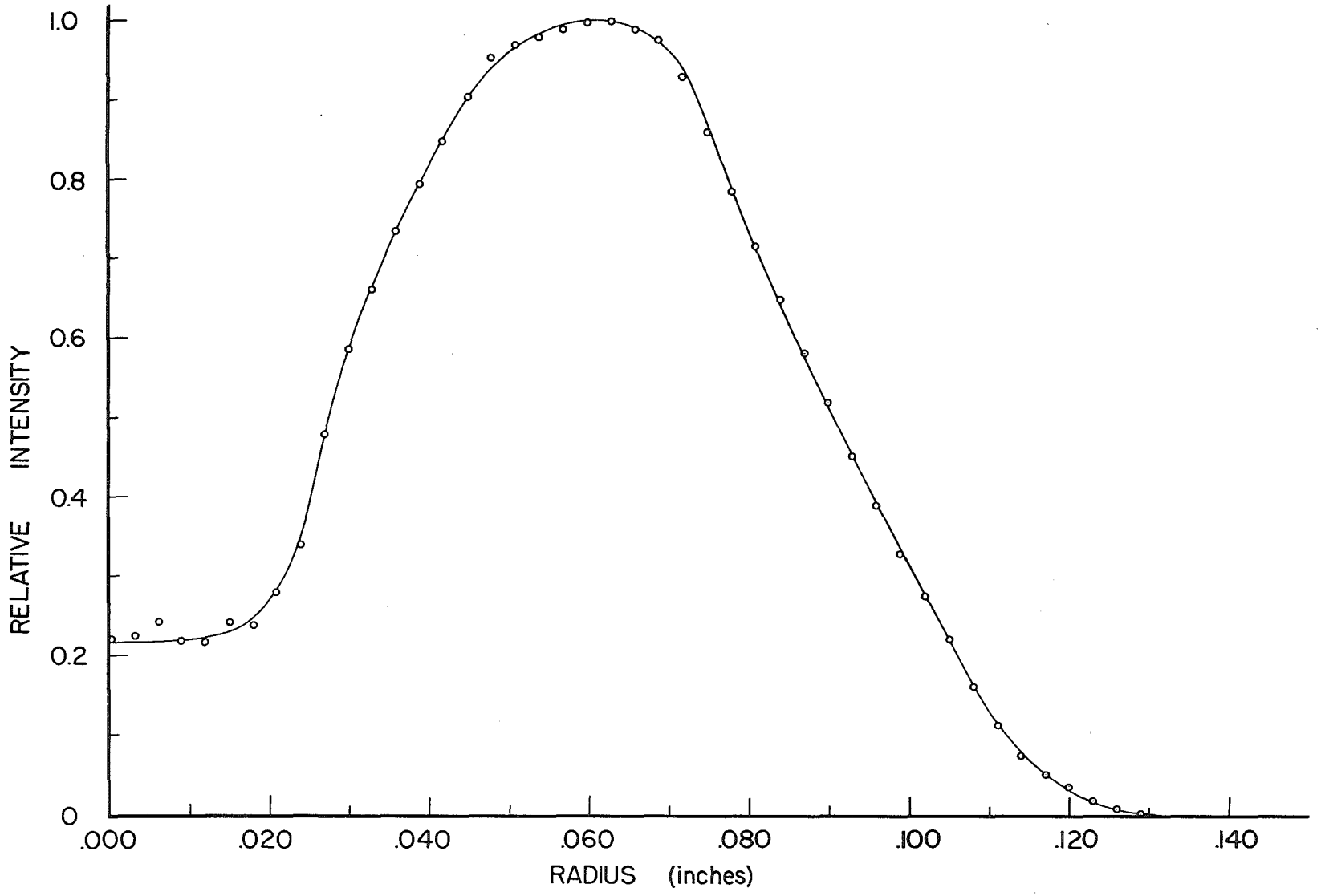

Fig. 5-9 Radial Intensity; Argon Atom Line 4158.59Å; Average Net Power 15,000 Btu/hr

temperature at horizontal increments of 0.004 in. from the axis of the plasma jet was determined by comparing the radial spectral line intensity with the theoretical relative intensity of the spectral line (see Appendix E). The temperature profiles in the argon plasma jet determined at the two power levels are shown in Figure 5-10.

5.3 DETERMINATION OF RADIAL DISTRIBUTION OF RADIATIVE POWER DENSITY IN AN ARGON PLASMA JET

The bolometer and plasma torch were positioned as shown in Figure 5-11 with the optical system providing a five-fold magnification of the image of the plasma jet in the plane of the bolometer sensing element. The bolometer was calibrated in this arrangement as discussed in Appendix B. Care was taken to place the bolometer element at a position in the image of the plasma jet corresponding to the height in the plasma jet at which the lateral spectral line intensity was measured.

The lateral intensity distribution of the continuum radiation was measured by traversing the bolometer horizontally across the image of the plasma jet. Readings of the bolometer output signal were recorded at 0.050 in. increments at the lower intensities, and at 0.025 in. increments at the higher intensities. These increments correspond to 0.010 in. and 0.005 in. increments in the plasma jet, respectively. Readings of the voltage drop across the plasma torch were recorded simultaneously with each bolometer output signal. The net power input to the plasma was calculated for each reading. These values were then averaged to compute the average net power for each traverse.

The lateral intensity distribution of the continuum radiation

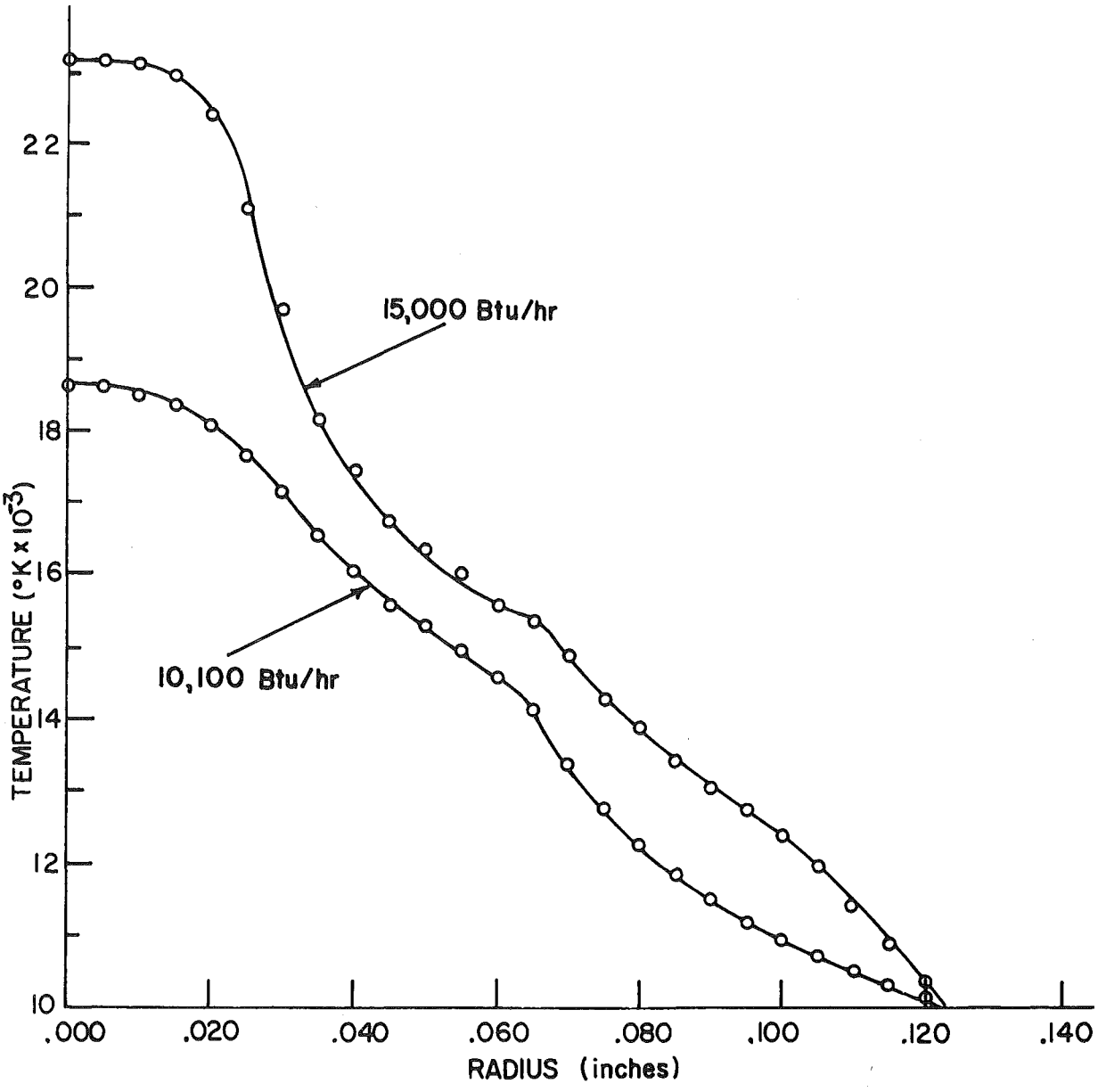

Fig. 5-10 Temperature Profiles of Plasma Jet

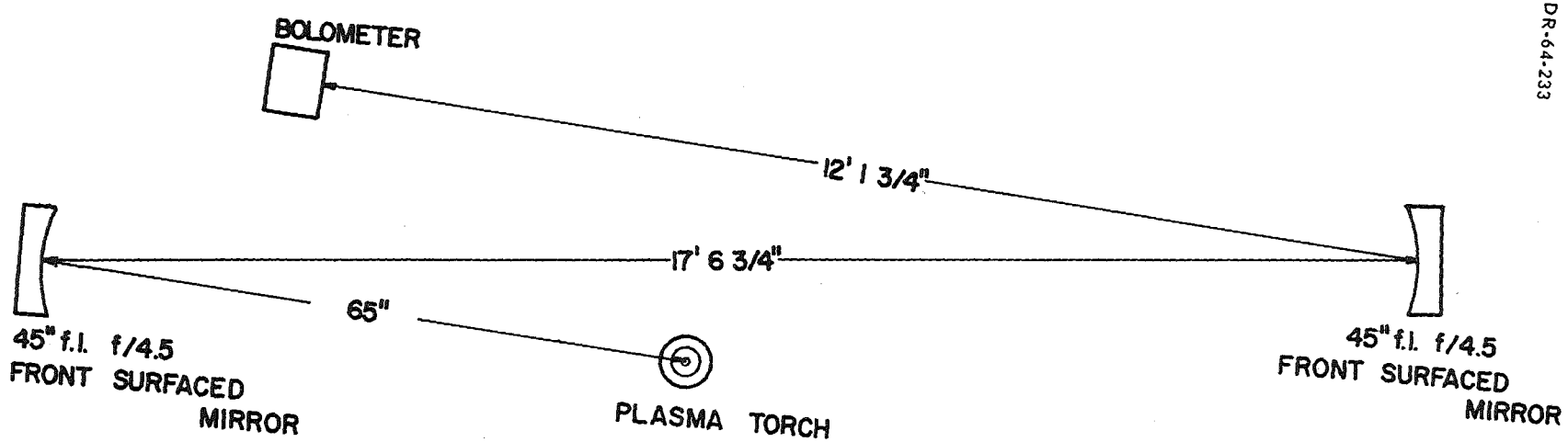

Fig. 5-11 Mirror Arrangement; Pointwise Measurements 5:1 Magnification

was measured at three power levels. The data from these measurements are shown in Figures 5-12, 5-13, and 5-14. The smooth curves drawn through these points were folded at the maximum intensity and a symmetrical lateral intensity distribution was drawn between the experimental curves for each traverse. These folded curves are shown in Figures 5-15, 5-16, and 5-17. The lateral intensity of the continuum radiation was read from these folded curves at 0.004 in. increments. These data were inverted to radial distributions using the computer program (Ref. 17). The resulting radial distribution of the radiative power density in the argon plasma jet at three power levels is shown in Figure 5-18.

5.4 DETERMINATION OF CONTINUUM RADIATION AS A FUNCTION OF TEMPERATURE

Ideally, the lateral intensity of the continuum radiation should have been measured at the same power levels as those at which the temperature was determined. However, it is nearly impossible to operate the plasma torch at a predetermined power level, because the voltage drop across the torch cannot be precisely predicted. As a result, the radiation traverses were taken at different power levels than the temperature traverses. A linear interpolation technique was used to adjust the temperature profiles and radial distributions of the radiative power density to the same power levels. The method of interpolation and sample calculations are shown in Appendix F. Figure 5-19 shows the final results of the temperature-radiation determination. The theoretical models discussed in Chapter 4 are shown for comparison.

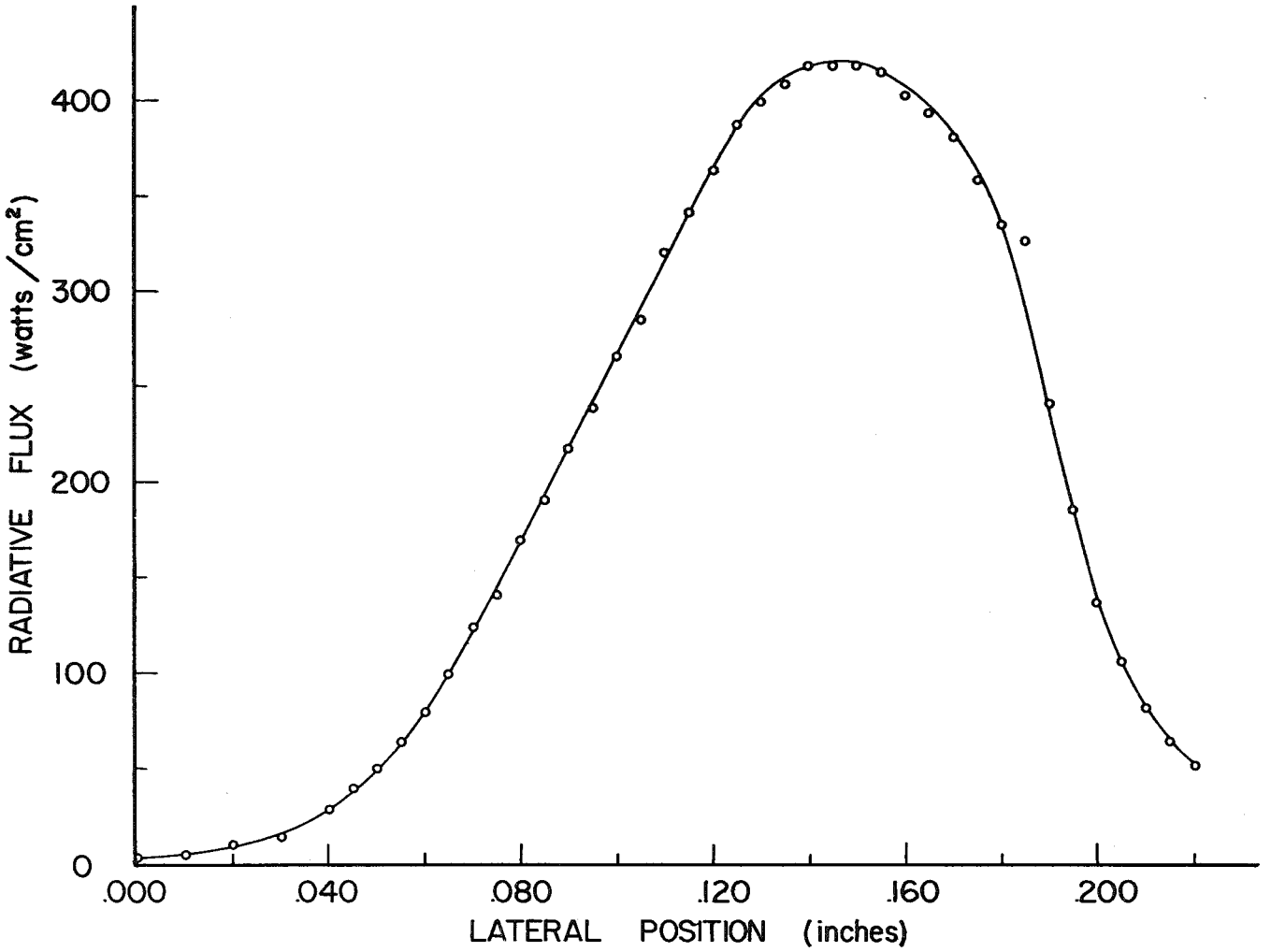

Fig. 5-12 Lateral Radiative Flux; Average Net Power 12,100 Btu/hr

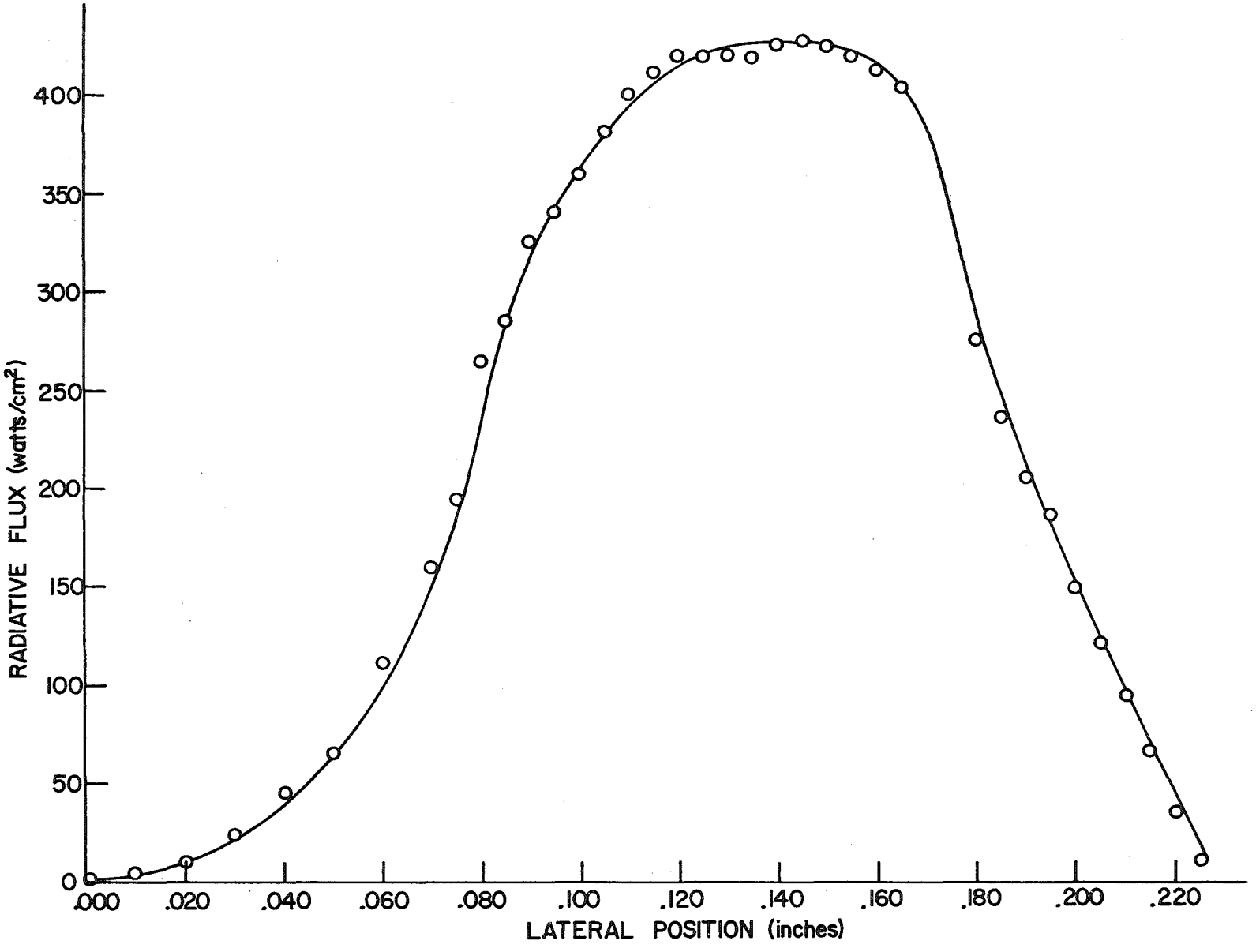

Fig. 5-13 Lateral Radiative Flux; Average Net Power 13,800 Btu/hr

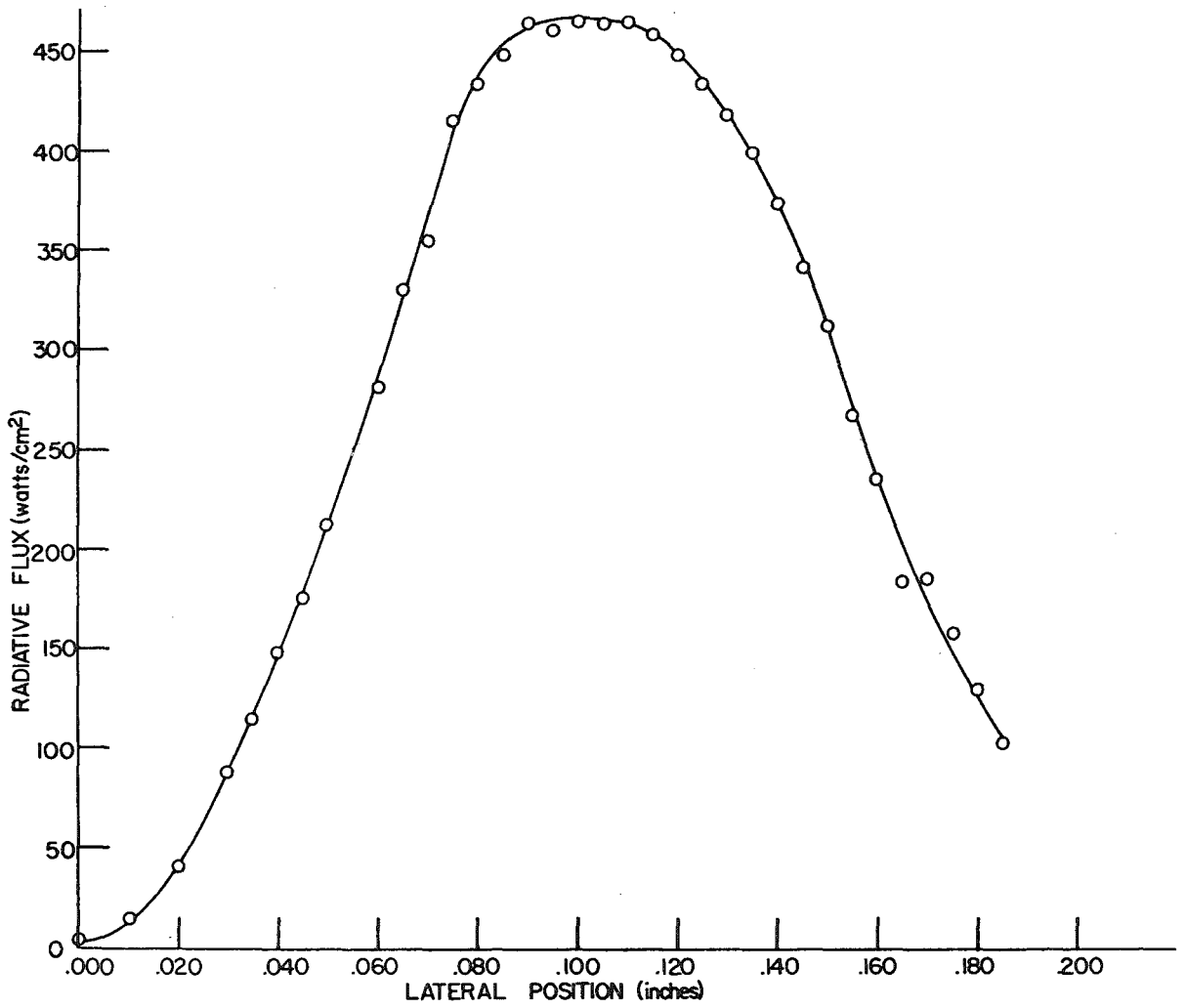

Fig. 5-14 Lateral Radiative Flux; Average Net Power 17,200 Btu/hr

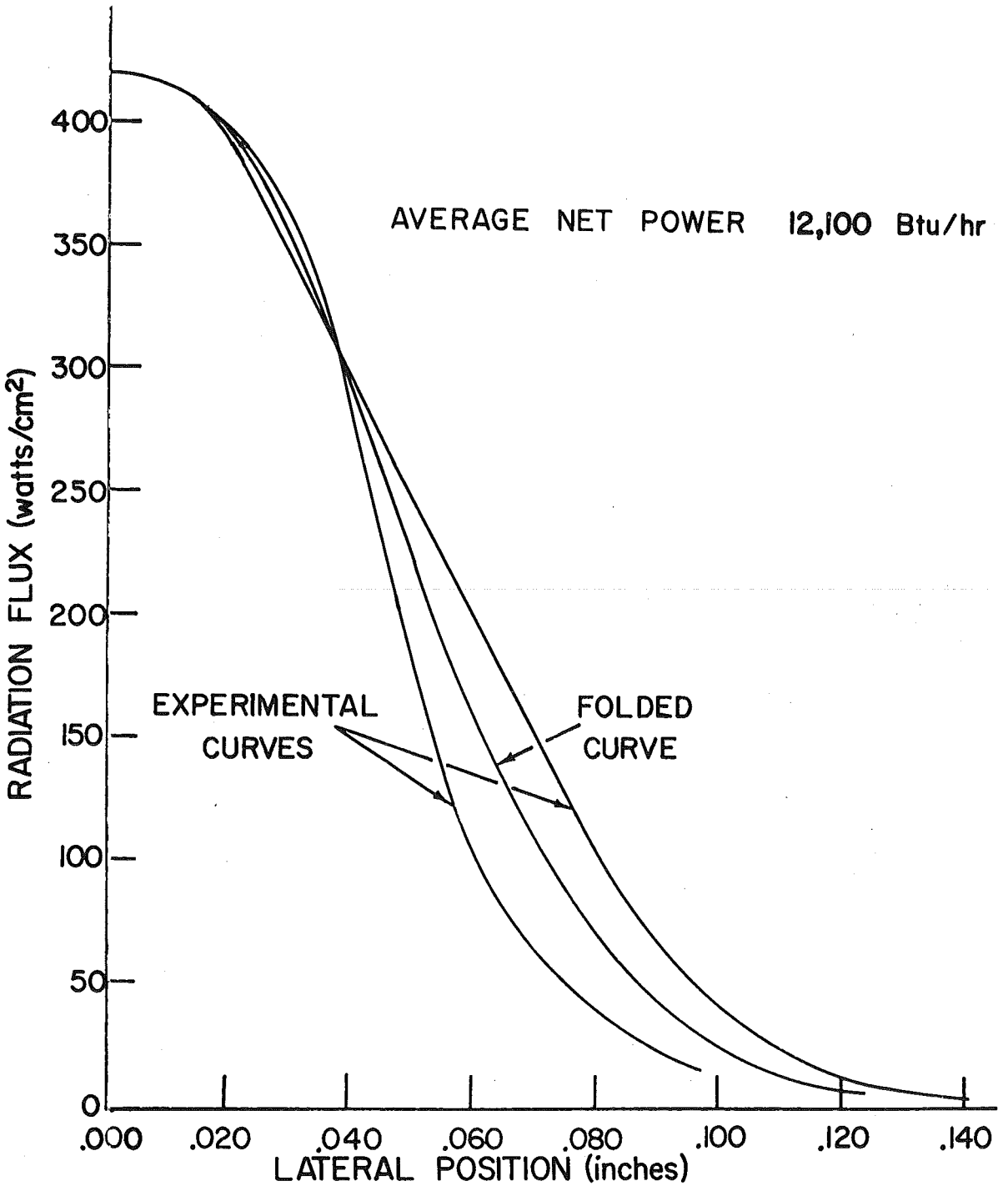

Fig. 5-15 Folded Lateral Radiative Flux

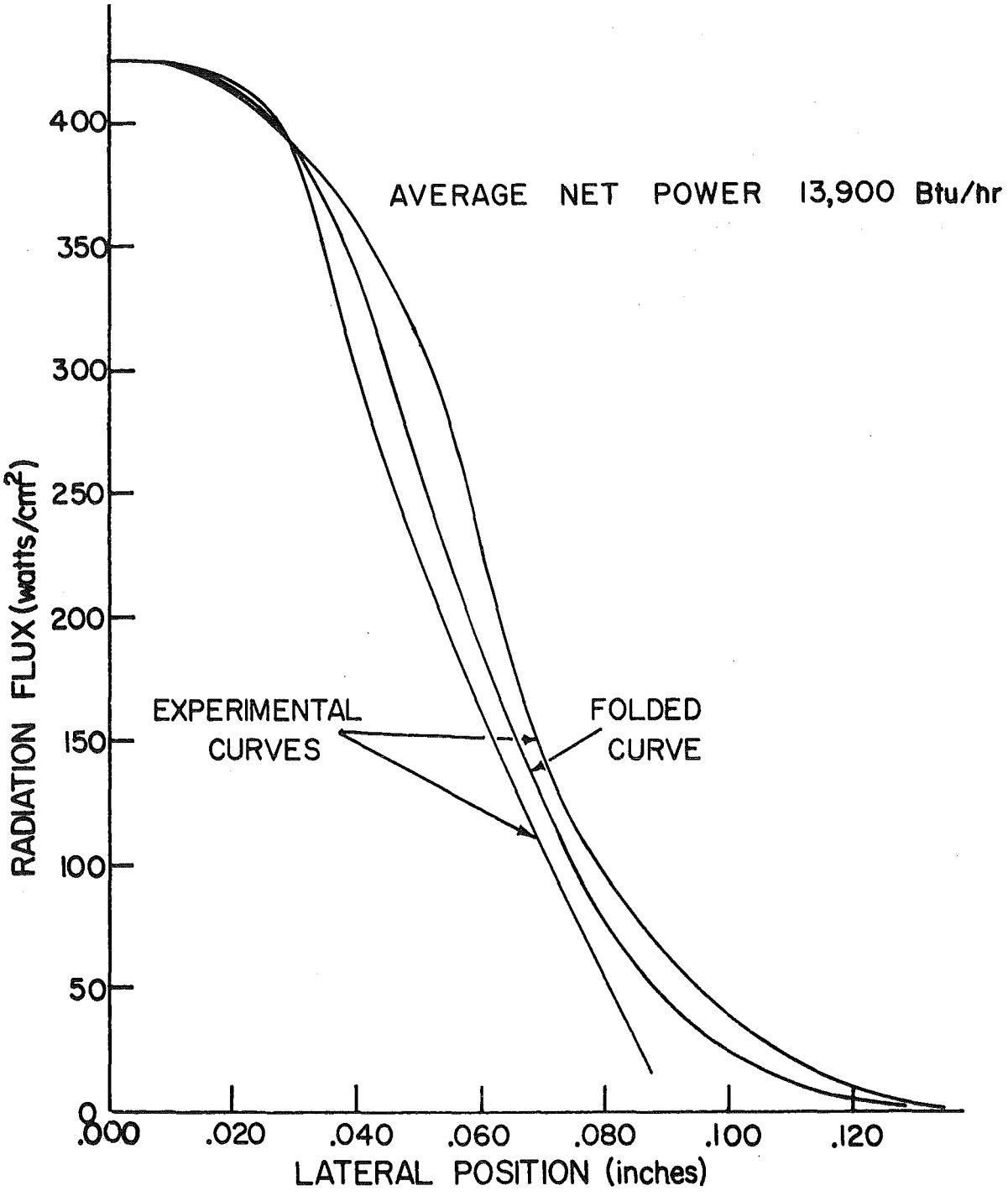

Fig. 5-16 Folded Lateral Radiative Flux

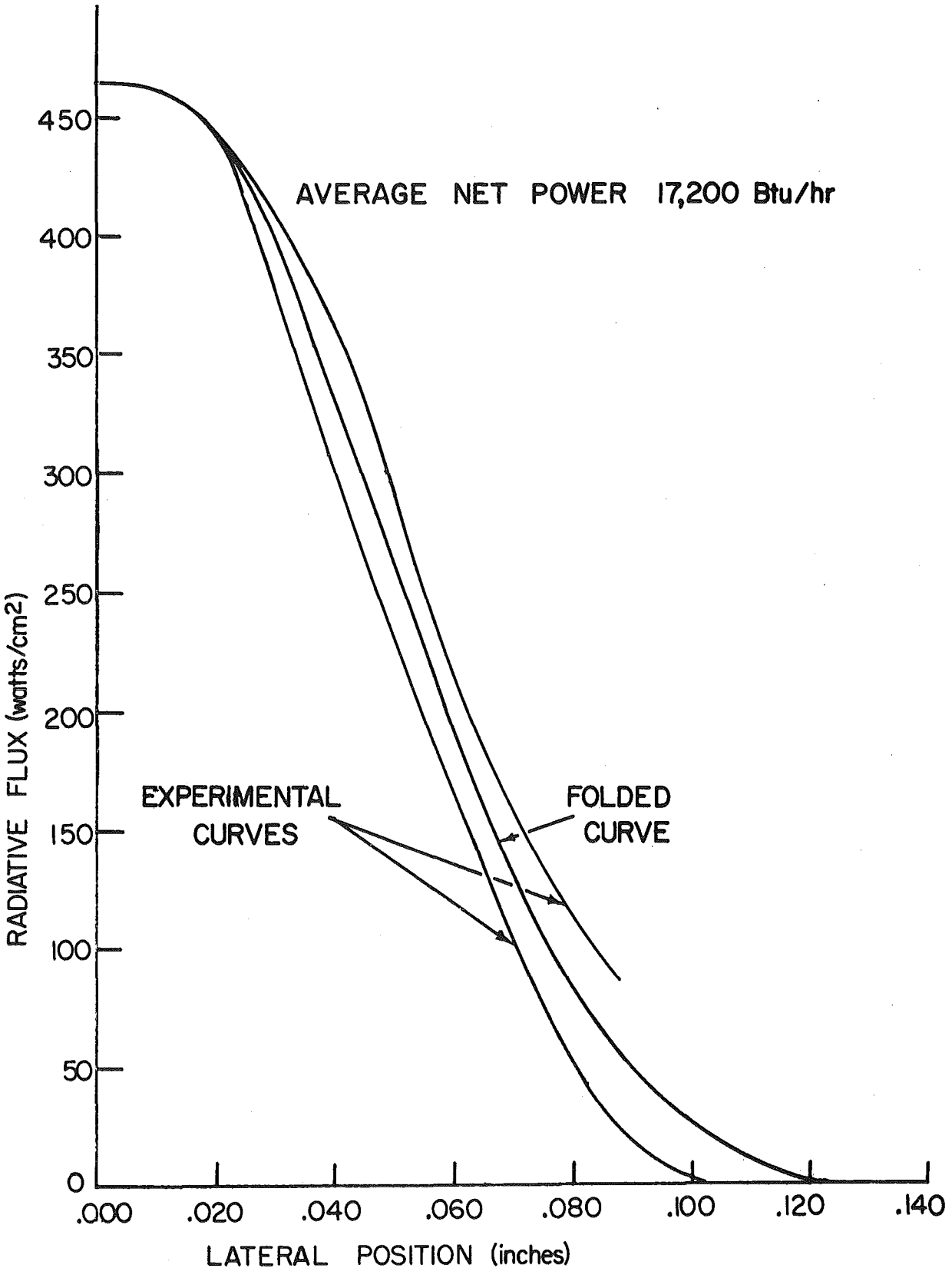

Fig. 5-17 Folded Lateral Radiative Flux

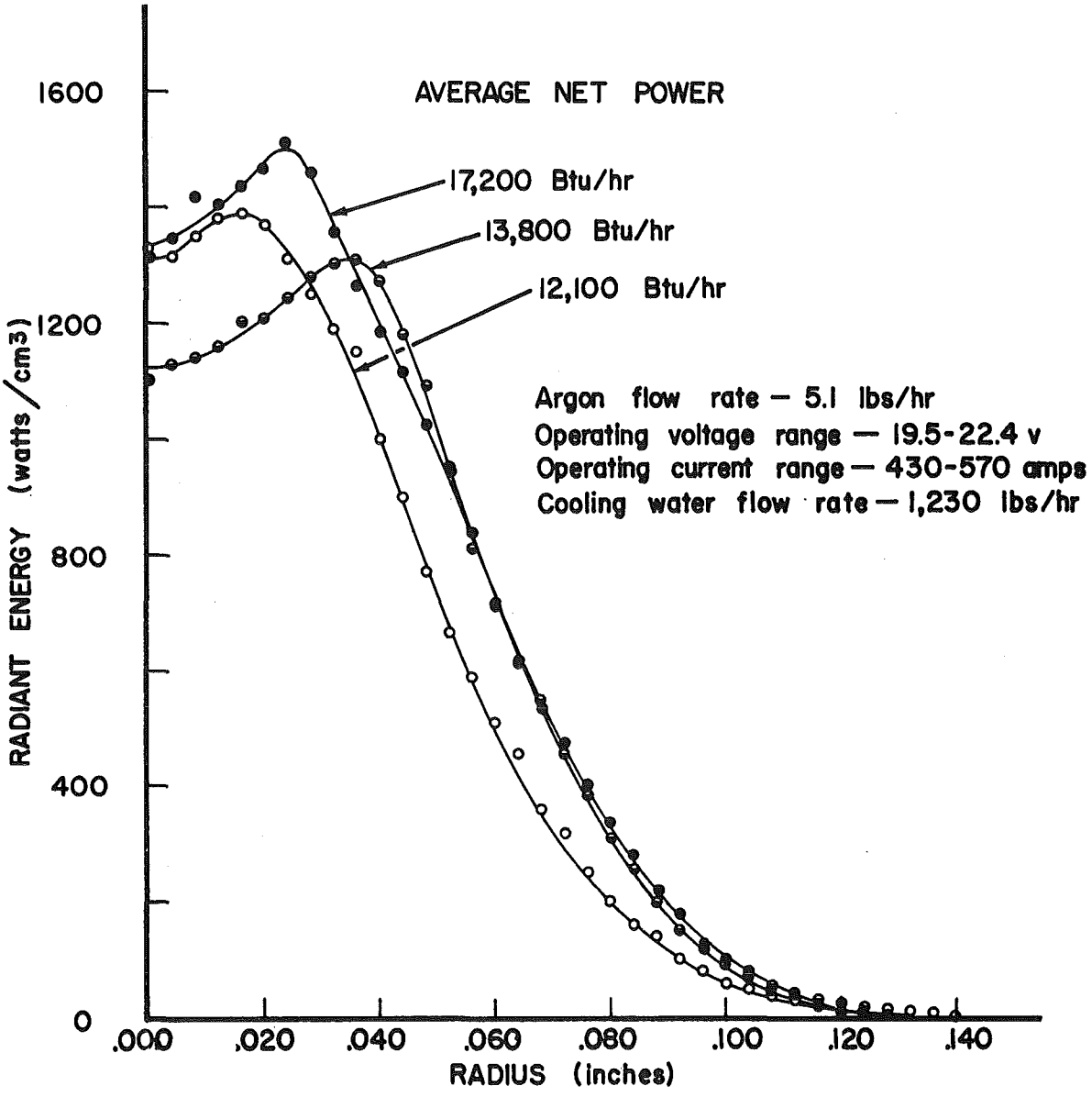

Fig. 5-18 Radiant Energy Transfer as a Function of Radius

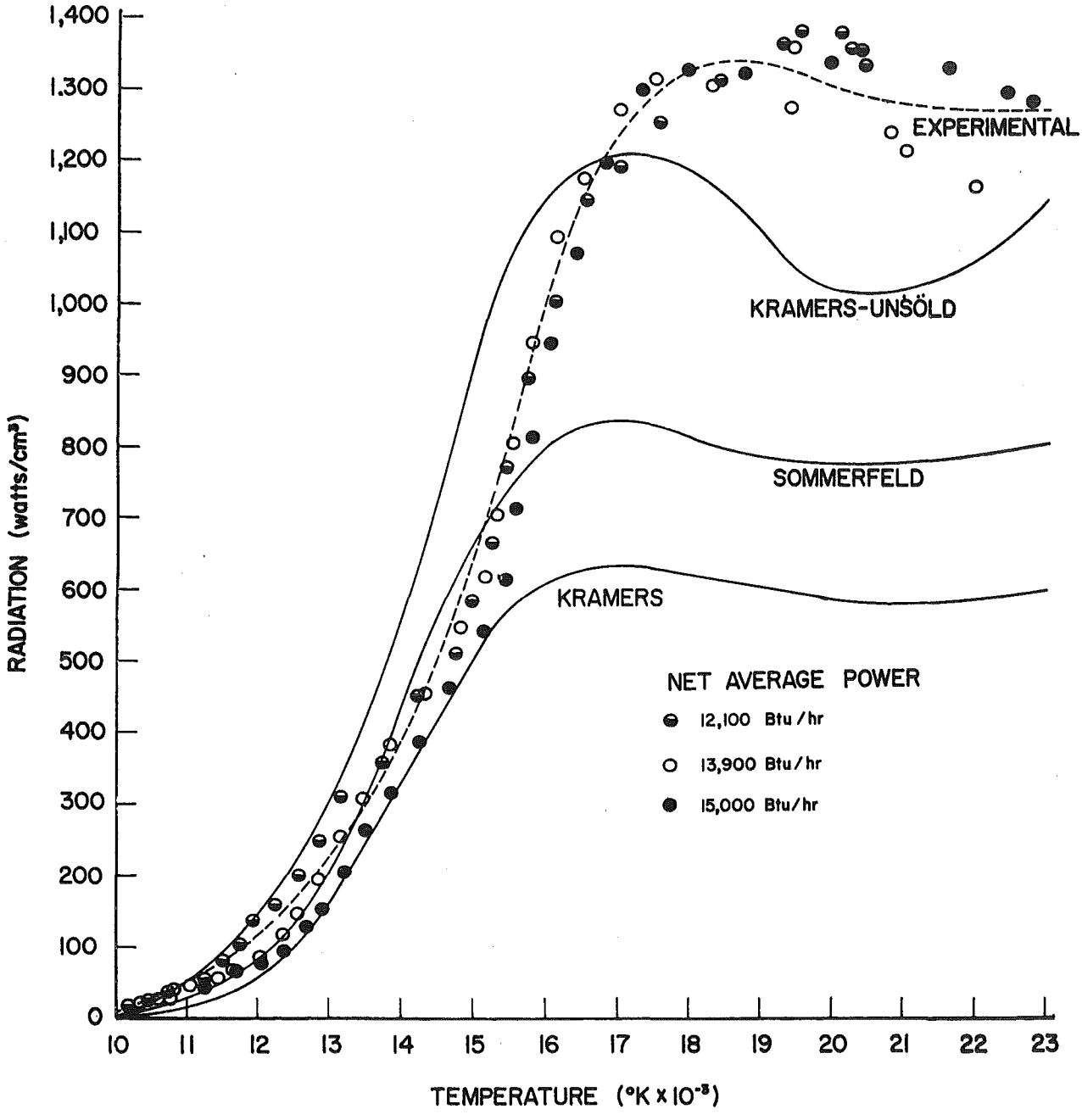

Fig. 5-19 Radiation from an Atmospheric Argon Plasma as a Function of Temperature

5.5 DISCUSSION OF RESULTS

About three minutes is required to make one traverse across the image of the plasma jet with the spectroscope. Since two traverses are required to determine the lateral spectral line intensity distribution, the plasma torch must operate with negligible power fluctuations for about seven minutes. Due to the fluctuations of the voltage drop across the plasma torch, it was very difficult to maintain steady operation of the torch for this length of time. In practice, as many as ten pairs of traverses were made before one pair was obtained during which the power remained nearly constant. Notice on Figure 5-2 the sudden jumps in the recorder chart trace between 8.25 min. and 8.50 min. This is an example of the difficulties caused by variations in the voltage drop across the plasma torch. In the case of this particular trace, the voltage was unsteady for only about ten seconds and then returned to its original value. A smooth curve was drawn through the unsteady region and the data were taken from this curve. If the voltage had settled to a new value following this disturbance, the traverse would have been useless.

The spectroscopic traces, Figures 5-2, 5-3, 5-4, and 5-5, show an asymmetry about the maximum. Some of this asymmetry is due to hysteresis in the recorder, but some is also caused by an asymmetry in the plasma jet. The latter effect is due to some misalignment of the nozzle over the electrode, which causes the arc to be distributed non-uniformly around the electrode. The effects of the asymmetry do not appear in the final results because of the folding procedure which was used. The

alignment of the nozzle was found to be very critical in reducing this asymmetry.

The data of the lateral radiative flux, Figures 5-12, 5-13, and 5-14, show some scatter in the data points and an asymmetry about the maximum. The scatter is due to voltage fluctuations. As about thirty minutes was required to make each of these traverses, it was impossible to avoid this scatter. The error introduced because of this scatter and the asymmetry shows up in Figure 5-18. Although it is difficult to determine the magnitude of this error, it does not appear to be prohibitive, judging from the results.

The final results shown in Figure 5-19 also exhibit scatter in the data points. This scatter is not severe except in the points above 19,000°K. This scatter and any error in the results are the accumulation of experimental errors and the errors incurred in the manipulation of the data. The experimental curve has been drawn by hand as the best apparent representation of the results. Due to the scatter of the points above 19,000°K, this portion of the curve cannot be considered as reliable as the portion below 19,000°K.

The experimental results indicate that both bremmstrahlung and recombination are important sources of the radiation emitted from an atmospheric argon plasma over the range of temperatures investigated. The Kramers-Unsöld model predicts the radiation emitted from an atmospheric argon plasma reasonably well from 10,000°K to 17,000°K.

There are several possible reasons for the discrepancy between the experimental data and the Kramers-Unsöld model. The extensive

experimental measurements and data processing necessary to arrive at the results increases the possibility of errors. Some of these errors show up as scatter in the data, but a systematic error could contribute to the discrepancy between the theoretical model and the experimental data. The cutoff frequency, which is not accurately known, has been assumed to be independent of temperature. Finally, the approach used of adding the radiation predicted by the Kramers model from the doubly ionized atoms to that predicted from the singly ionized atoms is probably not a good approximation.

A model, shown in Figure 5-20, was formulated to check the folding technique and method of inversion used to obtain the experimental curve on Figure 5-19. The section through the thickest portion of the plasma jet was divided into rectangular elements of volume 0.01 cm. thick having an area of one square centimeter. The value of the radiation at each radius was taken from the experimental curve on Figure 5-19. The contributions from the elements were added and the resulting value was compared with the maximum lateral radiative flux measured. The calculations are shown in Appendix F. The agreement with the measured values is good, which verifies the general method of arriving at the results.

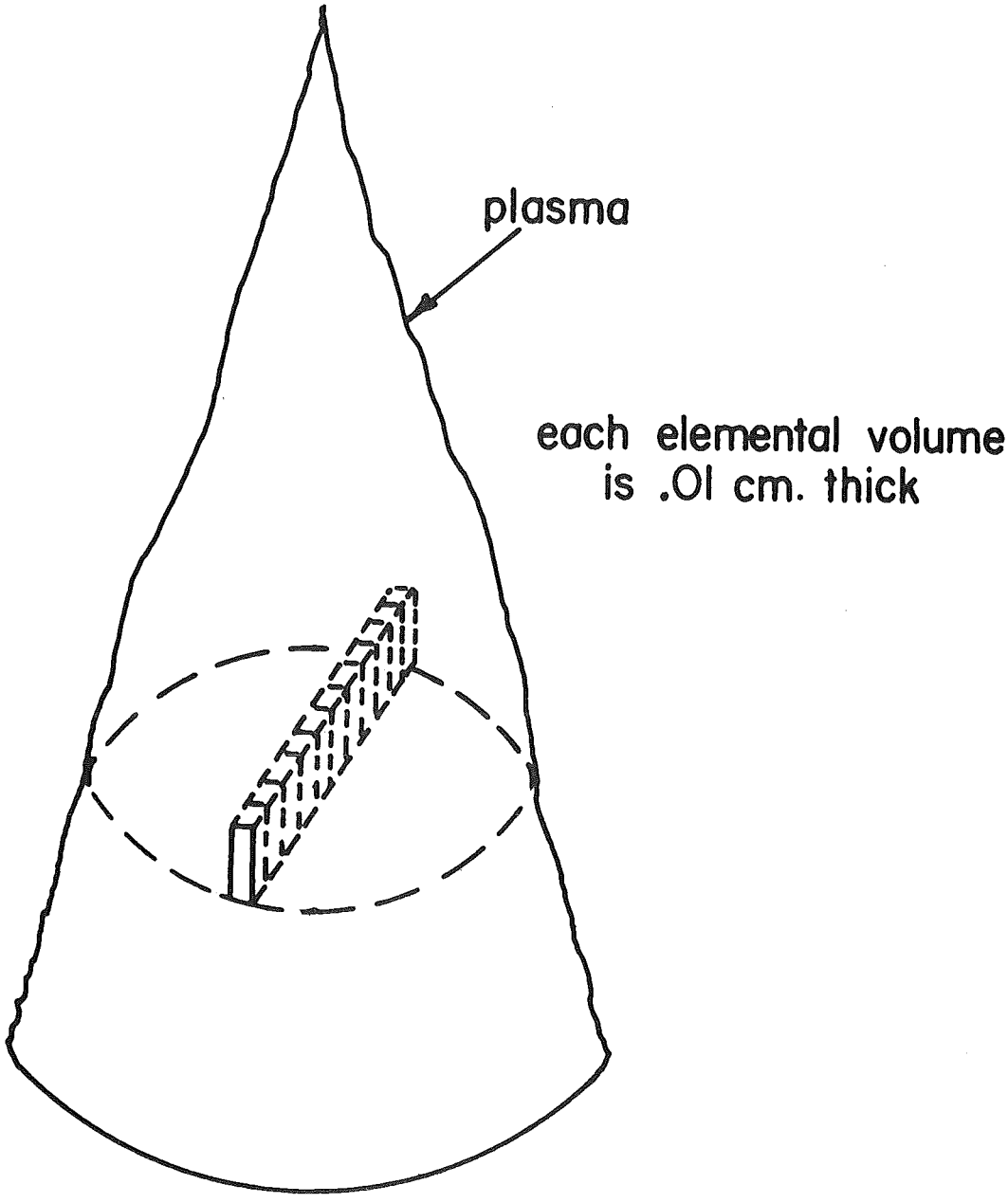

Fig. 5-20 Model used to Confirm Inverted Radiative Flux Data

CHAPTER 6

CONCLUSIONS

The first conclusion to be drawn from the experimental results is that radiation is an important mode of heat transfer from an argon plasma jet generated in a plasma torch and exhausted to atmospheric pressure. Radiant energy transfer from the argon plasma jet studied accounts for as much as 18 per cent of the net power input to the plasma.

The determination of the actual radiative heat transfer from the argon plasma and the plasma torch indicates that a large amount of energy is radiated from the core of plasma within the exit nozzle. The intensity of the radiation from the hot core of plasma greatly exceeds the intensity of the radiation from the plasma jet. This additional radiation is significant and must be considered in an overall energy balance about a plasma torch.

The energy radiated from an atmospheric nitrogen plasma jet is less than 1 percent of the net power input to the plasma, up to 100,000 Btu/hr net power input. The total radiation from a nitrogen plasma jet exhausted to the atmosphere is negligible for the flow rate and nozzle configuration investigated.

The radiation from an atmospheric argon plasma which is assumed to be in local thermodynamic equilibrium can be predicted reasonably well with the Kramers-Unsöld model from 10,000°K to 17,000°K.

The thermistor bolometer is well suited to measure the radiation emitted by a laboratory plasma. It is sensitive over a wide range of the spectrum and its calibration curve is linear. The measurements are made without disturbing the flow in the plasma jet.

BIBLIOGRAPHY

1. Servo Corporation of America, "Servotherm Thermistor Heat Detector Cells." Technical Bulletin TB 1300-6, Hicksville, L.I., N.Y.

2. Servo Corporation of America, "Properties of Infrared Transmitting Materials." Hicksville, L.I., N.Y.

3. Werneburg, J., "Untersuchung uber die Warmstrahlung von Flammen." Forschung auf dem Gebiete des Ingenieurwesens, Vol. 10, No. 2, 1939, pp. 61-79.

4. Cabot Corporation, "Carbon Black Pigments." Boston, Mass., June, 1961.

5. Oster, L., "Emission, Absorption, and Conductivity of a Fully Ionized Gas at Radio Frequencies." Reviews of Modern Physics, Vol. 33, No. 4, Oct., 1961, pp. 525-543.

6. Kramers, H. A., "On the Theory of X-Ray Absorption and of the Continuous X-Ray Spectrum." Philosophical Magazine and Journal of Science, Vol. 46, No. 275, Nov., 1923, pp. 836-871.

7. Pomerantz, J., "The Influence of the Absorption of Radiation in Shock Tube Phenomena." Navord Report 6136, Aug. 15, 1958.

8. Lochte-Holtgreven, W., "Production and Measurement of High Temperatures." Reports on Progress in Physics, Vol. 21, The Physical Society of London, 1958, pp. 312-383.

9. Bekefi, G. and S. C. Brown, "Emission of Radio Frequency Waves from Plasma." American Journal of Physics, Vol. 29, No. 7, July, 1961, pp. 404-428.

10. Drellishak, K. S., C. F. Knopp and A. B. Cambel, "Partition Functions and Thermodynamic Properties of Argon Plasma." Gas Dynamics Laboratory, Northwestern University, Report No. A-3-62, March, 1962.

11. Greene, J., "Bremsstrahlung from a Maxwellian Gas." AEC Research and Development Report, Princeton University, Nov. 3, 1958.

12. Olsen, H. N., "Partition Function Cutoff and Lowering of the Ionization Potential in an Argon Plasma." Physical Review, Vol. 124, No. 6, Dec., 1961, pp. 1703-1708.

13. Knopp, C. F., C. F. Gottschlich and A. B. Cambel, "A Spectroscopic Technique for the Measurement of Temperature in Transparent Plasmas." Gas Dynamics Laboratory, Northwestern University, Report No. B-2-61, ASTIA No. A.D.-277-360, July, 1961.

14. Compton, K. T., "Mobilities of Electrons in Gases." Physical Review, Vol. 22, No. 4, Oct., 1923, pp. 333-346.

15. Compton, K. T., "On the Motions of Electrons in Gases." Physical Review, Vol. 22, No. 4, Nov. 1923, pp. 432-446.

16. Cadek, F. C., "Measurement of Argon Transition Probabilities." M.S. Thesis, Northwestern University, June, 1963.

17. Enright, J. A., "A Spectroscopic Determination of Temperature and Velocity Distributions in an Argon Plasma Jet." M.S. Thesis, Northwestern University, June, 1963.

18. Nestor, O. H. and H. N. Olsen, "Numerical Methods for Reducing Line and Surface Probe Data." SIAM Review, Vol. 2, No. 3, July, 1960, pp. 200-207.

19. McAdams, Wm. H., Heat Transmission. McGraw-Hill Book Co., Inc., New York, Third Edition, 1954.

20. Hildebrand, F. B., Methods of Applied Mathematics. Prentice Hall Book Co., Englewood Cliffs, N.J., Jan., 1958.

15a. McGregor, W.K., "Spectroscopic Measurements in Plasmas", Physico-Chemical Diagnostics of Plasmas, ed. by T.P. Anderson, et. al., Northwestern University Press, 1964, pp. 143-146

APPENDIX A

EXPERIMENTAL APPARATUS AND PROCEDURE

A-1 PLASMA GENERATING FACILITY

A schematic layout of the plasma generating facility in the Northwestern Gas Dynamics Laboratory is shown in Figure A-1. Direct current power to operate the plasma torch is supplied by four Model SRH 444 Miller Electric Company arc welders. Each welder is capable of producing about ten kilowatts of d.c. power. The welders are arranged so that any number of units can be used to supply power to the torch. The units may be connected in series, in parallel, or in a series-parallel combination. A filter circuit is available which reduces the a.c. ripple in the welder output to less than one per cent of the nominal current. No change in the radiation from the plasma was observed in any of the experimental measurements upon incorporating the filters into the power circuit. The leads from the welders to the torch carry both the current and the cooling water. A high frequency starter manufactured by Thermal Dynamics Corporation is used to provide the breakdown voltage to initiate the arc. The welders are controlled by varying the voltage on the control windings of the transformers in the welders.

Water for cooling the torch is taken from the building supply. An auxiliary pump is available to increase the flow rate of the cooling water above that obtained using just tap pressure. This pump was not used in this experimental work. Nominal control of the water flow rate is provided by partially closing the shut-off valve from the building

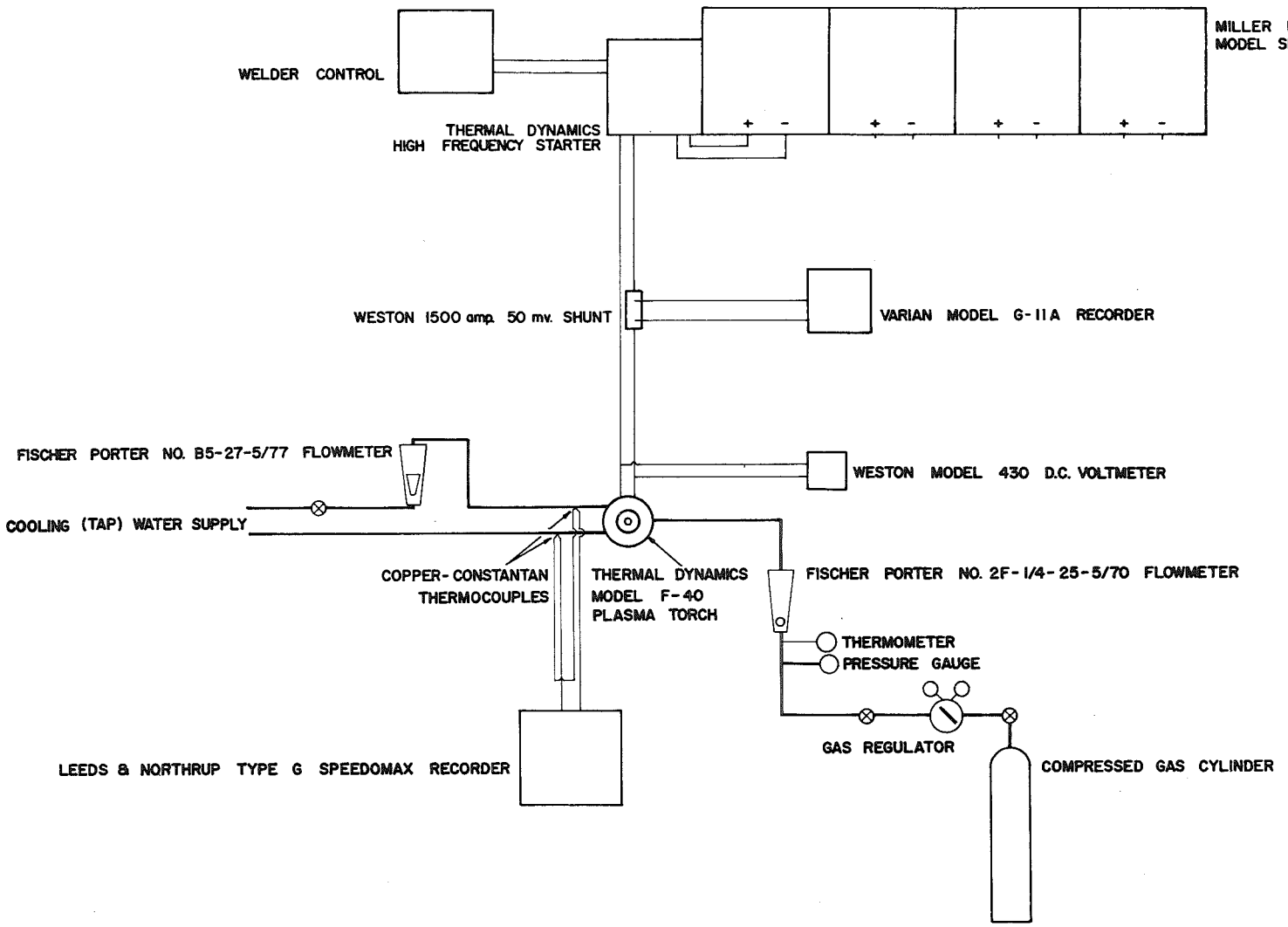

Fig. A-1 Plasma Generating Facility

supply.

The gas used to generate the plasma is supplied from ordinary high pressure cylinders. Gases of the highest purity available commercially were purchased from a local distributor of the Linde Company.

The entire plasma generating facility is operated from a remote control panel. Controls for the power supply--welders, filter circuit, and high frequency starter--as well as various gauges, flow meters, and recorders are housed in the control panel.

The d.c. current to the torch was determined by measuring the potential across a 1500 ampere 50 millivolt shunt manufactured by the Weston Electric Instrument Company which is in series with the power supply. This potential was measured with a Varian Associates, Inc., Model G 11 A strip chart recorder. The input resistance of this recorder has a minimum value of 1/2 megohm. The recorder was calibrated before each series of experimental runs using a Leeds and Northrup No. 8662 portable potentiometer. A typical recorder trace made during one of the experimental runs is shown in Figure A-2.

The voltage drop across the torch was measured with a Model 430 Weston voltmeter. Clip leads from this voltmeter were connected directly across the torch. With this arrangement, the voltmeter measures only the voltage drop across the plasma torch and does not include the voltage drop in the electrical leads from the welders to the torch.

Determination of the power loss from the torch to the cooling water was accomplished by measuring the flow rate of the cooling water and its temperature rise. The flow rate was measured with a Fischer

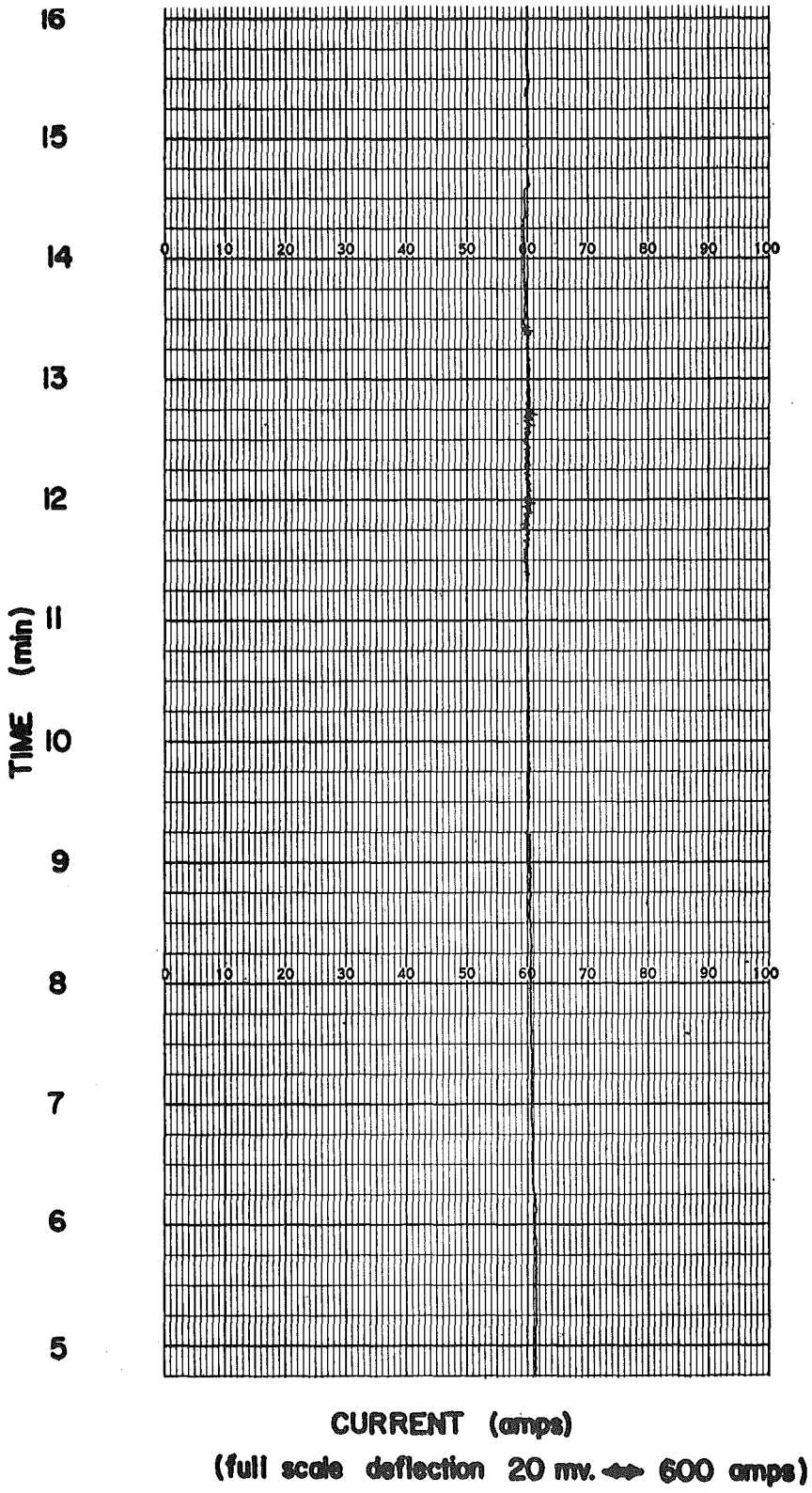

Fig. A-2 Typical Current Recorder Plot

Porter No. B5-27-5/77 rotameter located in the control panel. The temperatures of the incoming and outgoing cooling water were measured with copper-constantan thermocouples. The thermocouples, mounted in capillary glass tubing sealed with wax, were inserted in the water pipes directly upstream and downstream of the torch. The constantan leads from the thermocouples were commoned so that the e.m.f. between the copper leads was proportional to the temperature rise of the cooling water. This e.m.f. was measured with a Leeds and Northrup Type G Speedomax recording potentiometer. A typical trace made by the thermocouple recorder during one of the experimental runs is shown in Figure A-3.

The flow rate of the gas used to generate the plasma was measured with a Fischer Porter No. 2F-1/4-25-5/70 Tri-Flat variable area flow meter located in the control panel. A stainless steel float was used in the flow meter. The pressure and temperature of the incoming gas were indicated by gauges mounted in the control panel.

The seeder used to seed the plasma jet is a Sylco CCC Mark VII fine powder feeder manufactured by Sylvester and Company. In the seeder, the powder is metered from a vibrating storage tank by a feed screw to a carburetor where it is dispersed in the carrier gas stream. The feed screw has a variable speed drive which allows continuous adjustment of the powder feed rate from zero up to the maximum feed rate. A #57x51 nozzle insert manufactured by Thermal Dynamics Corporation was used in the plasma torch when seeding the plasma jet. This nozzle has a small hole through which the carrier gas and powder are injected radially

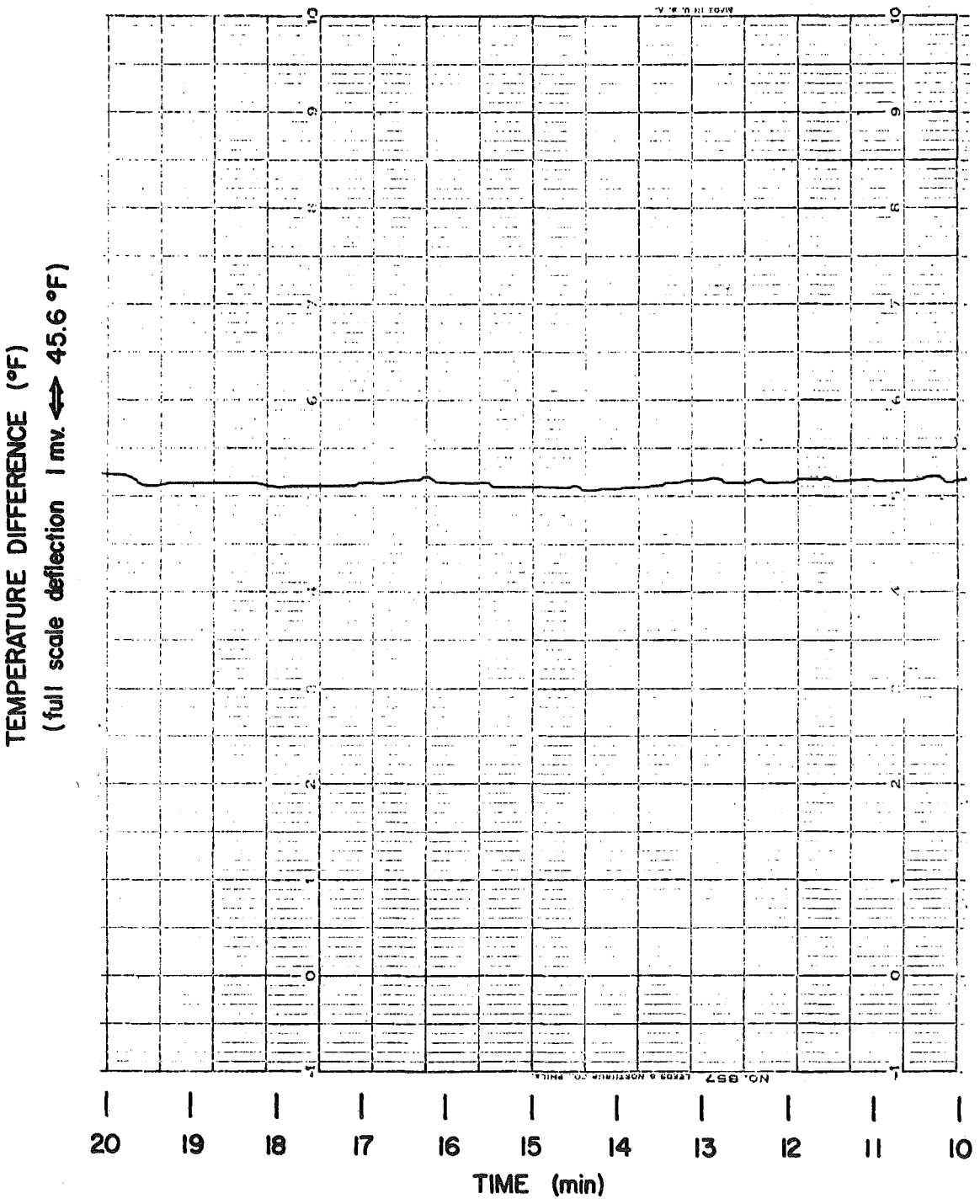

Fig. A-3 Typical Temperature Recorder Plot

into the plasma jet.

The carbon particles with which the plasma jet was seeded are manufactured by Cabot Corporation under the name of Supercarbovar. The particles have a mean diameter of 1.4×10^{-8} m. (Ref. 4). The same high purity argon used to generate the plasma was used as a carrier gas through the seeder.

A-2 EXPERIMENTAL PROCEDURE

The following start-up procedure was used at the beginning of each experimental run. The bolometer power supplies were turned on and, after a warm-up period of about one minute, the noise level in the bolometer circuit was read on the output voltmeter. No experimental measurements were made when the noise level exceeded three millivolts. The electrical current recorder and the thermocouple recorder were positioned with the recording pens on a unit interval chart line, and the charts were titled with a run number. The current recorder was calibrated at the beginning of each series of experimental runs. Since the thermocouple recorder has an internal calibration circuit it required only occasional calibration.

The gas supply to the torch was turned on and the pressure was adjusted with the gas regulator to 80 p.s.i.g. The cooling water was turned on and the flow rate was adjusted to the desired value. A flow rate was chosen which would give a maximum temperature rise of about 25°F.

The gas flow rate through the torch was set at its maximum value

of about 12 lbs/hr. With the main power to the torch turned off, the high frequency starter was held on. The ring of spark produced by the starter in the annular region between the electrode and nozzle was observed through the exit nozzle in a mirror held above the torch. The position of the nozzle over the electrode was adjusted so that the spark was evenly distributed around the electrode. The gas stream issuing from the exit nozzle was checked visually for water droplets which would indicate a water leak in the torch. In the absence of a water leak, the main power to the torch was turned on. The arc was struck by pressing the starter switch momentarily. The gas flow rate was then reduced to the desired operating value.

With the torch in operation, the clip leads from the Weston voltmeter were connected across the torch. The current recorder and a stopwatch were started simultaneously. One minute later the thermocouple recorder was started. After a final check of all of the instruments, the experimental readings were begun.

The gas temperature, pressure, and flow rate, and the cooling water flow rate were recorded at the beginning and end of each experimental run. The gas pressure and flow rate were observed to remain constant during the runs. The gas temperature was observed to drop very gradually during the runs. This is due to the cooling accompanying the expansion of the gas in the high pressure cylinder. This temperature drop was never more than $3^{o}F$ during an experimental run. The cooling water flow rate was observed to fluctuate randomly $\pm$ 5 per cent. The values of the gas pressure and flow rate used in the calculations

were those recorded at the beginning of each run. The average of the gas temperature at the beginning and end of each run was used in the calculations. The mean value about which the flow rate of the cooling water fluctuated was used in the calculations. This mean value did not vary during an experimental run.

APPENDIX B

CALIBRATION OF BOLOMETER

B-1 CALIBRATION APPARATUS

The bolometer was calibrated using a black surface of known temperature. The calibration for the total radiation measurements was accomplished by heating a hollow copper cone in a Hevi-Duti Type 62 electric furnace. The cone, shown in Figure B-1, was located so that its interior surface was visible from outside the furnace through a hole in the end of the furnace. Due to repeated heating and cooling, a heavy scale of copper oxide was formed on the entire surface of the cone, rendering it a nearly black surface. Iron-constantan thermocouples were located along the length of the cone in such a way that the temperature of the area of the cone viewed by the bolometer was known. A radiation shield made of asbestos board served to define the area from which the radiation was emitted and to shield the bolometer from the stray radiation emitted by the warm exterior surface of the furnace. A vertical copper plate was used as a radiation source to calibrate the bolometer for use with the optical systems which are described below. Its temperature was also measured with an iron-constantan thermocouple. The vertical copper plate served to define a focal plane for the optical systems. The thermocouple potentials were measured with the Leeds and Northrup No. 8662 portable potentiometer. The electric furnace has a maximum operating temperature of 1850°F.

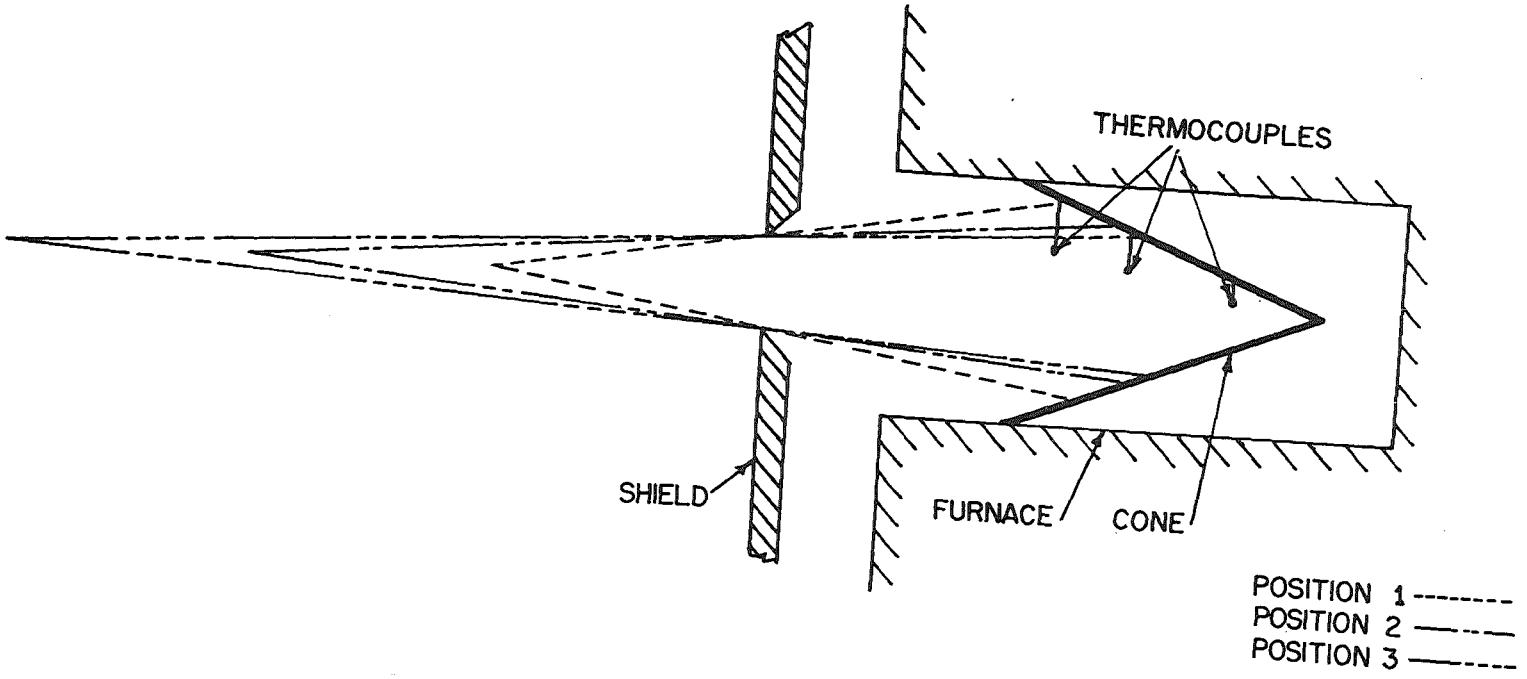

Fig. B-1 Experimental Set-Up for Total Radiation Calibration (vertical scale magnified 8 fold)

B-2 CALIBRATION OF BOLOMETER FOR TOTAL RADIATION MEASUREMENTS

Consider an element of black surface, dA_1, radiating in all directions from one side. Some of this radiation is intercepted by black element, dA_2, at a distance r from dA_1. The line connecting these two surface elements forms angles ϕ_1 and ϕ_2 with the normals to dA_1 and dA_2, respectively. The rate of radiant energy transfer, dq_{1-2}, from dA_1 to dA_2 is (Ref. 19)

$$dq_{1-2} = \frac{I_1 \, dA_1 \cos\phi_1 \; dA_2 \cos\phi_2}{r^2} \tag{B-1}$$

I_1 is the intensity of radiation from element dA_1. The elemental solid angle subtended by dA_2 at dA_1 is

$$d\omega_1 = \frac{dA_2 \cos\phi_2}{r^2}$$

Substituting, Eq. B-1 becomes

$$dq_{1-2} = I_1 \, dA_1 \cos\phi_1 \, d\omega_1 \tag{B-2}$$

The rate of radiant energy transfer, dq_1, from dA_1 in all directions is found by integrating over the complete hemispherical angle above dA_1

$$\frac{dq_1}{dA_1} = I_1 \int_0^{2\pi} \cos\phi_1 \, d\omega_1 \tag{B-3}$$

The quantity on the left hand side of Eq. B-3 is, by definition, the

emissive power of the black surface dA_1

$$W_1 = \sigma T_1^4 = \frac{dq_1}{dA_1}$$

where σ is the Stefan-Boltzmann constant, 0.1713×10^{-8} Btu/hr ft^2 $^oR^4$

T_1 is the temperature of black surface A_1 (^oR)

The quantity on the right hand side of Eq. B-3 may be integrated by noting that, due to the symmetry of the problem,

$$d\omega_1 = \frac{2\pi r \sin\phi_1 \, r\, d\phi_1}{r^2} = 2\pi \sin\phi_1 \, d\phi_1$$

Substituting these quantities into Eq. B-3

$$\sigma T_1^4 = I_1 \int_0^{\pi/2} 2\pi \cos\phi_1 \sin\phi_1 \, d\phi_1$$

$$= I_1 \frac{1}{2} \sin^2\phi_1 \Big|_0^{\pi/2}$$

$$= I_1 \pi$$

Thus the proportionality constant in Eq. B-1 for a black surface element, dA_1, is

$$I_1 = \frac{\sigma T_1^4}{\pi}$$

Eq. B-1 may now be used to evaluate the radiant heat transferred through an imaginary surface, A_2, at a distance r from a black surface A_1. For the purpose of calibrating the bolometer, the black surface, A_1, was taken as the hole in the radiation shield in front of the hot

black surface of the interior of the cone. The object is to find the radiative flux, F, at the bolometer element at distance r from the hole in the radiation shield. Since the bolometer was positioned on the axis of the cone, and since the plane of the radiation shield was perpendicular to the axis of the cone,

$$\phi_1 \cong 0°, \quad \phi_2 \cong 0°$$

For a distance r from the hole to the bolometer element much greater than the radius, r_1, of the hole in the radiation shield

$$\phi_1 = 0°$$

Likewise, since the bolometer element is very small (0.5 mm x 0.5 mm)

$$\phi_2 = 0°$$

Eq. B-1 becomes

$$dq_{1-2} = \frac{\sigma T_1^4}{\pi} \frac{dA_1\, dA_2}{r^2} \tag{B-4}$$

In order to find the radiative flux at the bolometer element due to the radiation from the entire area, A_1, of the hole, Eq. B-4 is integrated

$$\int \frac{dq_{1-2}}{dA_2} = \frac{\sigma T_1^4}{\pi} \int dA_1$$

However, since the bolometer element is very small, dA_2, may be taken as the area, δA_2, of the bolometer element. Performing the integration

$$\frac{q_{1-2}}{\delta A_2} = \frac{\sigma T_1^4 A_1}{\pi r^2} \qquad \text{(B-5)}$$

The quantity on the left of Eq. B-5 is recognized as the radiative flux, F, at the bolometer element. Thus, the calibration equation is

$$F = \frac{\sigma T_1^4 A_1}{\pi r^2} \qquad \text{(B-6)}$$

where F is the radiative flux at the bolometer element (Btu/hr ft^2)

σ is the Stefan-Boltzmann constant, 0.1713 x 10^{-8} Btu/hr ft^2 $^oR^4$

T_1 is the temperature of the black surface (^oR)

A_1 is the area of the black surface (ft^2)

r is the distance from the bolometer element to the black surface (ft)

As an example, one of the calibration points taken supplied the following data:

temperature of surface of cone in view of bolometer, 1,235^oF

distance from bolometer element to radiation shield, 24 in.

diameter of hole in radiation shield, 21/32 in.

bolometer output signal, 19.8 mv

Using Eq. B-6 to find the flux at the bolometer element,

$$F = \frac{(0.1713 \times 10^{-8})(1235 + 460)^4(\pi)(1/4)(0.656/12)^2}{\pi(24/12)^2}$$

$$= 2.64 \text{ Btu/hr ft}^2$$

To find the calibration value, the flux at the bolometer element is divided by the corresponding bolometer output signal in volts, giving

$$\frac{2.64 \text{ Btu/hr ft}^2}{1.98 \times 10^{-2} \text{ volts}} = 133 \text{ Btu/hr ft}^2 \text{ volt}$$

Figure B-2 shows the calibration data which were taken by Dowdy and Bowman.* The data were taken with the bolometer at three positions along the axis of the cone. The temperature of the cone was detected by three thermocouples, located as shown in Figure B-1. The scatter of the points on Figure B-2 is due to the fact that the temperature of the cone was not constant along its length. Referring to Figure B-1, the area of the cone viewed by the bolometer in position 1 is predominantly in the vicinity of thermocouple 1, while the area of the cone viewed by the bolometer in positions 2 and 3 is predominantly in the vicinity of thermocouple 2. Using only these data points, a straight line was drawn through the points as shown in Figure B-3. This is the calibration curve which was used for all of the total radiation measurements. This value for the calibration was checked several times over the months during which the experimental data were taken. The calibration value was always found to be within one per cent of that originally determined as shown in Figure B-3. The sample calculation of a calibration value shown above was taken from one of the later calibration checks.

*Research Assistants, Department of Mechanical Engineering, Northwestern University.

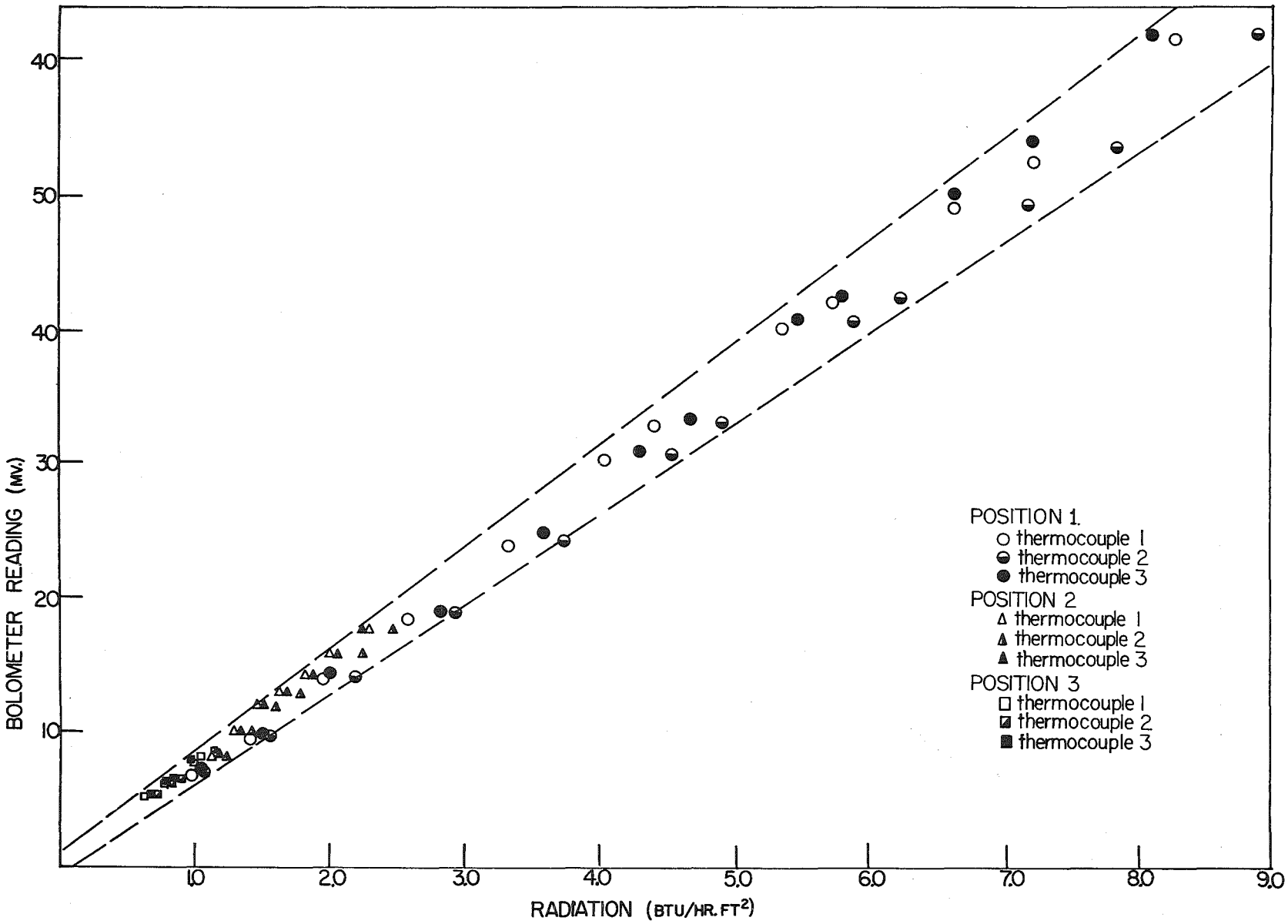

Fig. B-2 Calibration of Bolometer for Total Radiation

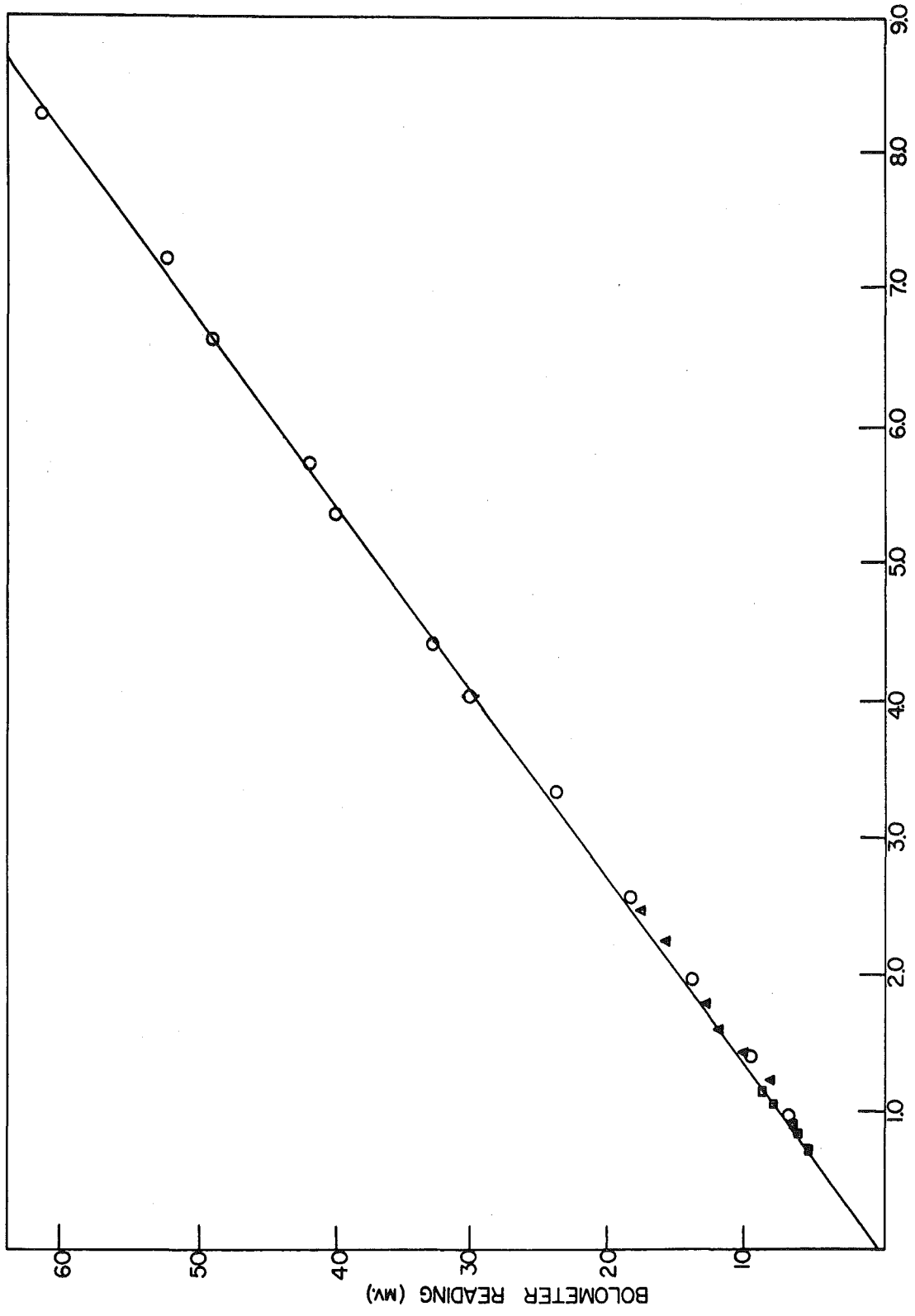

Fig. B-3 Calibration Curve for Total Radiation

B-3 CALIBRATION OF BOLOMETER FOR USE WITH OPTICAL SYSTEMS

The calibration of the bolometer for use with the optical systems shown in Figures 3-7 and 5-11 was somewhat simpler than the calibration technique used for total radiation measurements. For calibration with the optical systems, the copper plate was used as a radiation source in the furnace. The furnace and copper plate were positioned such that the plane of the copper plate defined one focal plane of the optical system. With the bolometer element in the other focal plane of the optical system, the bolometer element is effectively placed directly on the surface of the copper plate. Due to this fact, it is unnecessary to take into account the angular distribution of the radiation from the black surface as was done in Section B.2. Considering the copper plate as a black surface at temperature T, the radiative flux at the surface of this copper plate is σT^4. Dividing the value of the radiative flux at the surface of the plate by the corresponding output signal of the bolometer gives the calibration value. This calibration value already includes any effects of absorption within the optical system.

As an example, the data from one of the calibration points using the 5:1 magnification optical system shown in Figure 5-11 were as follows:

temperature of copper plate, 1,588°F

bolometer output signal, 31 mv

The radiative flux at the surface of the copper plate is

$$\sigma T^4 = (0.1713 \times 10^{-8})(1588 + 460)^4 = 2.96 \times 10^4 \text{ Btu/hr ft}^2$$

The calibration value is found by dividing the radiative flux at the

surface of the plate by the bolometer output signal in volts

$$\frac{2.96 \times 10^{4} \text{ Btu/hr ft}^2}{3.1 \times 10^{-2} \text{ volts}} = 0.96 \times 10^{6} \text{ Btu/hr ft}^2 \text{ volt}$$

The calibration curves obtained for use with the optical systems are shown in Figures B-4 and B-5.

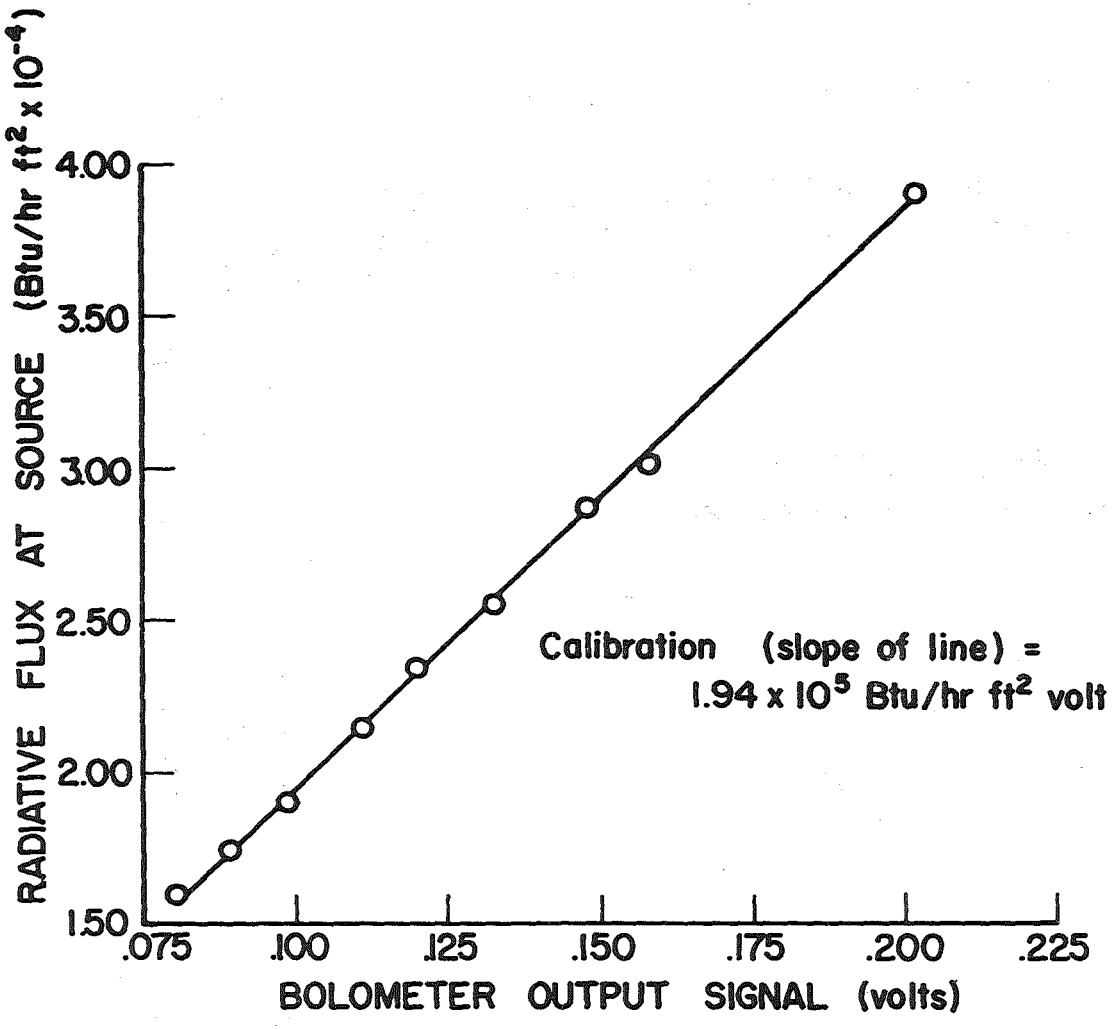

Fig. B-4 Calibration of Bolometer for Pointwise Measurements (2:1 magnification)

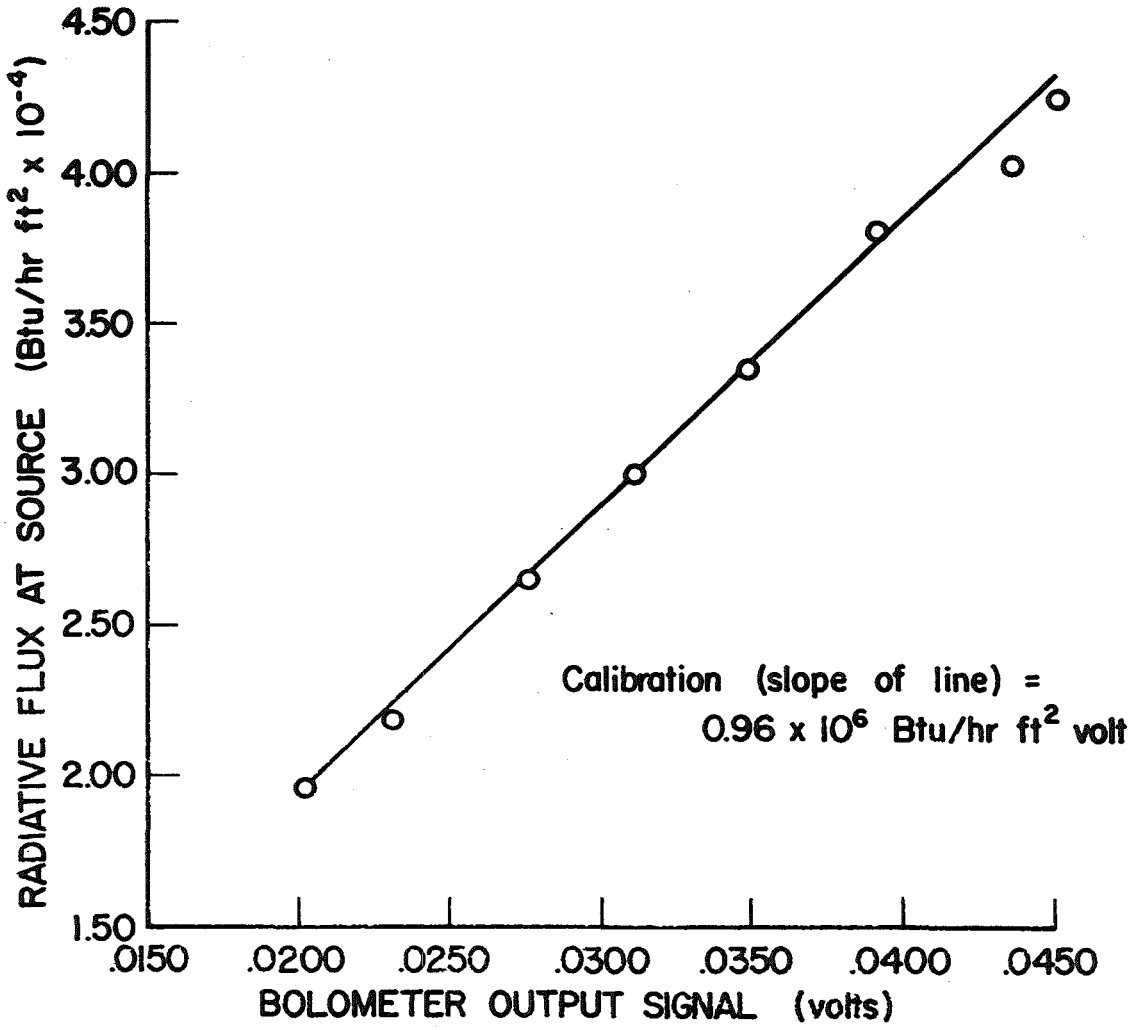

Fig. B-5 Calibration of Bolometer for Pointwise Measurements (5:1 magnification)

APPENDIX C

SAMPLE CALCULATIONS OF RESULTS IN CHAPTER 3

C-1 CALCULATION OF TOTAL RADIATION FROM PLASMA JET

One of the total radiation points shown on Figure 3-3 was calculated from the following data:

distance from bolometer to plasma jet 40 3/8 in.

voltage drop across plasma torch 21.8 v

cooling water flow rate 825 lbs/hr

current to torch 348 amps

cooling water temperature rise 15.7°F

bolometer output signal 77 mv

The gross power input to the torch is

$$(348 \text{ amps})(21.8 \text{ volts}) = 7{,}590 \text{ watts}$$

$$(7{,}590 \text{ watts})(3.415 \text{ Btu/watt hr}) = 25{,}900 \text{ Btu/hr}$$

The power loss to the cooling water is

$$(825 \text{ lbs/hr})(1.0 \text{ Btu/lb } ^\circ\text{F})(15.7 \ ^\circ\text{F}) = 12{,}900 \text{ Btu/hr}$$

The net power input to the plasma is

$$25{,}900 \text{ Btu/hr} - 12{,}900 \text{ Btu/hr} = 13{,}000 \text{ Btu/hr}$$

The area of the sphere on which the bolometer element lies is

$$4\pi \left(\frac{40.6 \text{ in}}{12 \text{ in/ft}} \right)^2 = 144 \text{ ft}^2$$

The radiative flux at the bolometer element is

$$(0.077 \text{ volts})(133 \text{ Btu/hr ft}^2 \text{ volt}) = 10.2 \text{ Btu/hr ft}^2$$

The total power radiated from the plasma jet (radiant power crossing the sphere in Figure 3-1) is

$$(144 \text{ ft}^2)(10.2 \text{ Btu/hr ft}^2) = 1,470 \text{ Btu/hr}$$

The per cent net power radiated is

$$\frac{1,470 \text{ Btu/hr}}{13,000 \text{ Btu/hr}} (100\%) = 11.3\%$$

C-2 CALCULATION OF TOTAL RADIATION FROM POINTWISE DATA

One of the experimental runs from which pointwise radiation data was taken was made under the following conditions:

optical system, two-fold magnification

average net power input, 11,300 Btu/hr

height of image of plasma jet, 2 1/8 in.

The diameter of the base of the cone, Figure 3-9, was taken as 5/16 in., the diameter of the exit nozzle opening. Radiation readings were taken at 1/8 in. vertical increments along the axis of the image of the plasma jet. As an example, consider the reading which was taken at a height of 1/2 in. along the centerline of the plasma jet. The area of a frustum of a right circular cone having a radius r_1 of the base and r_2 of the top and an altitude h is

$$\pi(r_1 + r_2) \times \sqrt{h^2 + (r_1 - r_2)^2}$$

Considering a vertical section through the axis of the conical plasma jet, the data for this example are found by considering the similar triangles

$$\frac{5/32}{17/16} = \frac{r_1}{17/16 - 15/32}$$

$$r_1 = 0.087 \text{ in}$$

$$\frac{5/32}{17/16} = \frac{r_2}{17/16 - 17/32}$$

$$r_2 = 0.078 \text{ in}$$

The height of the frustum under consideration in the plasma jet is 1/16 in. The area of this frustum is

$$\pi(.087 + .078)\sqrt{(.063)^2 + (.087 - .078)^2} = 0.033 \text{ in}^2$$

The bolometer output signal at this point was 3.9 volts (see Figure 3-8). Using the calibration value from Figure B-4, the radiative flux at the surface of the plasma jet at the vertical midpoint of this frustum of the cone is

$$(3.9 \text{ volts})(1.94 \times 10^5 \text{ Btu/hr ft}^2 \text{ volt}) = 7.6 \times 10^5 \text{ Btu/hr ft}^2$$

The radiant power crossing the surface of this frustum of the cone is

$$\left(\frac{0.033\ in^2}{144\ in^2/ft^2}\right)(7.6 \times 10^5\ Btu/hr\ ft^2) = 173\ Btu/hr$$

The total radiation from the cone was calculated by adding the contribution from each frustum of the cone, calculated as in the example above. The average net power input to the plasma was calculated by averaging the net power input at each radiation reading. The per cent net power radiated from the plasma jet was calculated by dividing the total radiation from the cone by the average net power input to the plasma.

C-3 CALCULATION OF ACTUAL RADIATIVE HEAT TRANSFER

The actual radiative heat transfer from the plasma and torch was calculated using the data on the angular distribution of the radiation from the torch by imagining the bolometer element to lie on a sphere whose center is the center of rotation of the plasma jet. The data were taken with the bolometer 47 5/8 in. from the center of rotation. As an example, consider the radiation reading taken at a viewing angle of 20°. The readings were taken at 5° increments at the higher intensities. The reading at 20° is considered to lie in the center of the area of the sphere included between the viewing angles of 17.5° and 22.5°. The area of a spherical segment of height h of a sphere of radius r is

$$2\pi rh$$

In terms of the quantities known in the experiment

$$h = r(1 - \cos\theta)$$

where θ is the viewing angle. The area of the spherical segment between the viewing angles of 0° and 17.5° is

$$2\pi\left(\frac{47.6 \text{ in}}{12 \text{ in/ft}}\right)^2(1 - \cos 17.5^\circ) = 4.55 \text{ ft}^2$$

The area of the segment of the sphere between the viewing angles of 0° and 22.5° is

$$2\pi\left(\frac{47.6 \text{ in}}{12 \text{ in/ft}}\right)^2(1 - \cos 22.5^\circ) = 7.52 \text{ ft}^2$$

The area of the ring-like element of the sphere, across which the radiation measured at a viewing angle of 20° passes, is

$$7.52 \text{ ft}^2 - 4.55 \text{ ft}^2 = 2.97 \text{ ft}^2$$

Consider the radiation reading taken at a viewing angle of 20° with the torch operating at an average net power input of 8,700 Btu/hr. The operating conditions at this point were:

voltage drop across torch 23.0 v

cooling water flow rate 645 lbs/hr

current to torch 240 amps

cooling water temperature rise 15.5°F

bolometer output signal 110 mv

The gross power input to the torch is

$$(23.0 \text{ volts})(240 \text{ amps})(3.415 \text{ Btu/watt hr}) = 18{,}800 \text{ Btu/hr}$$

The power loss to the cooling water is

$$(645 \text{ lbs/hr})(1.0 \text{ Btu/lb } ^\circ\text{F})(15.5 \ ^\circ\text{F}) = 10{,}000 \text{ Btu/hr}$$

The net power input to the torch is

$$18{,}800 \text{ Btu/hr} - 10{,}000 \text{ Btu/hr} = 8{,}800 \text{ Btu/hr}$$

The radiative flux at this viewing is

$$(0.110 \text{ volts})(133 \text{ Btu/hr ft}^2 \text{ volt}) = 14.6 \text{ Btu/hr ft}^2$$

The contribution to the actual radiative heat transfer passing across the segment of the sphere between 17.5° and 22.5° viewing angle is

$$(2.97 \text{ ft}^2)(14.6 \text{ Btu/hr ft}^2) = 43.4 \text{ Btu/hr}$$

The actual radiative heat transfer from the plasma and torch was calculated by adding the contributions passing across each ring-like segment of the sphere. The average net power input to the plasma was calculated by averaging the net power input at each radiation reading. The per cent net power radiated from the plasma and torch was calculated by dividing the total radiative power by the average net power input.

APPENDIX D

SAMPLE CALCULATIONS FOR THEORETICAL MODELS

D-1 SAMPLE CALCULATION FOR KRAMERS APPROXIMATION

The Kramers approximation is given by

$$P(T) = 1.4 \times 10^{-34} Z^2 n_e n_i T^{1/2} \left[e^{-840/T} - e^{-53,800/T} \right] \quad \text{watts/cm}^3 \quad (4\text{-}7)$$

As an example, consider a temperature of 19,000°K. From Drellishak's tables (Ref. 10) for the equilibrium composition of atmospheric argon plasma

$n_i^I = 1.84 \times 10^{17}$ cm^{-3}

$n_i^{II} = 1.08 \times 10^{15}$ cm^{-3}

$n_e = 1.87 \times 10^{17}$ cm^{-3}

where n_i^I, n_i^{II} are the number densities of the first and second ion, respectively. The contribution to the radiation from free-free electron-first ion collisions is

$$P_I(T) = (1.4 \times 10^{-34})(1)^2(1.87 \times 10^{17})(1.84 \times 10^{17})(1.9 \times 10^4)^{1/2} \times$$

$$\times \left[\frac{1}{e^{.0442}} - \frac{1}{e^{2.83}} \right]$$

$$P_I(T) = 596 \text{ watts/cm}^3$$

The contribution to the radiation from free-free electron-second ion collisions is

$$P_{II}(T) = (1.4 \times 10^{-34})(2)^2(1.87 \times 10^{17})(1.08 \times 10^{15})(1.9 \times 10^{4})^{1/2} \times$$

$$\times \left[\frac{1}{e^{.0442}} - \frac{1}{e^{2.83}} \right] = 14 \text{ watts/cm}^3$$

The radiation predicted by the Kramers approximation at 19,000°K is

$$596 \text{ watts/cm}^3 + 14 \text{ watts/cm}^3 = 610 \text{ watts/cm}^3$$

D-2 SAMPLE CALCULATION FOR SOMMERFELD APPROXIMATION

The Sommerfeld approximation is given by

$$P(T) = 1.4 \times 10^{-34} Z^2 n_e n_i T^{1/2} \bar{g}(T) \left[e^{-840/T} - e^{-53,800/T} \right] \quad \text{watts/cm}^3 \quad (4\text{-}8)$$

Again, consider a temperature of 19,000°K. The average Gaunt factor, $\bar{g}(T)$, at 19,000°K is given by Greene (Ref. 11) as 1.31. The radiation predicted at 19,000°K by the Sommerfeld approximation is

$$(610 \text{ watts/cm}^3)\ (1.31) = 800 \text{ watts/cm}^3$$

D-3 SAMPLE CALCULATIONS FOR KRAMERS-UNSOLD APPROXIMATION

The emission coefficient given by the Unsöld approximation is

$$\epsilon_\nu = 6.8 \times 10^{-45}\ Z^2\ \frac{n_e n_i}{T^{1/2}} \quad \text{watt sec/cm}^3 \quad (4\text{-}9)$$

The emission coefficient given by the Kramers approximation is

$$\epsilon_\nu = 6.8 \times 10^{-45}\ Z^2\ \frac{n_e n_i}{T^{1/2}}\ e^{-h\nu/kT} \quad \text{watt sec/cm}^3 \quad (4\text{-}3)$$

The combined Kramers-Unsöld model forces the emission coefficient of the Kramers approximation to match the emission coefficient of the Unsöld approximation at the cutoff frequency, ν_g , by adjusting the constant term in the Kramers emission coefficient. Equating the two emission coefficients at the cutoff frequency,

$$6.8 \times 10^{-45} Z^2 \frac{n_e n_i}{T^{1/2}} = CZ^2 \frac{n_e n_i}{T^{1/2}} e^{-h\nu_g/kT}$$

which gives

$$C = 6.8 \times 10^{-45} e^{h\nu_g/kT} \qquad \text{(D-1)}$$

as the constant term in the Kramers emission coefficient. The contribution to the radiation below the cutoff frequency from free-free and free-bound transitions is found by integrating the Unsöld emission coefficient from the lower limit of transmissibility of the sodium chloride window, ν_l , to the cutoff frequency, ν_g .

$$P(T) = \int_{\nu_l}^{\nu_g} \epsilon_\nu \, d\nu = 6.8 \times 10^{-45} Z^2 \frac{n_e n_i}{T^{1/2}} (\nu_g - \nu_l) \qquad \text{(D-2)}$$

The contribution to the radiation above the cutoff frequency from free-free transitions is found by integrating the Kramers emission coefficient from the cutoff frequency, ν_g , to the upper limit of transmissibility of the sodium chloride window, ν_u

$$P(T) = \int_{\nu_g}^{\nu_u} \epsilon_\nu \, d\nu$$

$$= \int_{\nu_g}^{\nu_u} CZ^2 \frac{n_e n_i}{T^{1/2}} e^{-h\nu/kT} \, d\nu$$

$$= CZ^2 (k/h) n_e n_i T^{1/2} \left(e^{-h\nu_g/kT} - e^{-h\nu_u/kT}\right)$$

Substituting for C and evaluating the constant term gives

$$P(T) = 1.42 \times 10^{-34} \, e^{14,400/T} \, Z^2 n_e n_i T^{1/2} \times \left(e^{-14,400/T} - e^{-53,800/T}\right) \qquad \text{(D-3)}$$

The upper and lower frequencies of transmissibility of the sodium chloride window are

$\nu_u = 11.2 \times 10^{14} \text{ sec}^{-1}$

$\nu_l = 0.175 \times 10^{14} \text{ sec}^{-1}$

The cutoff frequency is taken as

$\nu_g = 3.0 \times 10^{14} \text{ sec}^{-1}$

and is assumed to be constant with temperature.

Consider, as an example, a temperature of 19,000°K. The contribution to the radiation predicted by the Unsöld approximation is

$$P(T) = (6.8 \times 10^{-45})(1)^2 \frac{(1.87 \times 10^{17})(1.84 \times 10^{17})}{(1.9 \times 10^4)^{1/2}} (2.82 \times 10^{14})$$

$$= 478 \text{ watts/cm}^3$$

The contribution to the radiation predicted by the modified Kramers approximation is

$$P(T) = (1.42 \times 10^{-34})(e^{.758})(1.87 \times 10^{17})\left[(1)^2(1.84 \times 10^{17}) + (2)^2(1.08 \times 10^{15})\right](1.9 \times 10^{4})^{1/2}\left(e^{-.758} - e^{-2.83}\right)$$

$$= 602 \text{ watts/cm}^3$$

The radiation predicted by the Kramers-Unsöld model at 19,000°K is

$$478 \text{ watts/cm}^3 + 602 \text{ watts/cm}^3 = 1{,}080 \text{ watts/cm}^3$$

APPENDIX E

TEMPERATURE DETERMINATION

E-1 THEORY OF TEMPERATURE DETERMINATION

The electrons populating the higher energy levels of the excited atoms and ions in a plasma emit radiation of characteristic frequencies upon undergoing transitions to lower energy levels. The intensity of the radiation of any spectral line is given by (Ref. 16)

$$I_{\alpha\beta} = A_{\alpha\beta} h\nu_{\alpha\beta} \frac{n(T) g_\alpha e^{-E_\alpha/kT}}{\sum_{i=1}^{\infty} g_i e^{-E_i/kT}} \qquad \text{(E-1)}$$

where $I_{\alpha\beta}$ is the intensity of the radiation (watts/cm^3)

$A_{\alpha\beta}$ is the transition probability from state α to state β

$\nu_{\alpha\beta}$ is the frequency of the radiation (sec^{-1})

$n(T)$ is the number density of the atoms or ions emitting the radiation (cm^{-3})

g_i is the statistical weight of the i^{th} state

k is the Boltzmann's constant, 1.38 x 10^{-16} ergs/$^\circ$K

T is the temperature ($^\circ$K)

E_i is the excitation energy of the i^{th} state

The frequency of the spectral line is given by Planck's equation

$$h\nu_{\alpha\beta} = E_\alpha - E_\beta \qquad \text{(E-2)}$$

The quantity in the numerator of Eq. E-1 is the number atoms (considering an atom spectral line) in the α state as given by the

Boltzmann distribution. The quantity in the denominator of Eq. E-1 is the internal partition function of the atom. As the temperature rises at constant pressure, the decrease in the density of the gas and the destruction of atoms by ionization overtakes the increasing exponential and the intensity exhibits a maximum.

The theoretical relative intensity of the 4158.59 Å argon atom line, Figure E-1, was known (Ref. 13). The maximum intensity of this line occurs at 15,550°K. If the temperature at some point in the plasma jet is above 15,550°K, the experimentally measured spectral line intensity will also show a maximum. In this case it is unnecessary to measure the absolute intensity of the spectral line; the temperature in the plasma jet can be determined from the relative intensity of the spectral line by comparison with the theoretical relative intensity of the line.

The intensity of radiation emitted by a non-opaque plasma depends upon the depth of the plasma emitting the radiation. For the purpose of determining the temperature distribution in the plasma jet, the plasma is assumed to be optically thin. This assumption is supported by measurements in an argon plasma jet (Ref. 13). Under this assumption, the intensity of the characteristic radiation of a spectral line emitted by the plasma depends on the temperature distribution in the plasma jet and the thickness of the jet at the point of observation. The plasma jet is also assumed to have axial symmetry. Thus, the cross-section at any vertical height in the plasma jet is circular. The temperature distribution at any height in an axially symmetrical plasma jet will be a function only of the radius.

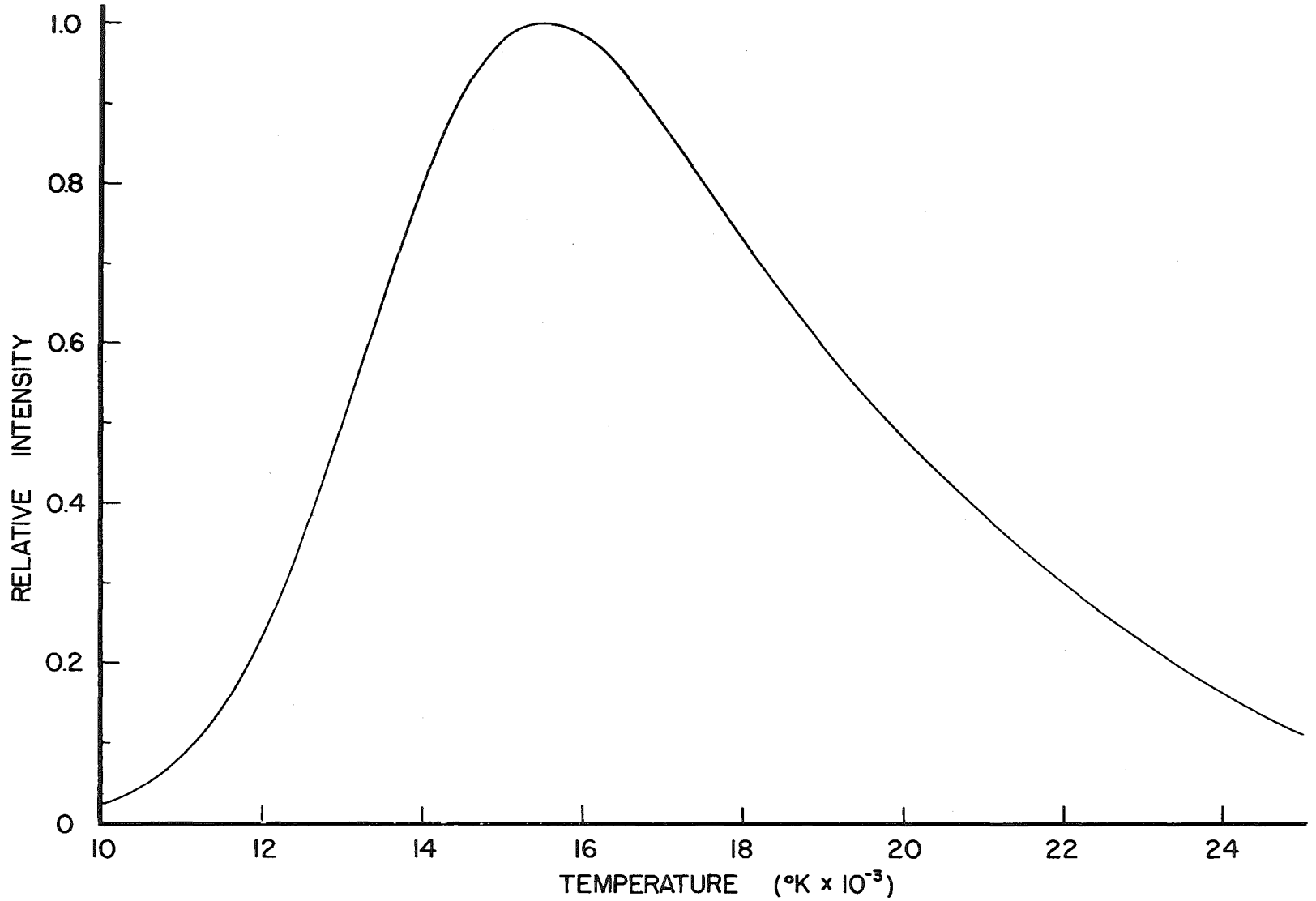

Fig. E-1 Theoretical Relative Intensity; Argon Atom Line 4158.59Å

E-2 ABEL INTEGRAL EQUATION

The intensity of the radiation viewed by the spectroscope is the sum of radiation emitted by each volume element throughout the depth of the plasma. Figures 5-6 and 5-7 show the spectral line intensity as functions of the lateral distance from the axis of symmetry of the plasma jet. The lateral spectral line intensity is an intensity, integrated over the depth of the plasma.

Assuming axial symmetry within the plasma jet, each horizontal cross-section is a circle. Define a rectangular coordinate system on this circle with its origin at the center of the circle as shown in Figure E-2 such that x represents the lateral distance from the axis of symmetry at which the spectroscope observes the radiation from the plasma. Denote the lateral spectral line intensity shown in Figures 5-6 and 5-7 by I(x). The object is to find a relationship between I(x) and I(r), the spectral line intensity as a function of the radial coordinate within the circle. The lateral spectral line intensity is given in terms of the radial spectral line intensity by the integral

$$I(x) = 2\int_0^Y I(r)\, dy$$

By definition of the coordinate systems

$$r^2 = x^2 + y^2$$

Y is the value of the coordinate y on the boundary of the circular cross-section of radius R, i.e.,

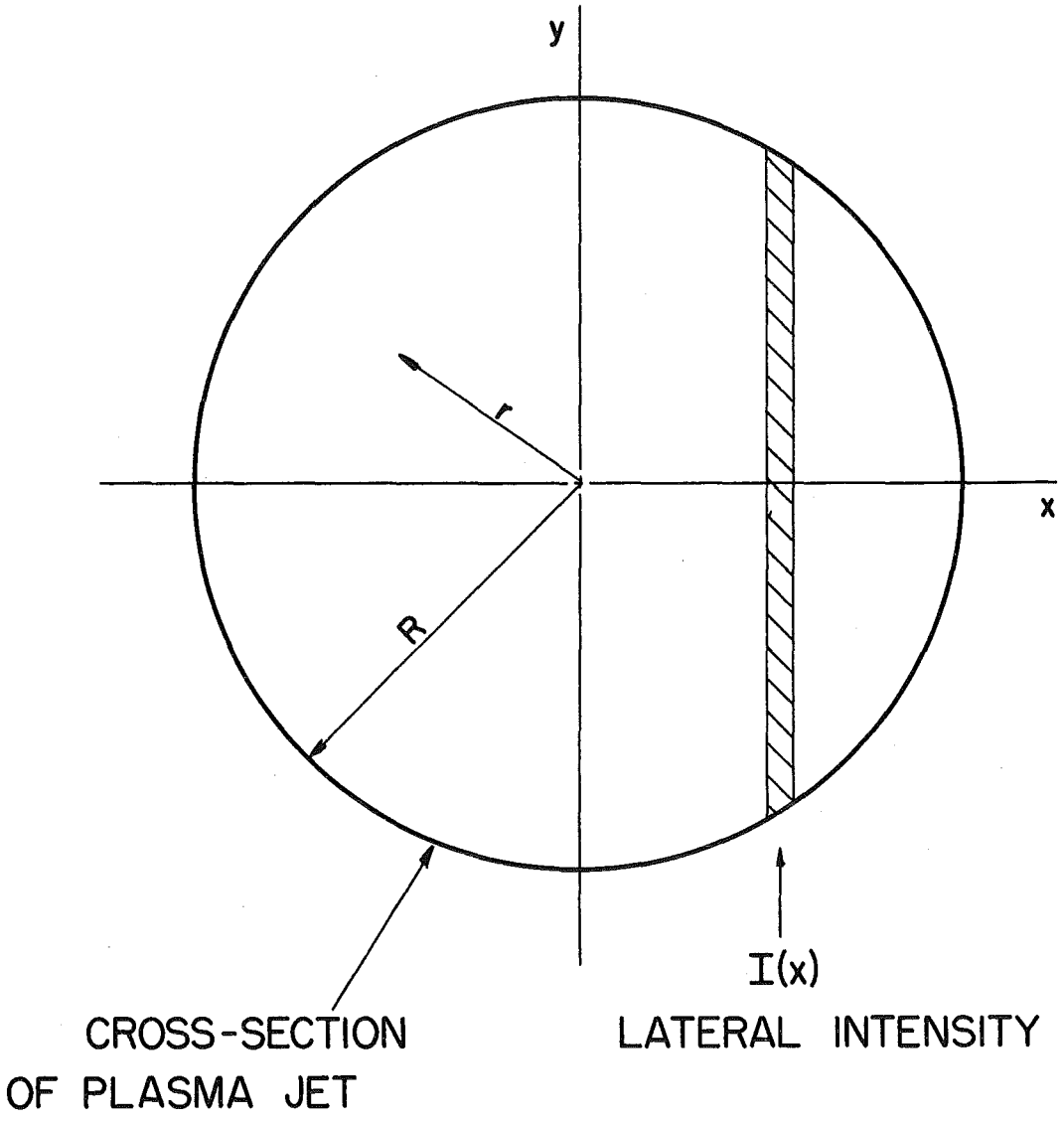

Fig. E-2 Derivation of Abel Integral

$$R^2 = x^2 + Y^2$$

Changing variables in the integral at a constant x

$$y = \sqrt{r^2 - x^2}$$

$$dy = \frac{r}{\sqrt{r^2 - x^2}}\, dr$$

$$I(x) = 2\int_0^{\sqrt{x^2 - R^2}} \frac{r\, I(r)\, dr}{\sqrt{x^2 - r^2}}$$

This is the Abel integral equation, which can be solved analytically (Ref. 20) giving

$$I(r) = -\frac{1}{\pi}\int_r^R \frac{I'(x)\, dx}{\sqrt{x^2 - r^2}}$$

where I'(x) is the derivative of I(x) with respect to x

Olsen (Ref. 16) has developed a numerical technique to evaluate this integral using data of the form of that in Figures 5-6 and 5-7. Enright (Ref. 17) has programmed this technique for use on an I.B.M. 709 digital computer. Enright's program was used to invert the experimental data.

E-3 SPECTROMETER ADJUSTMENTS FOR THE MEASUREMENT OF LATERAL SPECTRAL LINE INTENSITY

The spectrum of the radiation from an argon plasma consists of a series of spikes superposed on the slowly varying continuum radiation.

The spikes correspond to various spectral lines of the atoms and ions. Figure E-3 shows a spectrum of the plasma taken in the course of these experiments. This spectrum was taken with a minimum entrance and exit slit opening to provide maximum resolution.

Theoretically, the spectral lines should be very narrow. However, the spectral lines in a plasma are broadened due to various temperature and electric field effects. In order to measure the intensity of any spectral line, it is necessary to open the exit slit of the spectrometer so as to include all of the radiation under the desired spectral line.

Ideally, a spectral line should be chosen for the temperature determination which is isolated from all other lines. However, this is not the only factor to be considered in the choice. The 4158.59 Å atom line was chosen by other investigators for several reasons (Refs. 13, 16, 17). The 4158.59 Å line is flanked by two other lines, one at 4154.50 Å and one at 4164.18 Å. With the exit slit opened to receive all of the radiation under the 4158.59 Å line, the radiation from these other two lines will be included. Enright (Ref. 17) estimates that the 4154.50 Å line contributes a negligible amount of radiation to the readings. He also states that, although the radiation from the 4164.18 Å line is not negligible, the variation of the intensity of this line with temperature is nearly the same as for the 4158.59 Å. Therefore, a negligible error is introduced by including these two lines in the spectroscopic measurement of the lateral intensity of the 4158.59 Å line for the purpose of determining the temperature distribution in the plasma jet.

The necessary exit slit width was determined by measuring the width

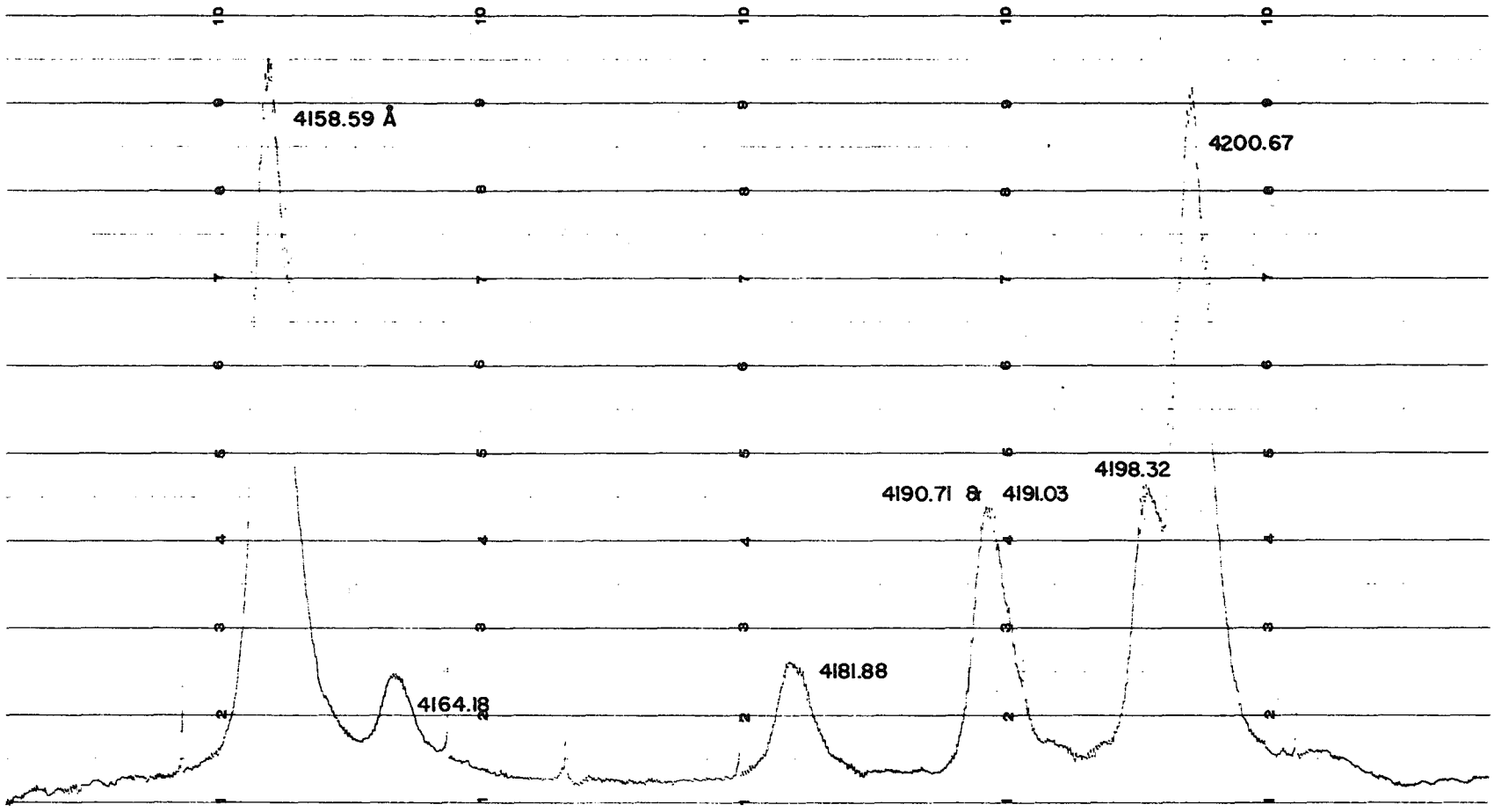

Fig. E-3 Spectrum of Argon Plasma; Slit Opening 1 Micron

of the 4158.59 Å line on Figure E-3 and dividing this width by the linear dispersion of the spectrometer at this wavelength, 43 Å/mm (Ref. 17). The exit slit width used was 208 microns greater than the entrance slit width. A spectrum of the plasma taken with the exit slit widened is shown in Figure E-4. The loss of resolution due to the wider exit slit opening is pronounced.

From the spectrum in Figure E-4, the setting of the spectrometer corresponding to the maximum intensity in the region of the 4158.59 Å line was determined. The measurements of the total lateral intensity of the line and continuum were made at this spectrometer setting. In order to determine what portion of this total lateral intensity was due to continuum radiation, the spectrometer was adjusted to receive the continuum radiation just to the left of the 4158.59 Å line in Figure E-4, but excluding all of the radiation from the line. A second traverse was made at this spectrometer setting to measure the continuum intensity. The continuum intensity was assumed to be the same underneath the 4158.59 Å line as slightly to the left of it, i.e., at slightly shorter wavelengths. The continuum intensity was measured at a wavelength of 4135 Å.

The traverses were made with an entrance slit width of 10 microns and an exit slit width of 218 microns. The entrance slit was opened this additional amount to increase the intensity of radiation received by the photomultiplier tube. The resulting additional loss of resolution does not effect the temperature determination.

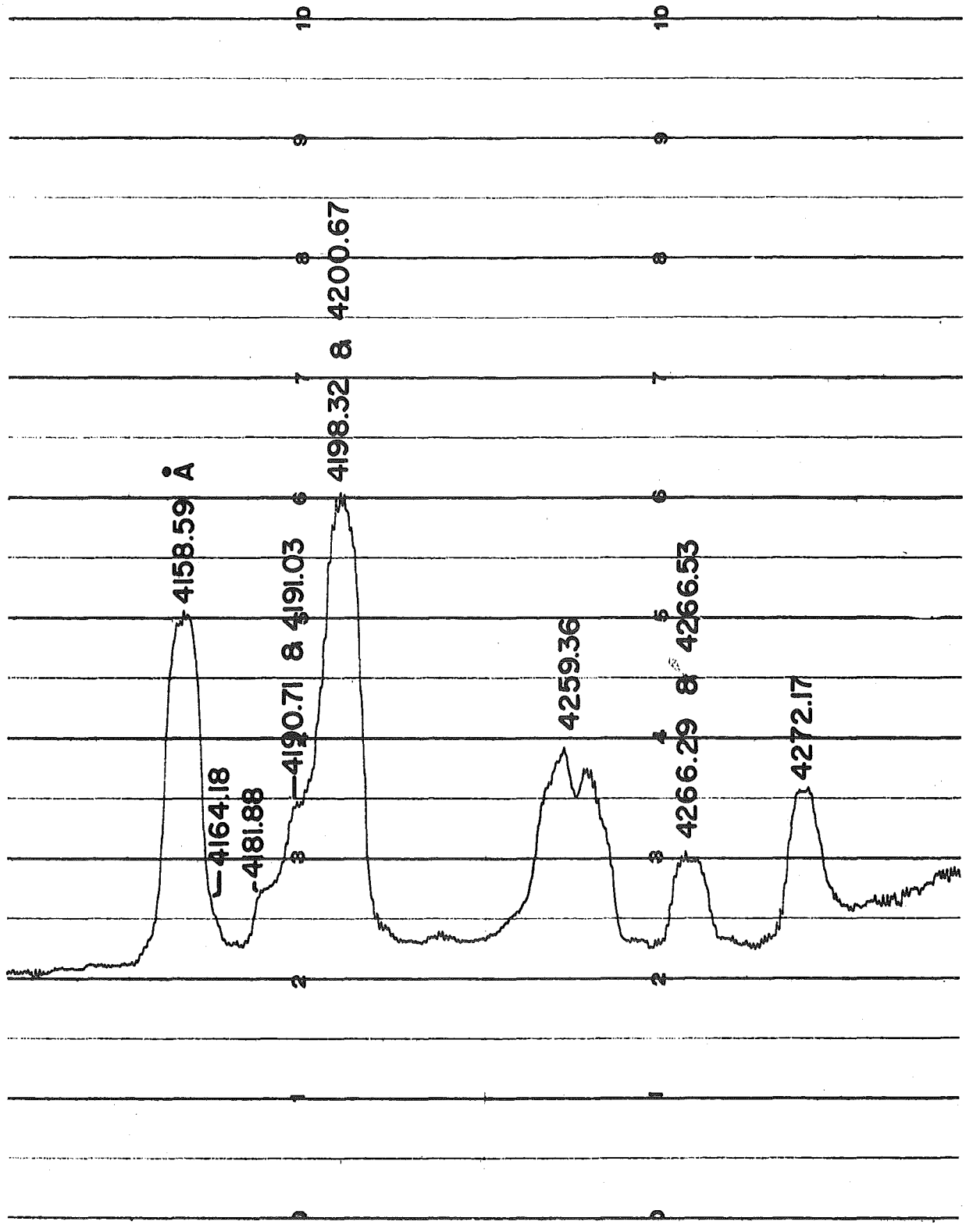

Fig. E-4 Spectrum of Argon Plasma; Slit Opening 209 Microns

APPENDIX F

CALCULATIONS OF TEMPERATURE-RADIATION DATA

F-1 INTERPOLATION OF TEMPERATURE RADIATION DATA TO COMMON POWER LEVELS

Ideally, the temperature profiles of the plasma jet, Figure 5-10, and the inverted radiation profiles, Figure 5-18, should have been determined at the same average net power input to the plasma. However, as has been explained in Section 5.4, it is impossible to operate the plasma torch at a predetermined power level. As a result, two temperature profiles were determined at an average net power input of 10,100 Btu/hr and 15,000 Btu/hr, while the three radiation profiles were determined at an average net power input of 12,100 Btu/hr, 13,900 Btu/hr and 17,200 Btu/hr. In order to determine the radiation as a function of temperature, these data were adjusted by means of a linear interpolation technique to common power levels.

To calculate the points on Figure 5-19 corresponding to 12,100 Btu/hr average net power, the two temperature profiles were used to interpolate to a temperature profile at 12,100 Btu/hr. At each 0.004 in. along the radius, the temperature difference, $\Delta T(r)$, between the temperature profile at 15,000 Btu/hr and the temperature profile at 10,100 Btu/hr was calculated from the profiles on Figure 5-10. The temperature difference $\Delta T'(r)$ between a hypothetical temperature profile at 12,100 Btu/hr and the measured temperature profile at 10,100 Btu/hr was calculated at each 0.004 in. along the radius using the interpolation technique of the following formula

$$\left(\frac{12,100 - 10,100}{15,000 - 10,100}\right)\Delta T(r) = \Delta T'(r)$$

The temperature at each 0.004 in. along the radius corresponding to an average net power input of 12,100 Btu/hr was found by adding the temperature difference, $\Delta T'(r)$, to the temperature at the same radius measured at 10,100 Btu/hr, following the formula

$$T_{12,100}(r) = T_{10,100}(r) + \Delta T'(r)$$

Using this method, the temperature profile measured at 10,100 Btu/hr can be interpolated to any desired power level, P_D, between 10,100 Btu/hr and 15,000 Btu/hr. The interpolation formula is

$$T_{P_D}(r) = T_{10,100}(r) + \left(\frac{P_D - 10,100}{15,000 - 10,100}\right)\Delta T(r) \qquad \text{(F-1)}$$

This equation was used to interpolate to temperature profiles at 12,100 Btu/hr and 13,900 Btu/hr average net power input. With the temperature profile known at the same power levels as each radiation profile, the points on Figure 5-19 were plotted.

In order to avoid extrapolating the temperature profile past the measured values, a similar interpolation technique was used to find a radiation profile at 15,000 Btu/hr by using the radiation profiles at 13,900 Btu/hr and 17,200 Btu/hr. The interpolation formula used is

$$R_{15,000}(r) = R_{13,900}(r) + \left(\frac{15,000 - 13,900}{17,200 - 13,900}\right)\Delta R(r) \qquad \text{(F-2)}$$

where $\Delta R(r)$ is the difference in radiation at each radius r between the radiation profile at 17,200 Btu/hr and the radiation profile at 13,900 Btu/hr.

The radiation profile at 15,000 Btu/hr obtained by applying Eq. F-2 was compared with the measured temperature profile at 15,000 Btu/hr to determine the third set of points on Figure 5-19.

For example, consider a radius of 0.020 in. in the plasma jet. From Figure 5-10, the temperature at a radius of 0.020 in. at 15,000 Btu/hr is 22,500°K; the temperature at 10,100 Btu/hr is 18,050°K. Thus the temperature difference, $\Delta T(r)$, at a radius of 0.020 in. is 3,950°K. Using Eq. F-1, the temperature corresponding to an average net power input of 12,100°K at this radius is

$$T_{12,100}(.020) = 18,050 + \left(\frac{12,100 - 10,100}{15,000 - 10,100}\right)(3,950)$$

$$= 19,660 \ ^{\circ}K$$

Referring to Figure 5-18, the radiation at a radius of 0.020 in. at an average net power input of 12,100 Btu/hr is 1,380 watts/cm^3. This is one of the points plotted on Figure 5-19. Likewise, at a radius of 0.020 in. the temperature corresponding to an average net power input of 13,900 Btu/hr is

$$T_{13,900}(.020) = 18,050 + \left(\frac{13,900 - 10,100}{15,000 - 10,100}\right)(3,950)$$

$$= 21,110 \ ^{\circ}K$$

Referring to Figure 5-18, the radiation at a radius of 0.020 in. at an average net power input of 13,900 Btu/hr is 1,200 watts/cm^3. This is another point on Figure 5-19.

Again, at a radius of 0.020 in., the radiation from Figure 5-18 at an average net power input of 17,200 Btu/hr is 1,470 watts/cm^3, and the radiation at 13,900 Btu/hr is 1,220 watts/cm^3. The difference in radiation from these two profiles at a radius of 0.020 in. is 260 watts/cm^3. Using Eq. F-2, the radiation corresponding to an average net power input of 15,000 Btu/hr at this radius is

$$R_{15,000}(.020) = 1,220 + \left(\frac{15,000 - 13,900}{17,200 - 13,900}\right)(260)$$

$$= 1,310 \text{ watts/cm}^3$$

From Figure 5-10, the temperature at a radius of 0.020 in. and at an average net power input of 15,000 Btu/hr is 18,300°K. This is also a point on Figure 5-19.

F-2 CHECK ON TEMPERATURE-RADIATION DATA

A check on the experimental curve drawn on Figure 5-19 was made. Using the interpolation technique discussed above, the temperature at 0.004 in. increments along the radius was found at an average net power input of 12,100 Btu/hr. The plasma was imagined to be divided into incremental volumes one centimeter square and 0.01 centimeters thick along a diameter as shown in Figure 5-20. The radiation, in watts/cm^3, was found at each increment along the radius for an average net power

input of 12,100 Btu/hr, by using the temperature at each increment as calculated with the interpolation formula, Eq. F-1, and reading the radiation corresponding to each temperature from the experimental curve on Figure 5-19. The radiation emitted by each elemental volume in Figure 5-20 is 0.01 times the value read from Figure 5-19, since the volume of each element in Figure 5-20 is 0.01 cm^3. The contributions to the radiation from the elemental volumes along the radius were added and the result was doubled to include the contributions along the diameter in the plasma jet. Doubling the contributions from the elements along the radius counts the elemental volume at the center of the plasma jet twice. Therefore, the contribution from the elemental volume at the center was subtracted once. The resulting figure should agree with the maximum value of the lateral radiative flux which was measured at 12,100 Btu/hr. Performing the calculation indicated gives a maximum lateral radiative flux of 404 watts/cm^2. Referring to Figure 5-12, the maximum measured value of the radiative flux was 418 watts/cm^2. A similar calculation of the radiative flux at an average net power input of 13,900 Btu/hr gives a value of 428 watts/cm^2. Referring to Figure 5-13, the maximum measured value of the radiative flux at this power level was 426 watts/cm^2.

Referring to Figure 5-14, the maximum measured radiative flux at an average net power input of 17,200 Btu/hr was 465 watts/cm^2. This value may be interpolated to correspond to an average net power input of 15,000 Btu/hr in a manner similar to that indicated in Eq. F-2. The calculation gives

$$F_{max}\,(15{,}000) = 426 + \left(\frac{15{,}000 - 13{,}900}{17{,}200 - 13{,}900}\right)(465 - 426)$$

$$= 439 \ \text{watts/cm}^2$$

Using the temperature profile at an average net power input of 15,000 Btu/hr on Figure 5-10, and the experimental curve on Figure 5-19, the calculated maximum radiative flux is 450 watts/cm^2 .

These results may be summarized as follows.

Average Net Power Input (Btu/hr)	Maximum Lateral Radiative Flux watts/cm^2		% Error (from measured value)
	Calculated	Measured	
12,100	404	418	-2.9
13,900	428	426	+0.5
15,000	450	439	+2.5